

Relativity: Introducing relativity and quantum theory by ruler and compass geometry of phase

William G. Harter and Tyle C. Reimer

University of Arkansas, Department of Physics, Fayetteville AR 72701

(Dated: April 6, 2017)

Abstract

A quantitatively precise and logically compelling Occam's Razor introduction to special relativity and quantum theory can be done with a few simple steps aided by ruler and compass. A number of concepts that students invariably find arbitrary, mysterious, or quasi-paradoxical are elegantly resolved.

The development models pairs of laser beams or cavity modes that produce a Minkowski coordinate lattice geometry in space-time and a reciprocal lattice geometry in per-space-time (Fourier space). This leads to a revealing roadmap for classical mechanical and quantum variables that derives and clarifies their differential relations yet requires little more than high-school trigonometry.

This geometric approach improves both conceptual visualization and the computational techniques for these subjects while showing they are really two sides of a single subject. Such a unified approach could allow these pillars of modern physics to be introduced earlier and in greater depth in a growing range of physics curricula. It also reveals heretofore hidden insight and provides new avenues for research.

(At current date above, this is undergoing final review and editing)

CONTENTS

I. Introduction to relativity	4
II. Novel reviews of trigonometry and its applications	7
A. Complex algebra and calculus	10
B. Phasors and complex wave functions	12
1. A phasor clock has only one hand!	14
2. At c the phasor clocks freeze!	14
3. What's waving? (... and what's not?)	15
III. Space-time vs Per-space-time: Fourier's keyboard of the Gods	17
A. c -Scaled wave graphs and Doppler shifts	18
B. Evenson's axiom and Doppler shifts	21
C. Rapidity and its Doppler shift arithmetic	22
IV. Wave-zero 2-CW coordinate grids	25
A. Geometry of Minkowski phase and group wave-lattices	28
B. Understanding relativity parameters and transformations	29
C. Invariance of phase to Lorentz transformation	33
D. Thales-Euclid means and geometry of hyperbolic invariants	34
E. PW Sums of multiple CW harmonics and Doppler effects	37
V. Properties and applications of relativity geometry	41
A. Space-proper-time plots and the stellar-aberration angle	41
1. TE-Waveguide geometry	44
2. Wave parameter variation with group velocity	46
3. Table II - Relativity ratios versus rapidity- ρ , guide angle- σ , and $\beta=u/c$	48
VI. Relativity gives basic wave mechanics of matter	49
A. What <i>is</i> energy?	51
1. What's the matter with energy?	52
2. How light is light?	55
VII. Relativity geometry of Hamiltonians and Lagrangian	57

A. Phase and action related to Lagrangian and Hamiltonian functions	57
B. Hamiltonian, Poincare invariants, and Legendre contact transformation	58
C. Hamilton-Jacobi quantization	62
VIII. Relativity geometry of quantum transitions	66
A. Symmetry and conservation principles	66
B. Single-photon transitions and Feynman diagram geometry	67
1. Photon transitions obey rocket-science formula	68
2. Geometric level and transition sequences	70
3. Half-sum-and-difference transition web	71
IX. Accelerated frames and optical Einstein-elevator	74
A. Metrology in accelerated frames	79
B. Mechanics in accelerated frames	82
X. Variation and quantization of Optical Amplitudes	85
A. Quantizing Maxwell waves	90
1. Quantum numbering of photons and modes	91
2. Quantum wave normalization	93
3. Relativistic 1-CW covariance of Poynting flux	94
4. Relativistic 2-CW invariance of cavity quanta	95
B. E-Field 2-CW flux relations	96
C. Photon-number vs. Coherent-alpha waves	97
1. Fuzzy hyperbolas vs. fuzzy coordinates	98
XI. Appendix	101
A. The Purest Light and a Wave-Resonance Hero —Ken Evenson (1932-2002)	101
List of Figures	103
List of Tables	106
References	107

I. INTRODUCTION TO RELAWAVITY

For well over a century the introductory teaching of special relativity (SR) and quantum mechanics (QM) has been problematic for critically thinking students who seek conceptual comprehension. A paraphrasing of many such student comments might be, “*I didn’t understand all that, but I don’t think our professor did, either!*”

In spite of such doubts, many thousands of students of physics, chemistry, engineering, and now even biological sciences have soldiered through SR and QM to create a vast technology based on them with new sciences still arising from these pillars of modern physics. Beginnings of QM by Planck¹ (1900), of QM and SR by Einstein^{2,3,4} (1905), and QM matter waves by DeBroglie⁵ (1923) were great advances in a theory related to electromagnetic (EM) wave phenomena that still yields new applications and theory.

Yet, doubts about establishing basic SR or QM axioms may cause enough discomfort for an SR or QM professor to exclaim, “*Just trust me! This all works out in the end!*” Such painful beginnings cannot be healthy for the science or for the society that supports it. Evidence of this is seen in the plethora of painful popular attempts to describe either SR or QM. All this begs us to apply Occam’s Razor.

The following article describes the result of decades long search⁶ at the University of Arkansas for a technically sweet front-end to modern SR and QM physics education as well as improved ways to develop classical mechanics (CM). The upshot is that SR and QM merge into a single subject and need not, indeed *should not*, continue to be taught separately. Space-time SR aberrations and related QM Lagrangian and Hamiltonian variables are constructed by a single elegant logic involving a few ruler and compass strokes derived from geometry of laser wave cavity interference.

Such a simple development allows younger students to begin acquiring understanding of modern physics theory while relating it to classical geometry and mechanics going back to Thales (600 BCE), Euclid (300BCE), and Galileo (1500ACE). This effort extends work by the Feynman, Leighton, and Sands projects of 1964 at CalTech that gave *The Feynman Lectures in Physics*⁷, (*The lectures online*)[?].

Full Disclosure: One of the authors (WGH) was a grad student of Richard P. Feynman and William G. Wagner (a co-author of Feynman’s text on Gravitation⁸) at CalTech and UCI between 1964 and 1968. The current project began at Georgia Tech⁹ in 1985 and

continued at UAF from 2001 to the present¹⁰.

In order to be self-contained, this exposition begins with a novel and refreshing geometric review of trigonometry of the six circular and six hyperbolic sine-tangent-secant and complementary cosine-cotangent-cosecant functions. The circular six are functions of unit-circle sector area σ while the hyperbolic six depend on unit-hyperbola sector area ρ and all reveal some little known relations.

A “trigonometric road-map” (TRM) relates twelve trig functions and shows that hyperbolic sine and cosine sum and difference give the \pm exponentials: $e^{\pm\rho} = \cosh \rho \pm \sinh \rho$. Hyperbolic functions with real exponential power series derived from interest-rate formulae are simpler than circular functions that involve the mysterious $i = \sqrt{-1}$ in complex exponentials $e^{\pm i\sigma} = \cos \sigma \pm i \sin \sigma$. So the former serve to derive the latter in a first step to show the role of complex wave functions $Ae^{\pm i(kx - \omega t)}$ in QM and SR theory and how real exponentials $e^{\pm\rho}$ rescale wavevector k , wave angular frequency ω , and wave amplitude A .

Later $e^{+\rho}$ and $e^{-\rho}$ are seen to be blue and red Relativistic Doppler shifts while σ is the stellar-aberration or waveguide-beam-entry angle¹¹. Both measure first order relativistic effects that are well known such as police Doppler radar. Second-order effects such as Lorentz contraction are immeasurably tiny at terrestrial speeds and much more mysterious. Yet second-comes-first in standard¹² SR texts. Here a first-things-first approach based on Doppler shifts turns out to be clearer and quicker and a lot more revealing.

This involves matching a “trigonometric road-map” (TRM) with a diagram of wave interference geometry for colliding laser plane waves that is named the “Relativity Baseball-Diamond” (RBD). The RBD is constructed from real-wave zeros that trace space-time Minkowski grids. So the logic of this development involves comparing TRM geometry based on unassailable mathematical axioms with a RBD geometry of SR and QM wave mechanics based on potentially assailable physical axioms having several challenging issues including uncertainty, non-locality, and space-time aberration.

The physical axioms for SR are picked with Occam’s Razor in mind¹³. Beside the time reversal symmetry axiom there is one axiom that is (or should be) a classroom show-stopper. That axiom demands that the speed of light *en vacuo* be the same constant for all observers. We prefer to name this *Evenson’s Axiom: All colors go the same speed $c=299,792,458\text{m}\cdot\text{s}^{-1}$* after Kenneth Evenson¹⁴ who measured c using overtones in a laser frequency chain in 1972. Later he worked to establish c as the definition of the meter, thus setting the stage

for a precision revolution that included, among other things, ultra-high resolution laser spectroscopy, the Global Positioning System, and the LIGO projects.

It is important to emphasize how counter-intuitive a super-constant c would be to Galileo and should be to anyone first dealing with SR. (It has been called the *Roadrunner Axiom* after Chuck Jones' cartoons.) Galileo could be excused if he assumed c was infinite ($c=\infty$) so then all would see the same c . But, how can a *finite* c be so regarded the same by all? A demystifying answer to this and other apparent paradoxes is based primarily on Doppler shifts.

A prerequisite to deriving SR and QM fundamentals involves thought experiments with Evenson's axiom that show why *en vacuo* c has to be constant. An ideal blue-green $600THz$ laser beam may be seen to lack a "birth certificate" in the sense that it might be made by an approaching laser operating below $600THz$ as well as a receding laser with output above $600THz$. One needs to explain clearly why all $v=600THz$ beams share the same $\lambda=0.5 \mu m$ wavelength of a co-moving $600THz$ laser and how this implies the same *en vacuo* speed $c=\lambda \cdot v$.

Full understanding of Doppler effects requires a review of wave mechanics that follows the introduction of the geometry of the TRM and RBD. This involves two complimentary four-dimensional theaters, space-time (\mathbf{x}, ct) and per-space-time $(c\mathbf{k}, \omega)$. The first examples are limited to two-dimensional graphs of space-time (x, ct) and per-space-time (ck, ω) . In later sections it will be shown that TRM plots occupy both (\mathbf{x}, ct) and $(c\mathbf{k}, \omega)$ as well as space-space (x, y) plots and per-space-per-space (ck_x, ck_y) plots.

Michelson and Morely¹⁵ showed wave interference is a fine way to measure relative space-time. The *relawavity* shows wave interference is also a fine way to *think* about things relative. By ruler & compass it derives and clarifies Lorentz-Einstein formulae, Lagrangians, Hamiltonians, Feynman diagrams, and Compton effects including wave frame dynamics for "Einstein elevator" acceleration.

II. NOVEL REVIEWS OF TRIGONOMETRY AND ITS APPLICATIONS

Every scientific calculator has an SIN button and, as we tell our home-churched students, this is not such a bad thing. In fact it stands for Slope of INcline and (multiplied by 100) gives the percent of grade or ratio of altitude gained over road distance traveled along the freeway bypass around their town. Next to SIN is a COS or COmplimentary Slope giving ratio of level distance over road distance. Fig. 1a is a plot of sine ($\sin \sigma = \frac{3}{5}$) and cosine ($\cos \sigma = \frac{4}{5}$) of angle $\angle\sigma=36.87^\circ$ that makes 3:4:5 triangles. Angle in radians $\sigma=0.6435=\pi\frac{36.87^\circ}{180^\circ}$ is also total sector area for a unit ($B=1$) circle. (That is π for $\sigma=\pi$.) Fig. 1 uses a non-standard convention to plot complimentary $\cos\sigma$ as a vertical projection while $\sin\sigma$ is horizontal. This is done to match Minkowski plots later on where space x is plotted on horizontal axis and time t on the vertical axis. It is complimentary to a standard Newtonian plot of x (vertical) versus time (horizontal).

The result of pressing a calculator TAN button for angle $\angle\sigma=36.87^\circ$ is the TANgent or $\tan\sigma=\frac{3}{4}$ (the ratio $\tan \sigma = \frac{\sin \sigma}{\cos \sigma}$) labeling the hypotenuse of a smaller 3:4:5 triangle on top of Fig. 1a. That tangent line is also the altitude of the largest 3:4:5 triangle in Fig. 1a, and it encloses the upper σ -sector. The three circular functions $\sin \sigma$, $\cos \sigma$, and $\tan \sigma$ are sufficient for elementary physics but it helps to have three more that are inverses of the primary three. The secant($\sec \sigma = \frac{1}{\cos \sigma} = \frac{5}{4}$), cosecant($\csc \sigma = \frac{1}{\sin \sigma} = \frac{5}{3}$), and cotangent as plotted in Fig. 1b to show *two* additional (and larger) 3:4:5 triangles. (Study carefully the mid and lower right hand side of Fig. 1b.)

A TRM suitable for SR and QM functions and theory involves replacing six circular functions in Fig. 1b with six hyperbolic functions as shown in Fig. 2 and Fig. 3 that play similar roles in labeling coordinates, tangents, and their intercepts around an equilateral hyperbola. Each circular function (such as $\sin \sigma = \frac{3}{5}$) is like an “urban dweller” that has a “country cousin” (for $\sin \sigma = \frac{3}{5} = \tanh \rho = \frac{3}{5}$) with same numerical value ($\frac{3}{5}$ here) that is a function of hyperbolic sector area ($\rho = 0.6931$ with angle $\tanh \rho = \frac{3}{5}$ in this example) as listed on top of Fig. 2 and plotted nearby. For each country-urban pair there is a flipped pair (here: $\tan \sigma = \frac{3}{4} = \sinh \rho$) that shares a value $\frac{3}{4}$ in that example) for the same hyper sector $\rho = 0.6931$ or angle $\angle\nu= 30.96^\circ$) and corresponding circle sector ($\sigma=0.6435$ or angle $\angle\sigma=36.87^\circ$).

A circle-hyperbolic (“urban-country”) pair $\sin \sigma = \frac{3}{5} = \tanh \rho$ and $\tan \sigma = \frac{3}{4} = \sinh \rho$

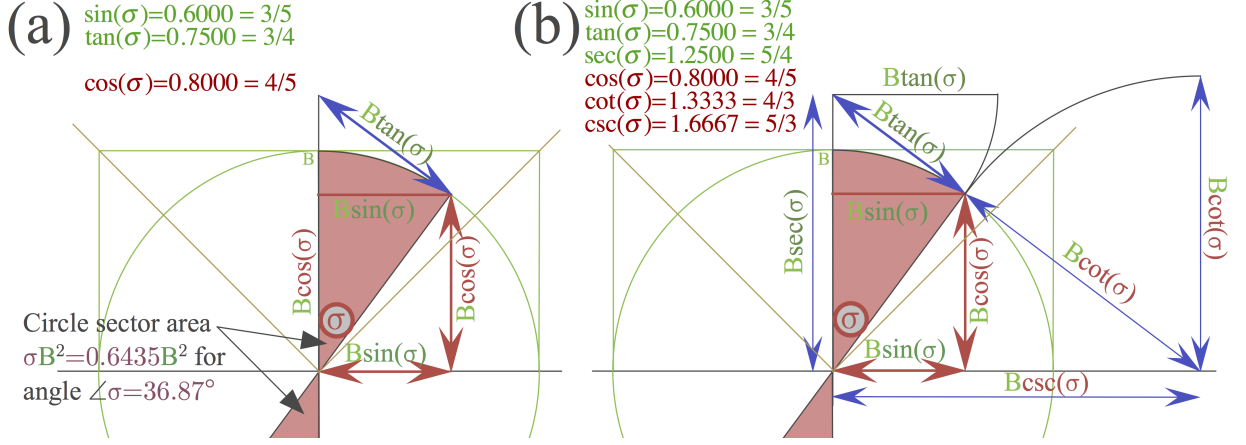


FIG. 1: Circular TRM's (a) Primary circular function triplet. (b) Full TRM sextet of circular functions.

is listed on top left of Fig. 2 and plotted to the right below. (Fig. 2 plots hyperbolic- ρ labels. Fig. 1b plots circular σ -labels.)

Total area ρ of sector pairs sandwiched between opposite sides of a hyperbola is derived by an integral similar to one giving total sector area σ between opposite sides of a circle. See (70) in Sec. IX, near the end. Preparing TRM Fig. 2 for SR and QM theory requires several more lines, circles, tangents, and intercepts that will label wave coordinates for SR and physical quantities for QM. The resulting TRM is Fig. 3. Most of the figure lies within a square with 45° diagonal **OR**. Sides of **OR** have length equal to base B times sum of hyperbolic sine and cosine that is a rising (+) exponential.

$$Be^{+\rho} = B(\cosh \rho + \sinh \rho) = B\left(\frac{5}{4} + \frac{3}{4}\right) = 2B \quad (1)$$

To the left of **OR**'s base is a small square with 45° diagonal **OL** normal to **OR**. Sides of **OL** have length equal to base B times the difference of hyperbolic cosine and sine that is a decaying (-) exponential.

$$Be^{-\rho} = B(\cosh \rho - \sinh \rho) = B\left(\frac{5}{4} - \frac{3}{4}\right) = \frac{1}{2}B \quad (2)$$

In Fig. 3 a circle through point **P** of radius $B\sinh\rho$ bisects hyperbola baseline **OB** where square **OL** ends. Vector **OP** in Fig. 3 has components $(x,y)_{\mathbf{P}}=(B\sinh\rho, B\cosh\rho) = (B\tan\sigma, B\sec\sigma)$ at angle $\angle\rho=\nu=31^\circ$. Just below that is **OS** with components $(x,y)_{\mathbf{S}}=(B\sin\sigma, B\cos\sigma) = (B\tanh\rho, B\text{sech}\rho)$ at angle $\sigma=36.87^\circ$. The circular sine-and-cosine of circle angle/area σ

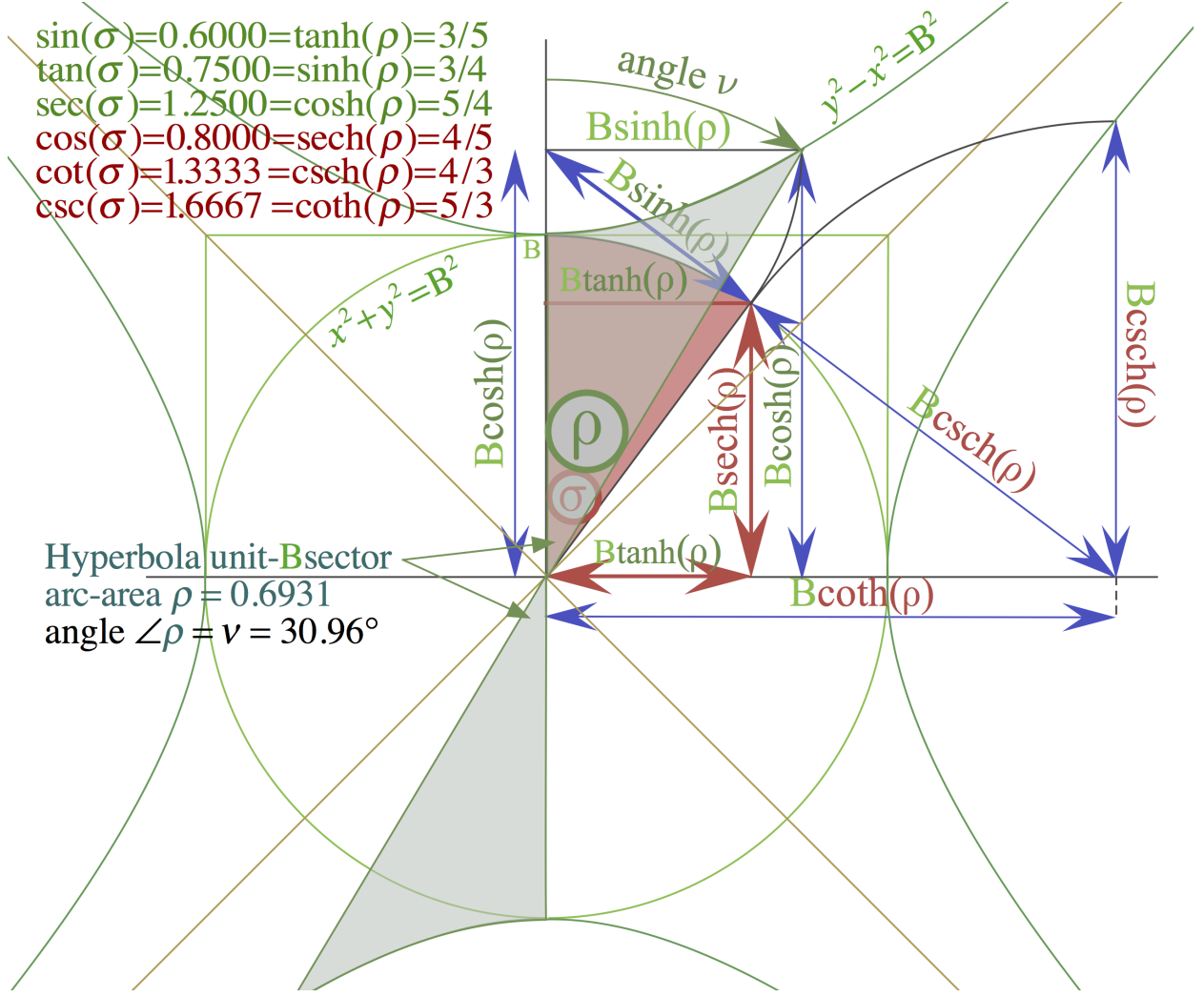


FIG. 2: TRM Hyperbolic labeling of Fig. 1b.

are natural coordinates for \mathbf{S} on the B -circle while hyperbolic sine-and-cosine of hyperbola angle/area ρ are natural coordinates for \mathbf{P} on the B -hyperbola, but either choice is correct. Point \mathbf{G} at $(x,y)_{\mathbf{G}}=(B\cosh\rho, B\sinh\rho)$ is a mirror reflection of \mathbf{P} thru the 45° line \mathbf{OR} . \mathbf{P} is a tangent point for a line \mathbf{RPI}_P of slope $\tanh\rho$ contacting the upper hyperbola. Similarly, \mathbf{G} is a tangent point for a line \mathbf{RGI}_G of slope $\coth\rho$ contacting the righthand hyperbola.

Tangent line \mathbf{RPI}_P crosses the vertical axis at a distance of $B\operatorname{sech}\rho$ from origin \mathbf{O} and ends on horizontal axis at \mathbf{I}_P , a distance $-B\operatorname{csch}\rho$ from \mathbf{O} . Tangent line \mathbf{RGI}_G ends on the vertical axis at \mathbf{I}_G a distance of $-B\operatorname{csch}\rho$ from origin \mathbf{O} after crossing the horizontal axes at distance $B\operatorname{sech}\rho$ from \mathbf{O} .

algebra and calculus of Fig. 3 promised in the introduction. Before doing that, notice that the slope of the line **OG** is also $\frac{\sinh\rho}{\cosh\rho} = \tanh\rho$, but line **OP** has inverse slope $\frac{\cosh\rho}{\sinh\rho} = \coth\rho$ as does the vertical hyperbolic tangent line through point **G**.

Calculus of Fig.3 geometry uses an infinite compounding limit of the interest rate- r formula.

$$e^{rt} = \lim_{n \rightarrow \infty} \left(1 + \frac{rt}{n}\right)^n \quad (3)$$

Infinite- n limit of binomial series is an exponential power- p series of $(rt)^p$ with $1/p!$ coefficients.

$$e^{rt} = 1 + rt + \frac{(rt)^2}{2} + \frac{(rt)^3}{2 \cdot 3} + \frac{(rt)^4}{2 \cdot 3 \cdot 4} + \frac{(rt)^5}{2 \cdot 3 \cdot 4 \cdot 5} + \frac{(rt)^6}{2 \cdot 3 \cdot 4 \cdot 5 \cdot 6} + \dots \quad (4a)$$

$$e^{-rt} = 1 - rt + \frac{(rt)^2}{2} - \frac{(rt)^3}{2 \cdot 3} + \frac{(rt)^4}{2 \cdot 3 \cdot 4} - \frac{(rt)^5}{2 \cdot 3 \cdot 4 \cdot 5} + \frac{(rt)^6}{2 \cdot 3 \cdot 4 \cdot 5 \cdot 6} - \dots \quad (4b)$$

Half-sum and half difference of $e^{\pm rt}$ series define the hyperbolic cosine ($\cosh(rt)$) and sine ($\sinh(rt)$).

$$\frac{e^{+rt} + e^{-rt}}{2} = 1 + \frac{(rt)^2}{2} + \frac{(rt)^4}{2 \cdot 3 \cdot 4} + \frac{(rt)^6}{2 \cdot 3 \cdot 4 \cdot 5 \cdot 6} - \dots = \cosh(rt) \quad (5a)$$

$$\frac{e^{+rt} - e^{-rt}}{2} = rt + \frac{(rt)^3}{2 \cdot 3} + \frac{(rt)^5}{2 \cdot 3 \cdot 4 \cdot 5} + \dots = \sinh(rt) \quad (5b)$$

Sum and difference gives equation (1) and (2) consistent with figures 2 and 3. Replacing rate r with imaginary rate ir where $i = \sqrt{-1}$ gives powers $i^0=1, i^1=i, i^2=-1, i^3=-i, i^4=1, i^5=i, i^6=-1, i^7=-i, \dots$ that repeat sequence- $(1, i, -1, -i)$ every 4th-power. Then hyper-sine-cosine becomes the circular-sine-cosine.

$$\frac{e^{+i rt} + e^{-i rt}}{2} = 1 - \frac{(rt)^2}{2} + \frac{(rt)^4}{2 \cdot 3 \cdot 4} - \frac{(rt)^6}{2 \cdot 3 \cdot 4 \cdot 5 \cdot 6} - \dots = \cos rt \quad (6a)$$

$$\frac{e^{+i rt} - e^{-i rt}}{2} = i rt - i \frac{(rt)^3}{2 \cdot 3} + i \frac{(rt)^5}{2 \cdot 3 \cdot 4 \cdot 5} - \dots = i \sin rt \quad (6b)$$

Sum and difference of this pair gives the Euler-DeMoivre formulae.

$$e^{+i\sigma} = \cos(\sigma) + i \sin(\sigma), \quad e^{-i\sigma} = \cos(\sigma) - i \sin(\sigma). \quad (7)$$

This is used to make wave functions and phasors that help to visualize wave mechanics.

B. Phasors and complex wave functions

A single continuous wave or 1-CW is plotted as a complex phasor array in a space-time plot of Fig. 4. Einstein's math teacher, Herman Minkowski¹⁶, chose the space-time (x, ct) convention plotting $space=x$ in horizontal direction and $c \cdot time=ct$ in along vertical axis. Lightspeed factor c makes the temporal ct -axis have the same spatial units as the x -axis and so the 1-CW moves along 45° lines of constant phase. Each phasor is like a clock sitting in a 300THz laser beam defined by wave function $\Psi_{k,\omega}(x, t) = Ae^{i(kx-\omega t)}$ and its space and time derivatives. (General exponential derivative: $\frac{d}{dt}e^{rt} = re^{rt}$ follows from Eq.(4a).)

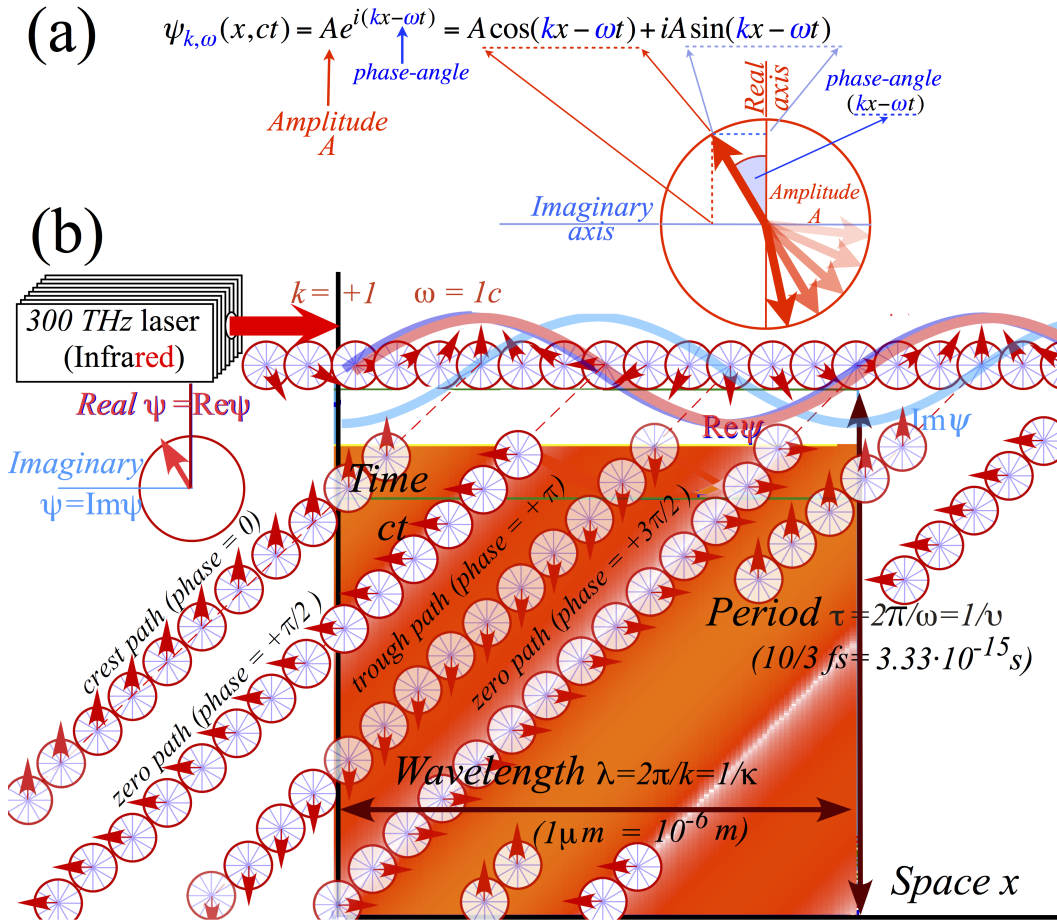


FIG. 4: (a) Single-phasor plot of wave-function at (x, ct) . (b) 1-CW Array of phasors at many (x, ct) -points.

Phasor plots in Fig. 4 are re-oriented by 90° in a non-conventional way so the real axis

points upward and the imaginary axis points to the left along beam-line. A $\Psi_{k\omega}$ pointing *up* corresponds to a real wave *crest* with phase angle $kx-\omega t = 0$, and where it points *down* corresponds to a real wave *trough* with phase angle $kx-\omega t = \pi$. In between are space-time points where $\text{Im-}\Psi_{k\omega}$ points *up* with phase angle $kx-\omega t = \pi/2$ or where $\text{Im-}\Psi_{k\omega}$ points *down* with phase angle $kx-\omega t = 3\pi/2$ for $\text{Im-}\Psi$ trough with phase angle $kx-\omega t = 3\pi/2$. These half- π tracks locate $(\text{Re}\Psi_{k\omega}=0)$ -lines such as the white line in lower right of Fig. 4(b). $(\text{Re}\Psi_{k\omega}=0)$ -lines mark (x, ct) grids in Sec. IV and help visualize relativity effects.

Space-time derivatives of phasor $\Psi_{k,\omega}(x, t) = Ae^{i(kx-\omega t)}$ sheds some light on its behavior.

$$\frac{\partial}{\partial x}\Psi_{k,\omega}(x, t) = \frac{\partial}{\partial x}Ae^{i(kx-\omega t)} = e^{i(kx-\omega t)} = -kA \sin(kx - \omega t) + ikA \cos(kx - \omega t) \quad (8a)$$

$$\frac{\partial}{\partial t}\Psi_{k,\omega}(x, t) = \frac{\partial}{\partial t}Ae^{i(kx-\omega t)} = -i\omega Ae^{i(kx-\omega t)} = \omega A \sin(kx - \omega t) - i\omega A \cos(kx - \omega t) \quad (8b)$$

(8b) shows imaginary part $\text{Im}\Psi_{k,\omega} = A \sin(kx - \omega t)$ multiplied by ω is real part of t -derivative $\frac{\partial}{\partial t}\Psi_{k,\omega}$. Note that wave imaginary part $\text{Im}\Psi$ in top of Fig. 4(b) is a quarter wavelength ahead of the real wave $\text{Re}\Psi$. This quite well matches an unfortunate mantra for US Stockholder-Driven corporations: *Imagination precedes Reality by exactly one Quarter!*

Needless to say, this rule does not always favor corporate research quality in the 21st century. Nevertheless, the concept of wave phase, indeed, *relative* phase, is an important key to understanding relativity, quantum mechanics, and dynamics of any oscillating or “wavy” system. If the relative phase between a pair of k_{AB} -coupled neighboring phasors is $\Delta\Phi = \Phi_A - \Phi_B$ then the rate of *A-to-B* energy or action transfer is proportional to the product of amplitudes $A \cdot B$ with coupling k_{AB} constant and $\sin \Delta\Phi$.

$$\text{Transfer } A\text{-to-}B \approx k_{AB} A \cdot B \cdot \sin \Delta\Phi$$

So if phasor A is *ahead* (that is *clockwise*) relative to phasor B, then A is feeding energy (or action) to B, and vice versa, if B is ahead of A then B is feeding A. In the beam phasor line of Fig. 4b each clock is ahead of the one to its right by $\Delta\Phi$ but behind the one to its left by the same amount $\Delta\Phi$. So as the clocks turn clockwise the wave will move left-to-right and with it, presumably, its energy or action. No phasor grows or shrinks as it passes on all that it gets. The actual speed of the wave is found by more elementary considerations of phase. Simply setting the phase equal to a constant (like 0 or $\pi/2$...in Fig. 4b) gives the equation for its path. $kx - \omega t = \text{const.} \Rightarrow x = \frac{\omega}{k}t + \frac{\text{const}}{k}$

The time coefficient $\frac{\omega}{k}$ is the 1-CW phase velocity that, in this case is that of light $\frac{\omega}{k}=c$. In the (x,ct) plot of Fig. 4b this makes 45° paths. Definitions of wave parameters like $\omega = 2\pi\nu$ and $k = 2\pi\kappa$ follows in Sec. III.

The concept of a 1-CW (that is a *Single-Continuous-Wave*) is greatly simplified here and in what follows. A CW-laser is standard jargon since the invention of the He-Ne laser in 1962. For our purposes of developing thought experiments we assume a perfect plane wave inside the beam such as is imagined in Fig. 4. The acronym CW can also mean *Coherent Wave* (elementary lasers are described by coherent states of photons) or *Colored Wave* (lasers are known for frequency or, if visible, *color* purity) or just plain *Cosine Wave* (that is the real part of the *Complex Wave* function $Ae^{i(kx-\omega t)}$.) This is to distinguish from a PW (that is a *Pulse-Wave* or *Packet-(of)-Waves* or *Particle-(like)-Wave*) that are made of many frequencies or colors combined to form localized pulses that act more like particles. Newton might have liked this kind of *corpuscle* if they had been available in 18th century laboratories. However, a laser CW would have given him “fits” as discussed in Sec. VI.

1. *A phasor clock has only one hand!*

While 1-CW phase can have great spectral purity and precision, the value of phase is only given modulo 2π . After each revolution by 2π the recording of time just starts over again. It is just a second-hand with no minute-hand or hour-hand (or week-hand, or-year-hand, etc.) to extend the range of a temporal record that space-time plots like Fig. 4 can provide. Evenson had to solve this in order to count 500-TeraHertz light waves and did so by producing harmonics and sub-harmonics using non-linearity of metal-insulator-metal diodes. Later work by Theodore Hensch and others involved PW lasers with “frequency-combs” of precisely spaced coherent Fourier components, essentially a clock with a thousand hands.

2. *At c the phasor clocks freeze!*

Fig. 4 can be viewed in some mind-bending ways. It is intended as a line of 20 phasor clocks attached to a CW laser with each turning at its $\omega=2\pi 300\text{THz}$ infrared frequency. Then each phase marches at the speed c of light through this line. Alternative extreme view has 20 frozen clocks being dragged past the laser at the speed c of light. (Actually we

would need about 20-thousand clocks so every pixel has a clock reading the correct value of *phase* $kx-\omega t$ assigned to the (x,ct) pixel.) Between the above two extremes are slower-moving-than- c clock-trains turning at a slower-than- ω angular frequency yet always leaving the same phase $kx-\omega t$ on each (x,ct) pixel! This bizarre property is due to *phase invariance*. [By the time you reach (23) in Sec. IV all this should become clearer.]

3. *What's waving? (... and what's not?)*

The most tenuous questions of light wave analysis lie in their axiomatic underpinnings. More simply, what is it that is waving up and down in the “real-part” $\text{Re}\Psi$ and/or in its t -derivative (scaled by angular frequency ω) that is the “imaginary-part” $\text{Im}\Psi$ plotted as sine-curves on the laser beam in Fig. 4?

The short answer is that $\text{Re}\Psi$ represents the electric field or **E**-field, and $\text{Im}\Psi$ represents $\dot{\mathbf{E}}/\omega$, the time derivative $\dot{\mathbf{E}}$ of \mathbf{E} scaled down by ω so the two form a quadrant of a rotating circular phasor Ψ . That conforms to Maxwell’s physics of **vector** fields transverse to the beam direction \mathbf{k} of wave propagation. Since it is impractical to draw **E**-vectors waving in and out of the page, we lay them onto the page going up and down in the direction of the time axis, and not where they should be.

This kind of plot does not spoil accuracy of later figures (Fig. 9 and Fig. 10) since they will be tracing the *zeros* or *nodes* of $\text{Re}\Psi$ waves at precisely the time instants that they occur. But, it does limit the display to the most elementary linear/plane polarized light wave. Nevertheless, this simplified stand-in for a real laser is enough to derive a wave-based formulation of elementary relativity and quantum theory.

Perhaps, it would be nice if light could be a 3-dimensional scalar wave such as the $\Psi(x,y,z,t)$ that appear in many textbooks, but those are not the optical cards that Nature has dealt us. Incidentally, that scalar view of Ψ is also an oversimplified stand-in, as well.

Real IR-to-UV laser beams have less than micron wavelengths traveling through beams that have more than a millimeter-wide Gaussian profile. That provides an ample region that is well described by a plane wave function $\Psi_{\omega,\mathbf{k}}(x,t)=Ae^{i(kx-\omega t)}$ if we avoid considering the complexity of possible polarization vector states normal to the beam axis \mathbf{k} .

So the wave’s amplitude oscillates sinusoidally as a function of space-time independent variables (x,t) . This happens while inverse-space and inverse-time wave parameters, such

as ω and \mathbf{k} described in following Sect. [III](#), do not “wave” at all. Instead they vary or “Doppler-shift” according to the velocity of source and observer but stay precisely fixed if that velocity is constant. Understanding Doppler shift is an important key to understanding relativity and quantum theory, and this is where that begins.

It might be worthwhile before beginning the next few sections to compare the trigonometry map of [Fig.3](#) to a map some pages ahead of relativistic physics in [Fig.19](#) or [Fig.25](#) that maps *relawavity* of relativistic quantum mechanics. These will be developed in the following sections. (Use click-linking of page and equation numbers.)

III. SPACE-TIME VS PER-SPACE-TIME: FOURIER'S KEYBOARD OF THE GODS

Physics students have to learn proper names for most physical units such as a *Joule* of energy, a *Newton* of force, or a *Watt* of power. Surprisingly there are no such names attached to most fundamental units, those of time (second) and space (meter). (One might argue for renaming the meter an *Evenson* after he helped redefine it. Or one could apply the name *Trump* to the 4.1-light year distance to the star α -Proxima, our nearest possibly habitable refuge from the former.)

Still, there are some more or less well established proper names for units of *per-space-time*. Most well known is the *Hertz* unit ($1 \text{ per second} = 1s^{-1}$) named after Heinrich *Hertz* (1857-1894), an inventor of radio transmission. Less well known among atomic and molecular spectroscopists is the *Kayser* unit of ($1 \text{ per centimeter} = 1cm^{-1}$) named after Heinrich *Kayser* (1853-1940) known for analyzing solar spectra. They were born only four years apart, but Hertz only lived 37 years while Kayser lived to 87.

These pioneers deserve a coordinate frame to compliment the Einstein-Minkowski (\mathbf{x}, ct)-frame. (Herman Minkowski¹⁷ (1864-1909) also died young at 45 shortly after failing to interest Einstein in his space-time plot. This may be due to Prof. Herman's calling Albert a "lazy dog" or another pejorative.) Fig. 5 relates a Kayser-Hertz (per-space κ , per-time ν) plot (on the left) to the usual (space x , time t) plot (on the right) that might be used to track water waves or sound waves. The primary objective of Fig. 5 is to review standard wave terms, notation, and velocity formulae.

A single Kayser-Hertz point or vector ($\kappa \frac{\text{(waves)}}{\text{meter}}, \nu \frac{\text{(waves)}}{\text{second}}$) produces one continuous wave (1-CW) that fills space-time with a wave having (wavelength $\lambda \frac{\text{meters}}{\text{(wave)}}$, wave-period $\tau \frac{\text{seconds}}{\text{(wave)}}$). Fig. 5 has wavenumber $\kappa = \frac{3}{2}$ waves per meter and wave-frequency $\nu = \frac{4}{5}$ waves per second in per-space-time. That is wavelength $\lambda = \frac{2}{3}$ meters per wave as well as wave-period $\tau = \frac{5}{4}$ seconds per wave in space-time. Kayser-Hertz space is better known as Fourier space where one imagines as a "control-panel" or "key-board" to produce waves in space-time. The name "Keyboard of the Gods" is coined to suggest that mortal musicians cannot control both frequency $\nu = 1/\tau$ and wavelength λ or wavenumber $\kappa = 1/\lambda$.

The idea of mapping an entire space-time wave like the 300THz wave in Fig. 4 from a single Kaiser-Hertz point ($\kappa \frac{\text{(waves)}}{\text{meter}}, \nu \frac{\text{(waves)}}{\text{second}}$) of Fourier space requires a stretch of imag-

ination. A wavelength or period in Fig. 4 involves a 2π phasor revolution as defined by wavefunction $\Psi_{k,\omega}(x,t) = Ae^{i(kx-\omega t)}$ whose parameters are *angular frequency* $\omega=2\pi v$ and *angular wavenumber* $k=2\pi \kappa$ or *wavevector* $\mathbf{k}=2\pi \boldsymbol{\kappa}$.

The letter k (or greek "kappa" κ) honors Kaiser, but Hertz is not so noticed. Instead the greek "nu" ν for number is used. Since ν is easily confused with velocity "v" we will use "omicron" (v) for number v of waves per second (frequency). Conventional Greek- l or "lambda" λ denotes wave-Length and Greek- t or "tau" τ stands for wave-Time period τ , again without a proper name.

Ideal Fourier models fix the $(k, \omega)=2\pi(\kappa, v)$ points in per-space-per-time. That determines wave velocity v or u in space-time. Fig. 5 lower right corner has a space/time formula for u as slope of wave paths.

$$\frac{\text{distance}}{\text{time}} = \frac{\text{wavelength}}{\text{wave period}} = \frac{\lambda}{\tau} = \frac{1/\kappa}{1/v} = \lambda v = \frac{v}{\kappa} = \frac{\omega}{k} = \frac{2/3}{5/4} = \frac{8}{15} = u \quad (9)$$

This often called *phase velocity* since it is the velocity of any particular phase, say zero phase: $0=kx-\omega t$. Solving this gives velocity or slope equation $x = \frac{\omega}{k}t \equiv u$ that agrees with (9) and has space-time slope relative to the vertical (time t or *period* τ) axis in Fig. 5. (It is a less familiar kind of slope.)

A vertical velocity vector \mathbf{v} in space-time (x,t) indicates a zero wave speed while a horizontal vector \mathbf{v} indicates infinite speed $v=\infty$. This inverts in per-space-per-time (k, ω) of Fig. 5 (left) where velocity is indicated by slope of \mathbf{v} relative to the horizontal (wavenumber $k=2\pi\kappa$) axis. This is a more familiar kind of slope. A horizontal \mathbf{v} has zero slope and indicates zero speed while vertical velocity (V) is ∞ . Soon there will be shown light wave examples of both these extremes!

A. c-Scaled wave graphs and Doppler shifts

Wave velocity $v=\frac{8}{15}$ is plotted with slope $\frac{8}{15}$ in per-space-per-time on lefthand side of Fig. 5 but the space-time slope on the righthand side has inverse $\frac{15}{8}$ slope relative to horizontal. If light speed is a super constant $c=2.99792458 \cdot 10^8 \text{ms}^{-1}$ it is convenient to rescale (9) to make c be *unit slope* in either plot.

$$c = \frac{\lambda}{\tau} = \frac{v}{\kappa} = \frac{\omega}{k} \text{ rescaled by } c \text{ to: } 1 = \frac{\lambda}{c\tau} = \frac{v}{c\kappa} = \frac{\omega}{ck} \quad (10)$$

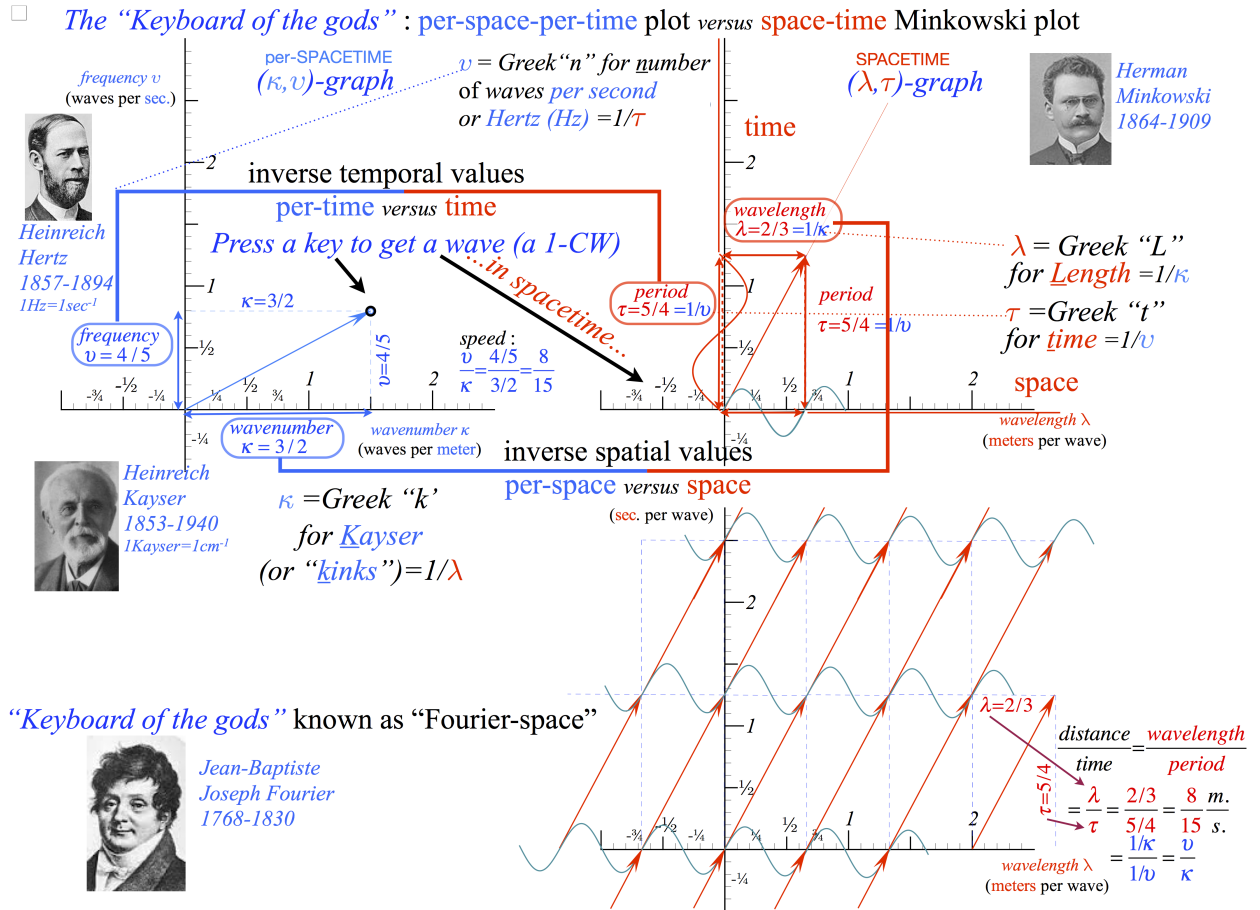


FIG. 5: Comparing a wave point in Kaiser-Hertz per-space-time to its Minkowski space-time view of resulting wave.

This was done in space-time (x, ct) -plot of Fig. 4 and now for per-space-time plot $(ck, \omega) = 2\pi(ck, \nu)$ on the lefthand side of Fig. 6 with its corresponding (x, ct) -space-time plot on the righthand side. Frequency units of both per-space-time axes are the same $\nu_A = 600\text{THz}$ units. The vertical ν -axis is directly so, but the horizontal ck -axis is indirectly so and without the c -factor, the κ unit is $\kappa_A = 2 \cdot 10^6$ waves per meter.

The vertical time ct_A axis of the $(x, ct) = (\lambda, c\tau)$ graph has the same $\frac{1}{2}$ -micron units of length that the horizontal space x_A -axis has. Without the c -scale factor the unit of time is $\tau_A = \frac{5}{3} fs = 1.667 \cdot 10^{-15} \text{ sec.}$ The units are assigned to a full blue-green 600THz wave made of two half waves, 1-peak and 1-trough separated by two real wave zeros $\sin 0$ and $\sin \pi$. When $\sin 0$ paths hit the vertical time axis a “hit” is recorded on the time axis in Fig. 6 at time units $\dots, -2, -1, 0, +1, +2, \dots$ each due to a period $\tau_A = \frac{5}{3} fs$.

Now consider the more rapid succession of “hits” for a line sloping into the negative direction so it has head-on collisions with the $\sin 0$ paths at time units $\dots -\frac{9}{4}, -\frac{6}{4}, -\frac{3}{4}, 0, \frac{3}{4}, \frac{6}{4}, \frac{9}{4}, \dots$ corresponding to a Doppler *blue-shift factor* of $\frac{4}{3}$. Then 600THz shifts to $\frac{4}{3}600 = 800\text{THz}$. A less rapid frequency of “hits” occurs along the path moving to the right and having rear-end collisions at $\dots -\frac{9}{2}, -\frac{6}{2}, -\frac{3}{2}, 0, \frac{3}{2}, \frac{6}{2}, \frac{9}{2}, \dots$ corresponding to a Doppler *red-shift factor* of $\frac{2}{3}$. Then 600THz shifts to $\frac{2}{3}600 = 400\text{THz}$.

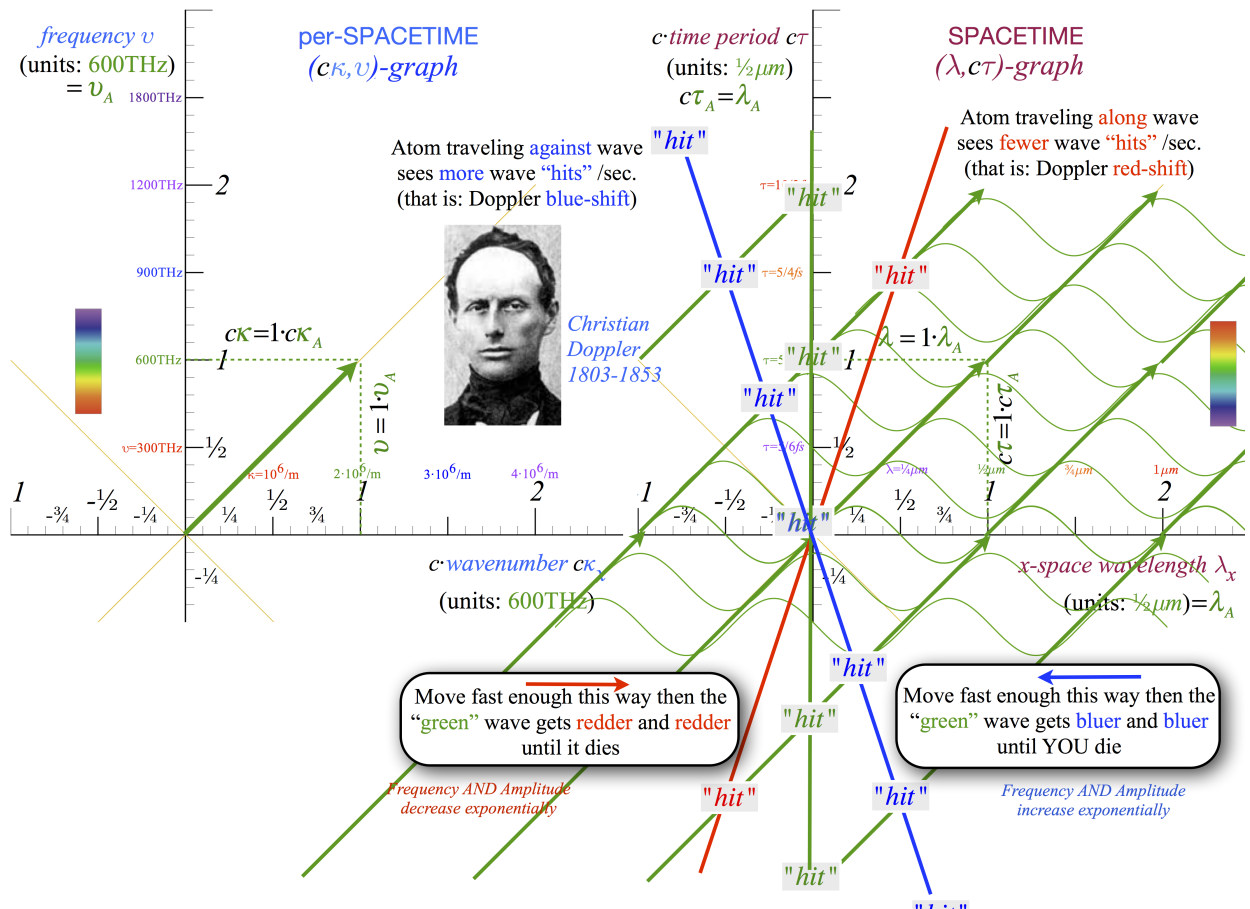


FIG. 6: 600THz plots c -scaled in per-space-time ($c\kappa, v$) and space-time (x, ct).

As will be shown, Doppler blue shift is limited only by infinite v and a red shift only by zero v in spite of the speed limit c for all hapless mortal travelers. If you go faster to the right (along light beam flow) the light becomes redder and weaker until it disappears. If you go faster to the left (against light beam flow) the light becomes bluer and stronger until *you* disappear! (Or die of γ -ray poisoning.)

B. Evenson's axiom and Doppler shifts

It has become traditional in quantum optics to imagine beams between a point B and a point A to be manned (or woman-ed) by live characters named Bob and Alice, respectively. Our Doppler thought experiment begins with Bob sitting stationary relative to Alice but millions of kilometers to the East of her (far right of Fig. 7) with Alice's laser shining on Bob. Unbeknownst to Bob, Alice is able to tune the laser on her spaceship and plans to do so as she accelerates toward Bob. Alice has cleverly programmed the laser to tune its frequency down with each increase of her velocity so Bob continues to see an unchanged 600 THz reading on his receiver-spectrometer. If Alice and Bob have a communication channel like a cell phone, Alice will also have to detune her end of that channel appropriately in order to not make Bob suspicious. (Bob assumes Alice is maintaining her stay-at-home role.)

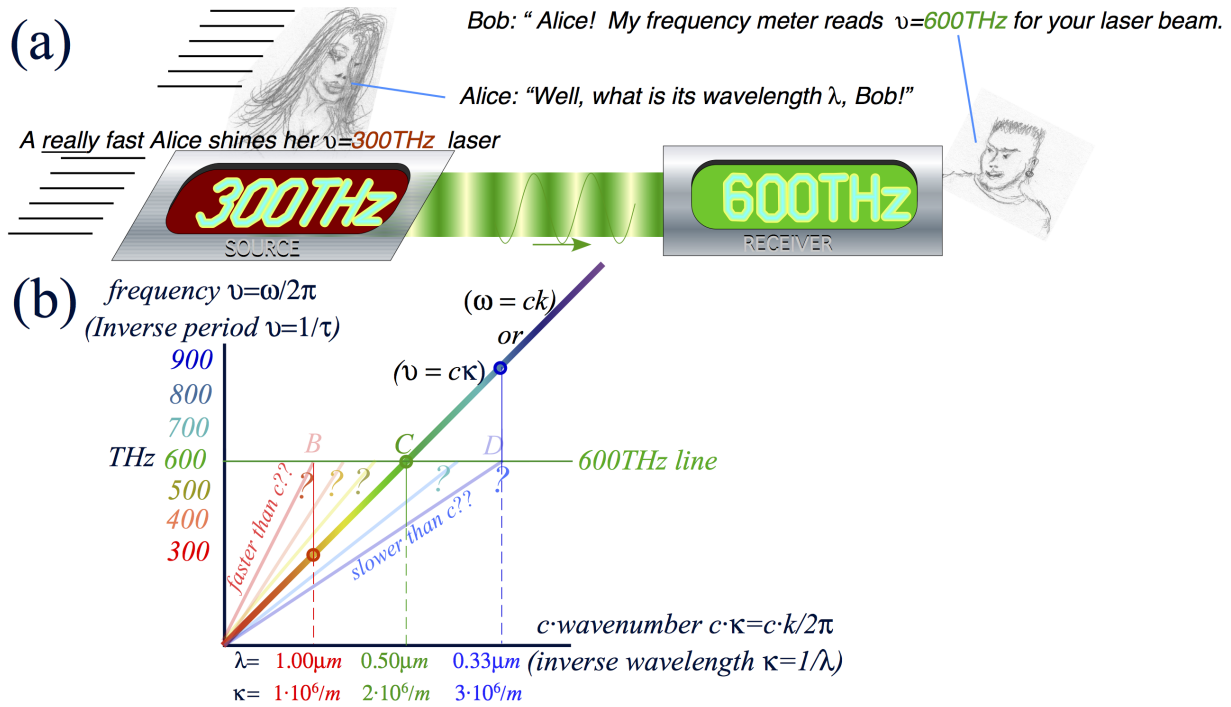


FIG. 7: Alice's 300THz laser approaches Bob. (a) Bob sees $\nu=600\text{THz}$. (b) What $\lambda=1/\kappa$ does Bob measure?

Now suppose Alice pauses her acceleration at a velocity corresponding to an octave Doppler blue factor of $b=2$, that is, while Bob thinks he is still receiving her steady blue-green 600 THz laser beam, she has actually down-tuned her laser to an infrared 300 THz as

in Fig. 7a. To check in with Bob, Alice must tune her phone receiver up by factor of 2 and her phone transmitter down by a factor of 2, just like her laser. (Tune-up-or-down by 2 is due to time reversal symmetry as explained below.)

Always the trickster, Alice asks Bob if he notices anything different about her laser beam. Bob replies, “It’s still your beautiful blue-green and reads 600 THz to 18 digits.” Alice says, “Okay, you’ve checked your frequency (ν)-meter, but what is your wavelength (λ)-measurement?”

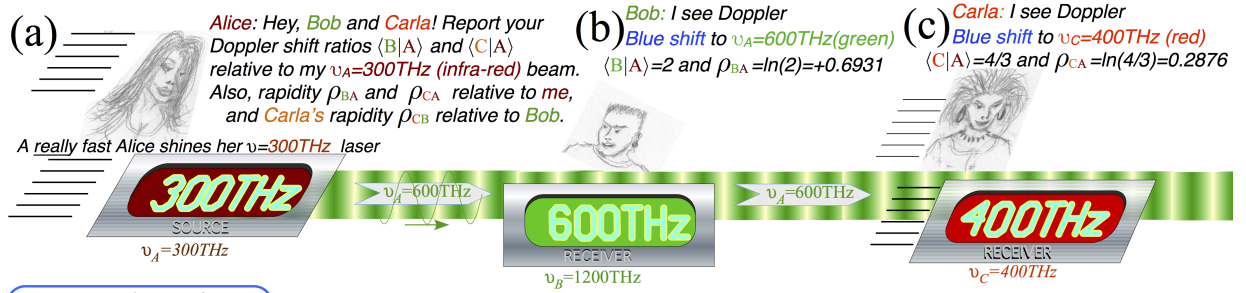
Alice’s leading question is a crucial one for relativity and quantum theory. She is asking if Bob is receiving some ‘phony’ kind of blue-green 600 THz, in this case, one that was produced by an infrared 300 THz laser moving very rapidly toward Bob. And, more generally, one may ask, “How many kinds of ‘phony’ blue-green, or of any other color or frequency, are possible in the vacuum of the universe?” One set of possibilities lies on the 600THz line of per-space-time ($c\kappa, \nu$) plot in center of Fig. 7b and includes B ($\lambda=1\text{micron}$ or $\kappa=1\cdot 10^6 m^{-1}$) thru C ($\lambda=\frac{1}{2}\text{micron}$ or $\kappa=2\cdot 10^6 m^{-1}$) to D ($\lambda=\frac{1}{3}\text{micron}$ or $\kappa=3\cdot 10^6 m^{-1}$). But, years of spectroscopy rule out ‘phony’ 600THz blue-green that do not have wavelength $\lambda=\frac{1}{2}\text{micron}$. The only choice in Fig. 7b is C and only possible 600THz light *speed* is $c = \frac{\nu}{\kappa} = \frac{600\cdot 10^{12}}{2\cdot 10^6} = 3\cdot 10^8 m\cdot s^{-1}$.

Alice could adjust her ship-and-laser to give any frequency to Bobs frequency meter. So any light Bob sees must fall on the 45° line of the ($c\kappa, \nu$) plot in Fig. 7b. This verifies Evenson’s Axiom requiring all 1-CW colors to march in lock-step at speed c .

A ($c\kappa, \nu$) plot is also called a *dispersion* plot. Points lying below the 45° line ($\nu=c\kappa$) belong to waves *slower* than vacuo light ($\nu/\kappa < c$). Those above are faster than c ($\nu/\kappa > c$). A waveform composed of sub or super luminal speeds would *disperse*, that is, super luminal components would outrun the sub luminal ones and thereby garble its initial waveform and information therein. Even a tiny frequency variation of speed c would give totally garbled light from galaxies millions (or billions!) of light-years away. (Goodbye Hubble images!)

C. Rapidity and its Doppler shift arithmetic

Thought experiments involving Doppler effects of relativistic quantum optics begs for a third member, Carla, on the SR optics team of Bob and Alice. Fig. 8 expands the Fig. 7 view in Bob’s frame with Alice approaching so Bob sees her infrared 300Thz source Doppler blue-shifted to green 600Thz. Carla is moving to the right more slowly than Alice so she also



Doppler ratio:

$$\langle R|S \rangle = \frac{v_{RECEIVER}}{v_{SOURCE}}$$

$$\rho_{RS} = \ln \langle R|S \rangle$$

or:

$$\langle R|S \rangle = e^{\rho_{RS}} = e^{-\rho_{SR}}$$

Definition of Rapidity ρ_{RS}

Bob-Alice Doppler ratio:

$$\langle B|A \rangle = \frac{v_B}{v_A} = \frac{600}{300} = 2$$

Bob-Alice rapidity:

$$\rho_{BA} = \ln \langle B|A \rangle = \ln \frac{2}{1} = 0.6931$$

$$\rho_{AB} = \ln \langle A|B \rangle = \ln \frac{1}{2} = -0.6931 = -\rho_{BA}$$

Carla-Alice Doppler ratio:

$$\langle C|A \rangle = \frac{v_C}{v_A} = \frac{400}{300} = \frac{4}{3}$$

Carla-Alice rapidity:

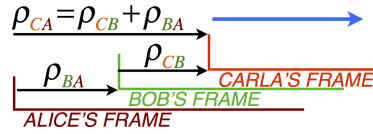
$$\rho_{CA} = \ln \langle C|A \rangle = \ln \frac{4}{3} = 0.2876$$

Galileo Galilei



1564-1642

Galileo's Revenge (part 1)
Rapidity adds just like Galilean velocity



Carla-Bob Doppler ratio:

$$\langle C|B \rangle = \frac{v_C}{v_B} = \frac{v_C}{v_A} \frac{v_A}{v_B} = \langle C|A \rangle \langle A|B \rangle = \frac{4}{3} \frac{1}{2} = \frac{2}{3}$$

Carla-Bob rapidity:

$$e^{\rho_{CB}} = e^{\rho_{CA}} e^{\rho_{AB}} = e^{\rho_{CA} + \rho_{AB}}$$

$$\rho_{CB} = \rho_{CA} + \rho_{AB} = 0.2876 - 0.6931 = -0.4055$$

$$= \ln \frac{4}{3} + \ln \frac{1}{2} = \ln \frac{2}{3}$$

FIG. 8: Doppler $\langle R|S \rangle$ and Rapidity ρ_{RS} (a) Alice's source and basic definitions. (b-c)

Example of rapidity addition

sees Alice's 300THz Doppler blue-shifted but only to red 400THz. A cartoon notation for speed shows v -meter&reader leaning into their direction of motion and trailing "contrail" lines. The speeds imagined here are truly enormous. It is later shown that Bob's Doppler shift of Alice's 300THz to his 600THz means she is approaching him at $\frac{3}{5}c$. (At that speed she could circumnavigate the Earth more than 4 times per second!)

In Fig. 8a Doppler shift ratio is defined by $\langle R|S \rangle = v_{RECEIVER}/v_{SOURCE}$. (Think R over S : $\langle R/S \rangle$.) Also given is a definition of *rapidity* ρ_{RS} as the natural logarithm of Doppler ratio ($\rho_{RS} = \ln \langle R|S \rangle$). The ρ_{RS} definition simplifies arithmetic of high-speed velocity addition where, as shown later by (6), velocity u_{RS} of R relative to S (in units of c) is hyper-tangent $\tanh \rho_{RS}$ of their relative rapidity ρ_{RS} . (Here: $\tanh(\ln 2) = \frac{3}{5}$.)

Fig. 8(b-c) shows how rapidity ρ_{CB} of Carla relative to Bob is the sum of rapidity ρ_{CA}

of Carla relative to Alice and the rapidity ρ_{AB} of Alice relative to Bob. Graph of equivalent sum $\rho_{CA} = \rho_{CB} + \rho_{BA}$ is in lower left of Fig. 8 and resembles Galilean velocity addition. However, ρ -sums are exact while Galileo's V-sums are approximate and fail badly at high speeds. ρ -sums have \pm sign rules: a (+)-sign for approach rapidity (blue shift) and (-)-sign for withdrawal rapidity (red shift). (Think of arrival of a friend as positive ρ while departure is negative ρ .) Note *Doppler-rule*: $\langle A|B \rangle = 1/\langle B|A \rangle$ and ρ -rule: $\rho_{AB} = -\rho_{BA}$ in Fig. 8.

IV. WAVE-ZERO 2-CW COORDINATE GRIDS

Optical single-Continuous Waves (1-CW) obey Evenson's Axiom and march lockstep en-vacuo at speed c with any and all other 1-CW going in a given direction $\hat{\mathbf{k}}$. Observer's motion along $\hat{\mathbf{k}}$ cannot alter 1-CW speed c , but will affect a 1^{st} -order Doppler shift $e^{\pm\rho}$ for both frequency $\omega = 2\pi\nu$ and wave-vector $\mathbf{k} = 2\pi\boldsymbol{\kappa}$ in each 1-CW per-space-time vector $K = (c\mathbf{k}, \omega)$. Following Fig. 8, observer motion along $\hat{\mathbf{k}}$ will shorten K by red-shift factor $e^{-\rho}$ while motion against $\hat{\mathbf{k}}$ will lengthen K by blue-shift factor $e^{+\rho}$.

$$K \xrightarrow[\text{red - shift}]{} K' = e^{-\rho}K = (c\mathbf{k}e^{-\rho}, \omega e^{-\rho}) \quad (11a)$$

$$K \xrightarrow[\text{blue - shift}]{} K' = e^{+\rho}K = (c\mathbf{k}e^{+\rho}, \omega e^{+\rho}) \quad (11b)$$

Fig. 9 has (x, ct) -plots of a head-on collision between wave e^{iR} moving right from Alice in Fig. 9a and wave e^{iL} moving left from Carla in Fig. 9c. It makes a wave-sum $e^{iR} + e^{iL}$ for Bob shown in Fig. 9b. Alice's wave has phase $R=kx-\omega t$ of a 1-CW moving rightward according to $x = \frac{\omega}{k}t + \text{constant}$ at speed $\frac{\omega}{k} = c$. Carla's wave has phase $L=-kx-\omega t$ of a 1-CW moving leftward according to $x = -\frac{\omega}{k}t + \text{constant}$. (Carla's wave has a $(-)k$.)

Fig. 9 has (ck, ω) -plots of a pair of K -vectors, \mathbf{R} from Alice and \mathbf{L} from Carla, that make vectors $\mathbf{P} = \frac{1}{2}(\mathbf{R} + \mathbf{L})$ and $\mathbf{G} = \frac{1}{2}(\mathbf{R} - \mathbf{L})$ describing 2-Continuous Wave (2-CW) structure Bob sees in Fig. 9b.

Zeros of the real part of the 2-CW seen in Fig. 9b trace a space-time coordinate grid of white lines. In elementary algebra, zeros are found by factoring. Plane wave-sum $e^{iR} + e^{iL}$ is factored as follows.

$$e^{iR} + e^{iL} = e^{i\frac{R+L}{2}} \left(e^{i\frac{R-L}{2}} + e^{-i\frac{R-L}{2}} \right) = 2e^{i\frac{R+L}{2}} \cos \frac{R-L}{2} = 2e^{-i\omega t} \cos kx \quad (12)$$

where: $R = kx - \omega t$ and: $L = -kx - \omega t$

Fig. 9b plots Real part of phase factor $e^{-i\omega t} = \cos \omega t - i \sin \omega t$ in dark blue and the Imaginary part in cyan. $e^{-i\omega t}$ is x -independent but is amplitude-modulated by Group factor $2\cos kx$, a time-independent 2-sided envelope. Group envelope zeros trace vertical coordinate lines in Fig. 9b and have zero x -velocity. This corresponds to a Group \mathbf{G} -vector with zero slope in per-space-time plot of Fig. 9d. The Phase \mathbf{P} -vector in Fig. 9d has infinite slope. This indicates an infinite velocity for phase zeros.¹⁸ They exhibit this every $\frac{1}{2}$ -period in (x, ct) plot Fig. 9b. Bob sees two "instantons" zip by in each period of $\tau_{\text{phase}} = \frac{5}{3} \cdot 10^{-15} \text{s} = \frac{5}{3} \text{fs}$.

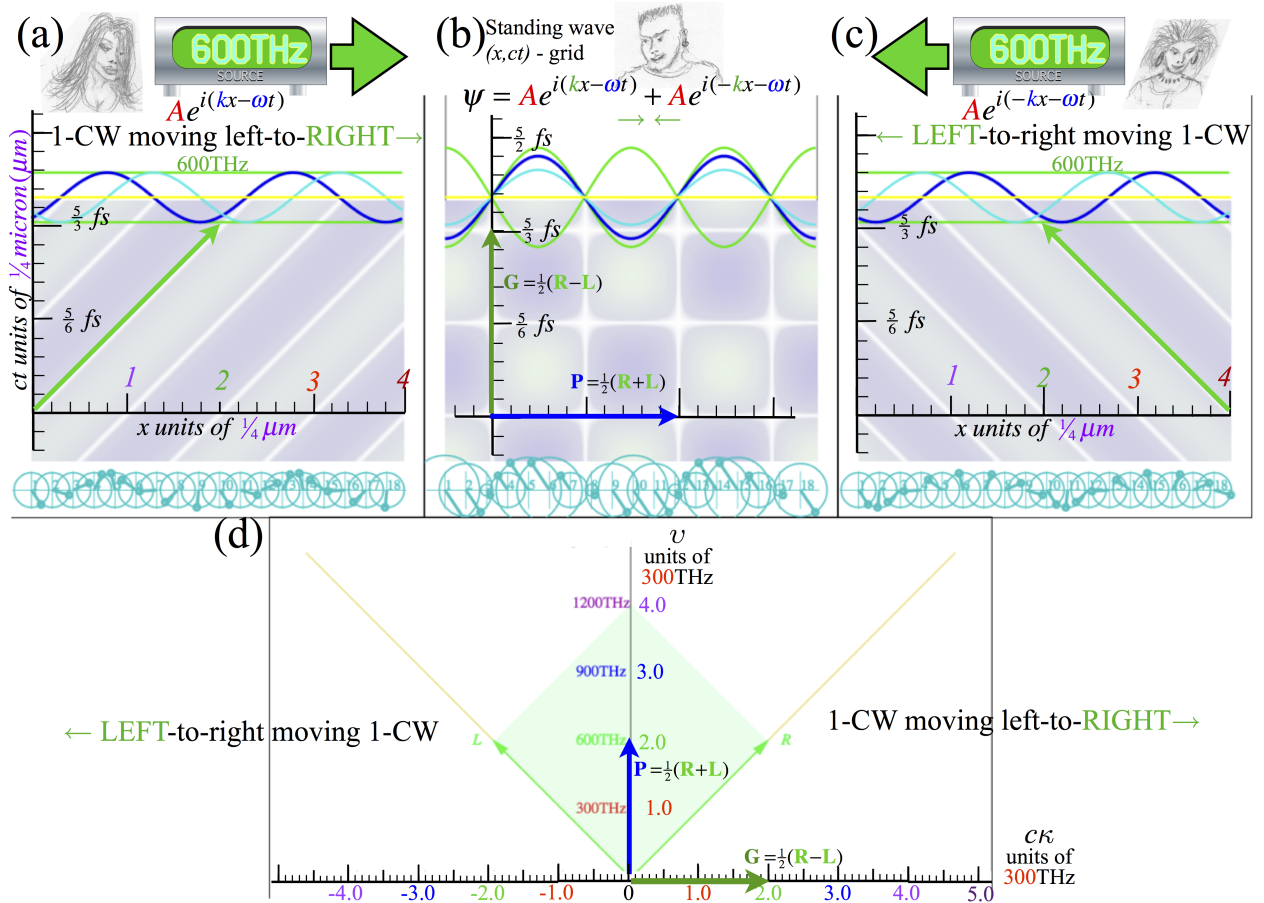


FIG. 9: (x, ct) wave plots (a) Alice's **R**-CW (b) Bob's Group **G** over Phase **P** (c) Carla's **L**-CW (d) (ck, v) plots of **P** over **G**

BohrIt Web Simulation: *Unshifted MultiPanel* ?

Bob's (ck, v) plot in Fig. 9b is what we call a "Relativity Baseball-Diamond" (RBD). Origin is *home-plate*, the **R**-vector is the *1st-baseline*, the **L**-vector is the *3rd-baseline*, **R**+**L** points to *2nd-base*, and Phase **P** = $\frac{1}{2}(\mathbf{R} + \mathbf{L})$ points to *Pitcher's mound*, and Group **G** = $\frac{1}{2}(\mathbf{R} - \mathbf{L})$ points to center of a *Grandstand*.

A sheared RBD is in Fig. 10d. It has a Doppler blue-shift $e^{\rho_{BA}} = 2$ of Alice's light to 1200THz (now *1st-baseline* is twice as long) combined with a Doppler red-shift $e^{-\rho_{BA}} = \frac{1}{2}$ of Carla's light to 300THz (now *3rd-baseline* is half as long). (ck, v) -plot geometry in Fig. 9d or Fig. 10d is reflected (literally, thru the diagonal) in the (x, ct) -plot in Fig. 9b or Fig. 10b, respectively. This is powerful! It's a ruler&compass derivation of Alice and Carla space-time (x', ct') and per-space-time (ck', v') coordinates as seen by Bob speeding toward Alice

(her beam blue-shifted to 1200Hz) and away from Carla (red shifted to 300THz) . Alice's

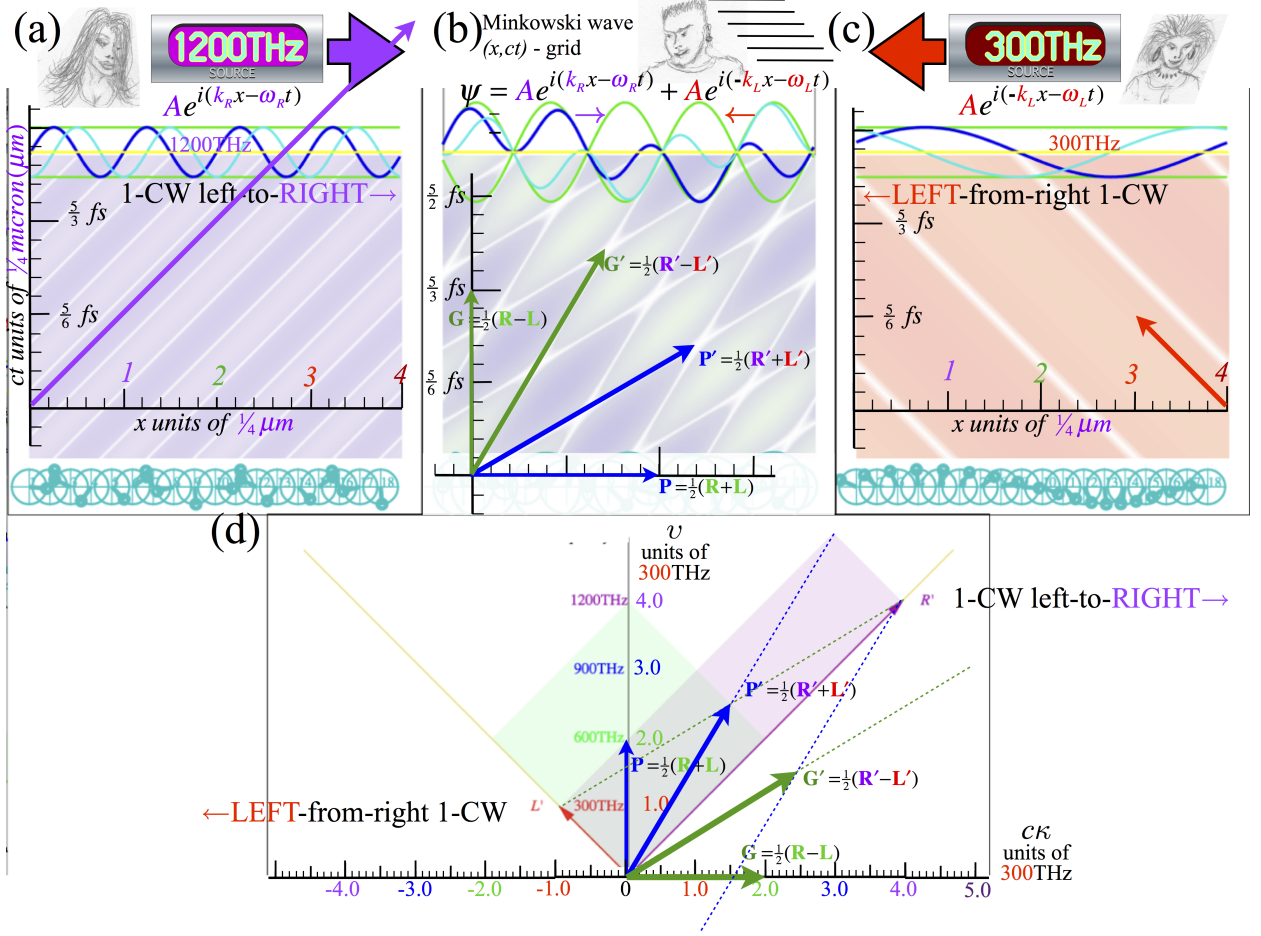


FIG. 10: (x, ct) wave plots (a) Alice's **R**-CW (b) Bob's Group **G'** over Phase **P'** (c) Carla's **L**-CW (d) (ck, v) plots of **P'** over **G'**

BohrIt Web Simulation: *Doppler Shifted MultiPanel* ?

rightward blue-shifted wave $e^{iR'}$ plus Carla's leftward red-shifted wave $e^{iL'}$ has factors like (12).

$$\Psi'(x, t) = e^{iR'} + e^{iL'} = e^{i\frac{R'+L'}{2}} (e^{i\frac{R'-L'}{2}} + e^{-i\frac{R'-L'}{2}}) = e^{i\frac{R'+L'}{2}} 2 \cos \frac{R'-L'}{2} = \Psi'_{phase} \Psi'_{group} \quad (13)$$

Zeros of Real parts of wave factors $\Psi_{phase} \Psi_{group}$ in (12) make a square "rest-frame" lattice in Fig. 9b.

$$0 = \text{Re } \Psi_{phase} = \text{Re } e^{i\frac{R+L}{2}} = \text{Re } e^{-i\omega_A t} = \cos \omega_A t \quad (14a)$$

define horizontal time - lines: $t = \pm \frac{\pi}{2\omega_A}, \pm \frac{3\pi}{2\omega_A} \dots$

$$0 = \text{Re } \Psi_{group} = \text{Re } e^{i\frac{R-L}{2}} = \text{Re } e^{-ik_A x} = \cos k_A x \quad (14b)$$

$$\text{define vertical } x \text{ - space - lines: } x = \pm \frac{\pi}{2k_A}, \pm \frac{3\pi}{2k_A} \dots \text{ (b)}$$

They are (x, ct) coordinate lines marking half-periods $\frac{\tau_A}{2} = \frac{\pi}{\omega_A} = \frac{1}{2\nu_A}$ and half-wavelengths $\frac{\lambda_A}{2} = \frac{\pi}{k_A} = \frac{1}{2\kappa_A}$ that lie mid-way between crests (lighter regions) and troughs (darker regions) in Fig. 9b. Its square lattice turns into a “moving-frame” rhombus lattice of Fig. 10b when the Doppler parameter ρ_{AB} is non-zero. Then Bob sees blue-shift $\langle B|A \rangle v_A = v_A e^{\rho_{AB}}$ going toward Alice’s v_A -laser source and red-shift $\langle B|C \rangle v_C = e^{-\rho_{BC}} v_C$ as he goes away from Carla’s v_C -laser. Time inversion flips roles of receiver-source pairs. That flips ratio $\langle R|S \rangle = v_{RECEIVER}/v_{SOURCE} \rightarrow \langle S|R \rangle$ while changing the \pm sign of $\rho_{AB} = -\rho_{BA}$ and relative velocity $u_{AB} = -u_{BA}$.

A single rhombus in “reciprocal” $(c\kappa, \nu)$ -per-space-time of Fig. 10d has geometry similar to every rhombus cell of (x, ct) wave zeros in Fig. 10b. This geometry also relates ρ_{AB} to u_{AB} as shown below.

A. Geometry of Minkowski phase and group wave-lattices

Bob sees Alice’s $v_A=600\text{THz}$ laser beam blue-shifted by $\langle B|A \rangle = e^{\rho_{BA}} = 2 = b_{BA}$ as he approaches her. So a vector $\mathbf{R}' = \begin{pmatrix} v \\ c\kappa \end{pmatrix}$ that Bob plots for Alice is her original vector $\mathbf{R} = v_A \begin{pmatrix} 1 \\ +1 \end{pmatrix}$ *doubled* in length by the blue shift to $\mathbf{R}' = b_{BA} v_A \begin{pmatrix} 1 \\ +1 \end{pmatrix} = v_A \begin{pmatrix} 2 \\ +2 \end{pmatrix}$ along the 1st baseline (45°) in Fig. 10d. This runs head-on into Carla’s $v_C=600\text{THz}$ laser beam that is red-shifted by $\langle B|C \rangle = e^{-\rho_{BC}} = \frac{1}{2} = r_{BC}$ as Bob runs away from Carla. So her original vector $\mathbf{L} = v_A \begin{pmatrix} 1 \\ -1 \end{pmatrix}$ is *halved* in length to $\mathbf{L}' = r_{BC} v_A \begin{pmatrix} 1 \\ -1 \end{pmatrix} = v_A \begin{pmatrix} \frac{1}{2} \\ -\frac{1}{2} \end{pmatrix}$ on 3rd baseline (-45°). (Evenson’s axiom confines 1-CW light to 1st-baseline for $+\kappa$ and to 3rd-baseline for $-\kappa$.)

Alice’s right-going vector \mathbf{R} (Bob’s view \mathbf{R}') and Carla’s left-going vector \mathbf{L} (Bob’s view \mathbf{L}') go according to (12) or (13) into a half-sum $\mathbf{P} = \frac{1}{2}(\mathbf{R} + \mathbf{L})$ (Bob’s view $\mathbf{P}' = \frac{1}{2}(\mathbf{R}' + \mathbf{L}')$) for phase wave factor.

$$\mathbf{P}' = \begin{pmatrix} v'_{phase} \\ c\kappa'_{phase} \end{pmatrix} = \frac{1}{2}(\mathbf{R}' + \mathbf{L}') = v_A \begin{pmatrix} \frac{1}{2}(e^\rho + e^{-\rho}) \\ \frac{1}{2}(e^\rho - e^{-\rho}) \end{pmatrix} = v_A \begin{pmatrix} \cosh \rho \\ \sinh \rho \end{pmatrix} = v_A \begin{pmatrix} \frac{5}{4} \\ \frac{3}{4} \end{pmatrix} \quad \text{or: } v_A \begin{pmatrix} 1 \\ 0 \end{pmatrix} \quad (15a)$$

Bob's View *Alice's View*

Group wave factor of (12) or (13) calls for a half-difference $\mathbf{G} = \frac{1}{2}(\mathbf{R} - \mathbf{L})$

$$\mathbf{G}' = \begin{pmatrix} v'_{group} \\ c\kappa'_{group} \end{pmatrix} = \frac{1}{2}(\mathbf{R}' - \mathbf{L}') = v_A \begin{pmatrix} \frac{1}{2}(e^\rho - e^{-\rho}) \\ \frac{1}{2}(e^\rho + e^{-\rho}) \end{pmatrix} = v_A \begin{pmatrix} \sinh \rho \\ \cosh \rho \end{pmatrix} = v_A \begin{pmatrix} \frac{3}{4} \\ \frac{5}{4} \end{pmatrix} \quad \text{or: } v_A \begin{pmatrix} 0 \\ 1 \end{pmatrix} \quad (15b)$$

Bob's View *Alice's View*

Slope of Bob’s group vector \mathbf{G}' in $(c\kappa, \nu)$ -plot of Fig. 10d is group wave velocity in c -units.

$$\frac{V^{group}}{c} = \frac{v'_{group}}{c\kappa'_{group}} = \frac{\sinh \rho}{\cosh \rho} = \tanh \rho = \frac{\frac{3}{4}}{\frac{5}{4}} = \frac{3}{5} \equiv \frac{u}{c} \equiv \beta \quad (16a)$$

This is the speed $\frac{u}{c} = \frac{3}{5}$ of Alice and Carla's *group* or *envelope* wave in Bob's space-time plot of Fig. 10b. u/c is the conventional *relativity-parameter* $\beta \equiv \frac{u}{c}$ for velocity of Alice and Carla relative to Bob. This group wave is for Alice or Carla a *standing* wave held by their laser cavities. In the same picture is the much faster *phase* or *carrier* wave that Bob would (if he could!) record going $\frac{5}{3}$ faster than light.

$$\frac{V^{phase}}{c} = \frac{v'_{phase}}{c\kappa'_{phase}} = \frac{\cosh \rho}{\sinh \rho} = \coth \rho = \frac{\frac{5}{4}}{\frac{3}{4}} = \frac{5}{3} \equiv \frac{c}{u} \equiv \frac{1}{\beta} \quad (16b)$$

After Fig. 9b we noted “instantons” seen by Bob that had infinite phase velocity. That is what Alice or Carla see for phase velocity in Fig. 10b while Bob sees two or three phase-zero white lines intersecting the dark blue wave curves near the top of the figure. There they have slowed down to a super-luminal speed (16b) of $\frac{u}{c} = \frac{5}{3}$. (**P** line slope $\frac{5}{3}$ is relative to x -axis in Fig. 10b but it is $\frac{3}{5}$ relative to ct -axis in reciprocal Fig. 10d. Recall that **P** and **G** lines get switched between reciprocal spaces.)

Fig. 11 shows detail in (a) per-Space-Time $(c\kappa, v)$ and (b) Space-Time $(\lambda, c\tau)$. In Fig. 11a, $(c\kappa, v)$ -coordinates of **P'** are proportional to $\kappa_{group} = 1/\lambda_{group}$ and $v_{group} = 1/\tau_{group}$ while $(c\kappa, v)$ -coordinates of **G'** are proportional to $\kappa_{phase} = 1/\lambda_{phase}$ and $v_{phase} = 1/\tau_{phase}$. In Fig. 11b, the interval between successive intercepts of **P'**-lines (or **G'**-lines) with the space x' -axis is proportional to wavelength λ_{phase} (or λ_{group}), and the corresponding intercept with time ct' -axis give the period τ_{phase} (or τ_{group}).

Table I. displays eight relativity parameters including Doppler shifts and wave velocities given as functions of rapidity ρ and of the old $\beta = \frac{u}{c}$ parameter. Numerical values for $\beta = \frac{3}{5}$ case are at bottom. Note that the ratio in column- $(1+n)$ is the inverse of the ratio in column- $(8-n)$ for $n < 8$. Some discussion is required of the Table I and plot thereof in Fig. 11 in order to avoid pitfalls in the application and interpretation of the ratios. This begins in the following section.

B. Understanding relativity parameters and transformations

Some of the parameters listed in Table I and plotted in Fig. 11 have famous names attached. In some cases there are several such names and contexts, and these will be

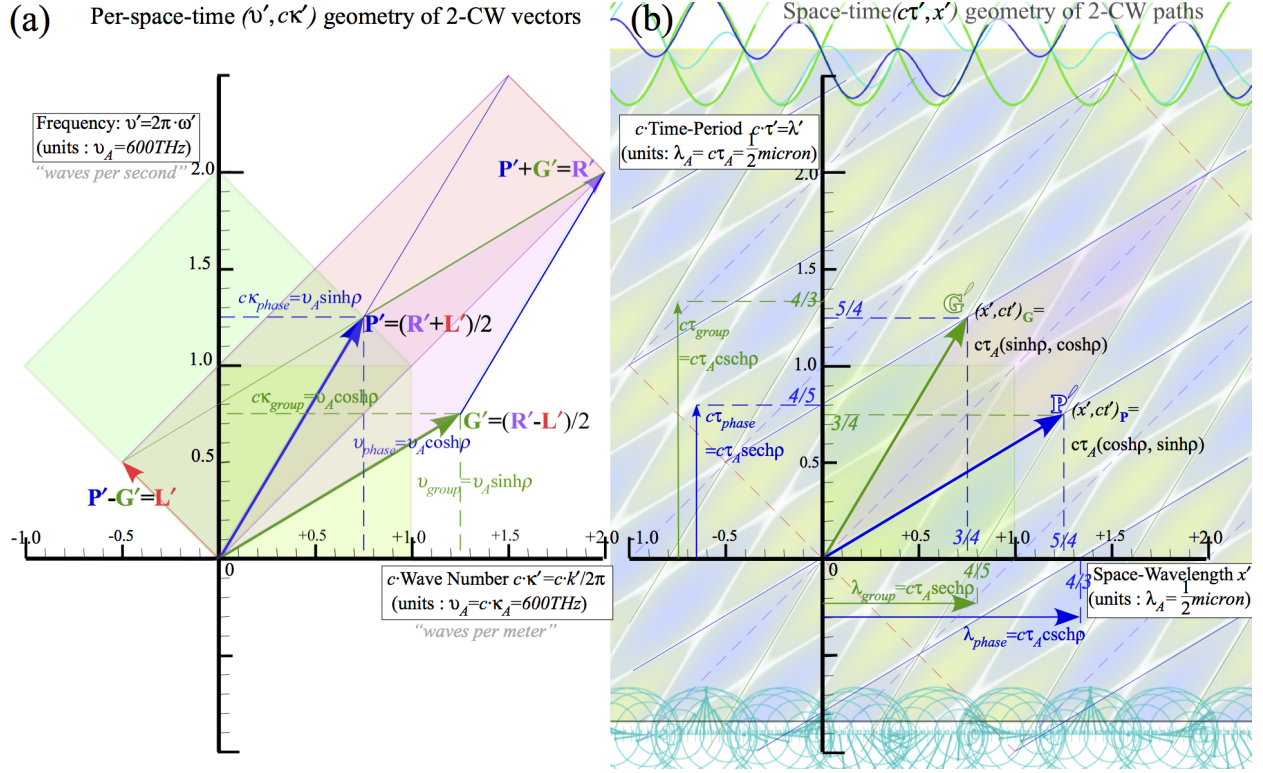


FIG. 11: Relativity parameters given as ρ -functions as they appear in (a) Per-space-time and (b) Space-time

recalled in due time. We begin with just two pairs of mutually reciprocal parameters $\text{sech } \rho$ and $\cosh \rho$ relevant to sophomore physics that belong to the following table entries.

$$\lambda_{\text{group}} = \lambda_A \text{sech } \rho = \lambda_A \sqrt{1 - \beta^2} \quad (17a)$$

$$v_{\text{phase}} = v_A \cosh \rho = \frac{v_A}{\sqrt{1 - \beta^2}} \quad (17b)$$

Sophomores learn two names: *Lorentz length contraction* and *Einstein time dilation*. Group velocity $V_{\text{group}} = c\beta = c \tanh \rho$ is derived in (16a). The β -forms in (17a)-(17b) follow by hyper-identity

$$\cosh^2 \rho - \sinh^2 \rho = 1. \quad (17c)$$

More difficult is learning what lies under these "contractions" and "dilations" and realizing that they are primary (really *secondary*) effects of greater but not-quite-canceling Doppler contractions and dilations.

By now it should be clear that the hyper-trigonometry lessons in Fig. 2 and Fig. 3 have

<i>phase</i>	$b_{RED}^{Doppler}$	$\frac{c}{V_{phase}}$	$\frac{\mathcal{K}_{phase}}{\mathcal{K}_A}$	$\frac{\tau_{phase}}{\tau_A}$	$\frac{v_{phase}}{v_A}$	$\frac{\lambda_{phase}}{\lambda_A}$	$\frac{V_{phase}}{c}$	$b_{BLUE}^{Doppler}$
<i>group</i>	$\frac{1}{b_{BLUE}^{Doppler}}$	$\frac{V_{group}}{c}$	$\frac{v_{group}}{v_A}$	$\frac{\lambda_{group}}{\lambda_A}$	$\frac{\mathcal{K}_{group}}{\mathcal{K}_A}$	$\frac{\tau_{group}}{\tau_A}$	$\frac{c}{V_{group}}$	$\frac{1}{b_{RED}^{Doppler}}$
<i>rapidity</i> ρ	$e^{-\rho}$	$\tanh \rho$	$\sinh \rho$	$\operatorname{sech} \rho$	$\cosh \rho$	$\operatorname{csch} \rho$	$\operatorname{coth} \rho$	$e^{+\rho}$
$\beta \equiv \frac{u}{c}$	$\frac{\sqrt{1-\beta}}{\sqrt{1+\beta}}$	$\frac{\beta}{1}$	$\frac{1}{\sqrt{\beta^2-1}}$	$\frac{\sqrt{1-\beta^2}}{1}$	$\frac{1}{\sqrt{1-\beta^2}}$	$\frac{\sqrt{\beta^{-2}-1}}{1}$	$\frac{1}{\beta}$	$\frac{\sqrt{1+\beta}}{\sqrt{1-\beta}}$
<i>value for</i> $\beta=3/5$	$\frac{1}{2}=0.5$	$\frac{3}{5}=0.6$	$\frac{3}{4}=0.75$	$\frac{4}{5}=0.80$	$\frac{5}{4}=1.25$	$\frac{4}{3}=1.33$	$\frac{5}{3}=1.67$	$\frac{2}{1}=2.0$

TABLE I: Relativity parameter formulae. Last row gives numeric values for blue-shift

$$b_{BLUE}^{Doppler}=2 \text{ or } \beta = \frac{u}{c} = \frac{3}{5}.$$

$\operatorname{sech} \rho$ and $\cosh \rho$ functions along with **R**, **L**, **P**, and **G** points in precisely the places they appear in Fig. 10 or Fig. 11. (All involve 3:4:5 triangles and $\operatorname{sech} \rho = \frac{4}{5}$.) Fig. 11b has two parallel **G**-lines (group velocity $\frac{3}{5}$) cross Bob's x' -axis at $x'=0$ and $x'=\frac{4}{5}x_A$, respectively. So Alice's standing wave is contracted to 80% (or $\frac{4}{5}$) of its original λ_A , that is, $\lambda_{group} = \lambda_A \frac{4}{5}$ as listed in Table I and Fig. 11b, and due to ((17a)).

Lorentz contraction comes with a well-worn paradox. Suppose Bob criticizes Alice for her 80% foreshortened meter-stick. (Actually, it is a *micrometer* stick if it holds two 600Thz standing $\lambda_A = \frac{1}{2}\mu m$ waves.) But, if Alice checks out Bob's equipment as well as he did hers, then she could reply, "No Bob! You're the one that's 80% short of a full deck!"

So begins a physical lovers' quarrel made all the worse by the fact that *both* parties are *right*. This also questions a relativity assumption that a Lorentz contraction of an ethereal light wave would imply the same contraction of a solid steel laser mount holding that wave.

This highlights a main point of relativity: *All* things are wavelike as in *quantum* wavelike. The steel mount obeys the same space-time rules as light itself while the standing wave in Alice's laser is behaving like a tiny mass making its own frame. Furthermore, both the tiny wave and its steel cavity must contract *together* to keep the laser in *resonance*. Waves are very particular about resonance.

As the GPS and LIGO projects have shown, quantum interference can be excruciating

exercise in precision of timing. While Lorentz contraction (17a) involves the “skin” or *group-envelope* of a wave, the v_{phase} dilation effect embodied by (17b) involves the “guts” or *phase frequency* of a wave (and an old showman’s adage, “*Timing is everything!*”) It has no famous name so let’s call it the *Planck frequency dilation effect* since, as seen later, v_{phase} is the “heartbeat” of quantum matter that gives it its energy.

Einstein time dilation is one of the more poorly explained effects since it involves Bob reading a moving clock (Alice’s in this case) located far down-track using co-observers (Bob’s in this case) that have clocks co-moving and synced with Bob’s. Imagine Alice’s clock in Fig. 11b to be passing thru point \mathbf{G}' at the instant Bob and observers occupy the horizontal dashed line where all their ct' clocks read $\frac{5}{4} = 1.25$ in Alice’s units. ($\tau_A = \frac{5}{3}$ femto seconds) That is a 25% dilation of 1.0 that Alice’s clock will read at the right end of the dashed line. (Alice is crossing a \mathbf{P}' line that is all $ct=1$.) So from that scenario her clocks appear 25% slower than Bob’s. This is another lover’s quarrel like that of the Lorentz effect.

Since that \mathbf{P}' line Alice just crossed points back to Bob’s time of ($ct' = \frac{4}{5} = 0.8$) she could claim to be even younger, 80% of Bob’s age. Time and space reading by non-local observers is problematic due to another 1st-order time shift (besides Doppler). It is future-to-past shift due to slope of \mathbf{P} and \mathbf{G} lines. As Alice passes Bob his observers further to her left get to look farther into Alice’s future while those further to her right can see farther into her past. This strange shift turns out to vary as $x \cdot \sinh \rho$.

The future-to-past time shift due to spatial position x is part of the famous¹⁹ *Lorentz space-time* $(x, ct) \leftrightarrow (x', ct')$. First, the *relativity* $(c\boldsymbol{\kappa}, v) \leftrightarrow (c\boldsymbol{\kappa}', v')$ *per-space-time transformation* (not properly due to Lorentz but quite similar in form) follows from definitions (15a) and (15b) of Bob’s phase vector \mathbf{P}' and group \mathbf{G}' vector in terms of Alice’s vectors of phase \mathbf{P} and group \mathbf{G} .

$$\mathbf{P}' = \begin{pmatrix} v'_{phase} \\ c\boldsymbol{\kappa}'_{phase} \end{pmatrix} = v_A \begin{pmatrix} \cosh \rho \\ \sinh \rho \end{pmatrix} = \begin{pmatrix} v_A \\ 0 \end{pmatrix} \cosh \rho + \begin{pmatrix} 0 \\ v_A \end{pmatrix} \sinh \rho = \mathbf{P} \cosh \rho + \mathbf{G} \sinh \rho \quad (18a)$$

$$\mathbf{G}' = \begin{pmatrix} v'_{group} \\ c\boldsymbol{\kappa}'_{group} \end{pmatrix} = v_A \begin{pmatrix} \sinh \rho \\ \cosh \rho \end{pmatrix} = \begin{pmatrix} v_A \\ 0 \end{pmatrix} \sinh \rho + \begin{pmatrix} 0 \\ v_A \end{pmatrix} \cosh \rho = \mathbf{P} \sinh \rho + \mathbf{G} \cosh \rho \quad (18b)$$

This gives a matrix $(c\boldsymbol{\kappa}', v') \leftarrow (c\boldsymbol{\kappa}, v)$ *per-space-time transformation* and its inverse $(c\boldsymbol{\kappa}, v) \leftarrow (c\boldsymbol{\kappa}', v')$.

$$\begin{pmatrix} v' \\ c\kappa' \end{pmatrix} = \begin{pmatrix} \cosh \rho & +\sinh \rho \\ +\sinh \rho & \cosh \rho \end{pmatrix} \begin{pmatrix} v \\ c\kappa \end{pmatrix} \Rightarrow \begin{pmatrix} v \\ c\kappa \end{pmatrix} = \begin{pmatrix} \cosh \rho & -\sinh \rho \\ -\sinh \rho & \cosh \rho \end{pmatrix} \begin{pmatrix} v' \\ c\kappa' \end{pmatrix} \quad (19)$$

Re-ordered c -scaled vector $(ck, \omega) = 2\pi(c\kappa, v)$ transforms just like $(\omega, ck) = 2\pi(v, c\kappa)$.

Bob's \mathbf{P}' vector shares a phase hyperbola with Alice's \mathbf{P} and similarly for \mathbf{G}' and \mathbf{G} .

$$\begin{aligned} \mathbf{P} - \text{hyperbola} : v^2 - c^2\kappa^2 &= v'^2 - c^2\kappa'^2 = v_A^2 \quad (\text{a}) \\ \mathbf{G} - \text{hyperbola} : c^2\kappa^2 - v^2 &= c^2\kappa'^2 - v'^2 = c\kappa_A^2 \quad (\text{b}) \end{aligned} \quad (20)$$

These hyperbolas (plotted in Fig. 2 and 3) are invariant to Lorentz-like transformation (18).

C. Invariance of phase to Lorentz transformation

A laser phasor sketched in Fig. 4 should be taken seriously as a gauge of time (clock) and of space (metric ruler) for giving time (wave period τ) and distance (wavelength λ) in Fig. 11b. A reading of phase ϕ by Alice at a space-time point must equal reading ϕ' by Bob in spite of unequal readings (x, t) and (x', t') for that point and unequal readings (ω, k) and (ω', k') for a laser group-wave or its phase-wave. (Here angular $(ck, \omega) = 2\pi(c\kappa, v)$ replace Kayser-Hertz $(c\kappa, v)$ to do phase calculations.)

$$\begin{aligned} \phi'_{\text{phase}} &\equiv k'_{\text{phase}}x' - \omega'_{\text{phase}}t' = k_{\text{phase}}x - \omega_{\text{phase}}t \equiv \phi_{\text{phase}} \\ \phi'_{\text{group}} &\equiv k'_{\text{group}}x' - \omega'_{\text{group}}t' = k_{\text{group}}x - \omega_{\text{group}}t \equiv \phi_{\text{group}} \end{aligned} \quad (21)$$

Bob's (ω', k') components are in (15) or (18). Alice's (ω, k) are the same with $\rho = 0$. This derives an Einstein-Lorentz Transformation (ELT) $(x, ct) \leftarrow (x', ct')$ of Bob's (x', ct') to Alice's (x, ct) .

$$\begin{aligned} \phi_{\text{phase}} &\equiv x' \frac{\omega_A}{c} \sinh \rho - t' \omega_A \cosh \rho = 0 \cdot x - \omega_A t \Rightarrow ct = ct' \cosh \rho - x' \sinh \rho \\ \phi_{\text{group}} &\equiv x' \frac{\omega_A}{c} \cosh \rho - t' \omega_A \sinh \rho = \frac{\omega_A}{c} x - 0 \cdot t \Rightarrow x = -ct' \sinh \rho + x' \cosh \rho \end{aligned}$$

ELT matrix and inverse resolve Bob-Alice space-time (Fig. 11b) and matches per-space-time form (19).

$$\begin{pmatrix} ct' \\ x' \end{pmatrix} = \begin{pmatrix} \cosh \rho & +\sinh \rho \\ +\sinh \rho & \cosh \rho \end{pmatrix} \begin{pmatrix} ct \\ x \end{pmatrix} \Rightarrow \begin{pmatrix} ct \\ x \end{pmatrix} = \begin{pmatrix} \cosh \rho & -\sinh \rho \\ -\sinh \rho & \cosh \rho \end{pmatrix} \begin{pmatrix} ct' \\ x' \end{pmatrix} \quad (22)$$

Quite similar invariant hyperbolas appear in space-time. A key space-time ρ -invariant is *proper time* τ .

$$(c\tau_A)^2 = (ct')^2 - (x')^2 = (ct'')^2 - (x'')^2 = .. \quad (23a)$$

$$c\tau_A = ct' \sqrt{1 - \frac{(x')^2}{(ct')^2}} = ct' \sqrt{1 - \frac{u^2}{c^2}} \quad (23b)$$

D. Thales-Euclid means and geometry of hyperbolic invariants

Re-examining Alice, Bob, and Carla laser thought experiment is instructive. Imagine as before, that Bob detects counter-propagating laser beams of frequency ω_R going left-to-right (due to Alice's laser) and ω_L going right-to-left (due to Carla's laser). We ask two questions:

- (1.) To what velocity u_E must Bob accelerate so he sees beams with equal frequency ω_E ?
- (2.) What is that frequency ω_E ?

Query-1 has Jeopardy-style answer-by-question: What group velocity (16a) does Bob see?

$$u_E = V_{group} = \frac{\omega_{group}}{k_{group}} = \frac{\omega_R - \omega_L}{k_R - k_L} = c \frac{\omega_R - \omega_L}{\omega_R + \omega_L} \quad (24)$$

Query-2 similarly: What ω_E is blue-shift $b\omega_L$ of ω_L and red-shift ω_R/b of ω_R ?

$$\omega_E = b\omega_L = \omega_R/b \Rightarrow b = \sqrt{\omega_R/\omega_L} \Rightarrow \omega_E = \sqrt{\omega_R \cdot \omega_L} \quad (25)$$

V_{group}/c is ratio of difference mean $\omega_{group} = \frac{\omega_R - \omega_L}{2}$ to arithmetic mean $\omega_{phase} = \frac{\omega_R + \omega_L}{2}$. Frequency $\omega_E = B$ is the geometric mean $\sqrt{\omega_R \cdot \omega_L}$ of left and right-moving frequencies defining the geometry in Fig. 12 as detailed in Fig. 12a. Line sum of $\omega_L = \omega_E e^{-\rho}$ and $\omega_L = \omega_E e^{+\rho}$ is bisected at center C of a circle connecting shifted phase vector \mathbf{P}' to its $\sqrt{\omega_R \cdot \omega_L}$ original \mathbf{P} .

Original \mathbf{P} (Pitcher's mound) is the geometric mean point $\sqrt{1 \cdot 4} = 2$ at Alice's base frequency of $B=v_A=600\text{THz}$. (Fig. 12 units are 300 THz.). That lets you construct points $\mathbf{P}, \mathbf{P}', \mathbf{P}'', \dots$ on a hyperbola that all frames will claim to also be their 600 THz invariant curve. Geometry begins by choosing to prick a \mathbf{C} -point ck with compass needle. Then compass pencil is set to point- \mathbf{P} , and arc $\mathbf{P} \mathbf{P}'$ is drawn to the next hyperbola point $\omega'(k)$ on the new axis ck . (Arc is optional if graph paper locates vertical \mathbf{PC} line.)

Time-symmetry axiom ($e^\rho e^{+\rho} = r \cdot b = 1$) implies phase points $\mathbf{P}', \mathbf{P}'', \mathbf{P}''', \dots$ lie upon equilateral hyperbolas ($xy=const.$ or $\omega_R \omega_L = \omega_A^2$) whose $\pm 45^\circ$ asymptotes frame Doppler-shifted rectangles that all have the same area $2\omega_A^2$ of the initial ($\rho=0$) baseball diamond

in Fig. 9d. Fig. 12b shows plots of top branches for two (ω', ck') -hyperbolas belonging to constants $\omega_A = 2$ and $\omega_A = 4$. This oblique $\pm 45^\circ$ view of the invariant hyperbolas emphasizes the Doppler shift ($r \cdot b = \text{const.}$) relations that are not obvious from the usual straight Cartesian invariant equations such as (23).

The geometry behind Fig. 12a or Fig. 12b is ancient and goes back to Thales of Miletus (circa 600BCE) about three centuries before Euclid. Thales construction of means follows from his proof by symmetry that each point on a circle subtends a right (90°) angle which in turn is based on inscribed rectangles (dashed lines in Fig. 12). The same geometry applies to half-sum and half differences of phase angles involved in the wave interference sum sketched in Fig. 13c for each pair of phasors added in Fig. 13d. That is the geometry of factoring equations (12) and (13) giving Minkowski grids.

Adding waves Ψ_A and Ψ_B gives new and valid $\Psi_{AB} = \Psi_A + \Psi_B$ solution to Maxwell wave equations due to linearity of differential equations. Then one may entertain a Galilean relativity of phase angular velocity ω as sketched in Fig. 13e, a 2nd-Galileo-revenge, the 1st being ρ -addition in Fig. 8, another argument of wave function exponentials. So Galilean addition of linear velocity fails so that we may trust it when adding lightwave phase angular velocity ω . Would we have it any other way?

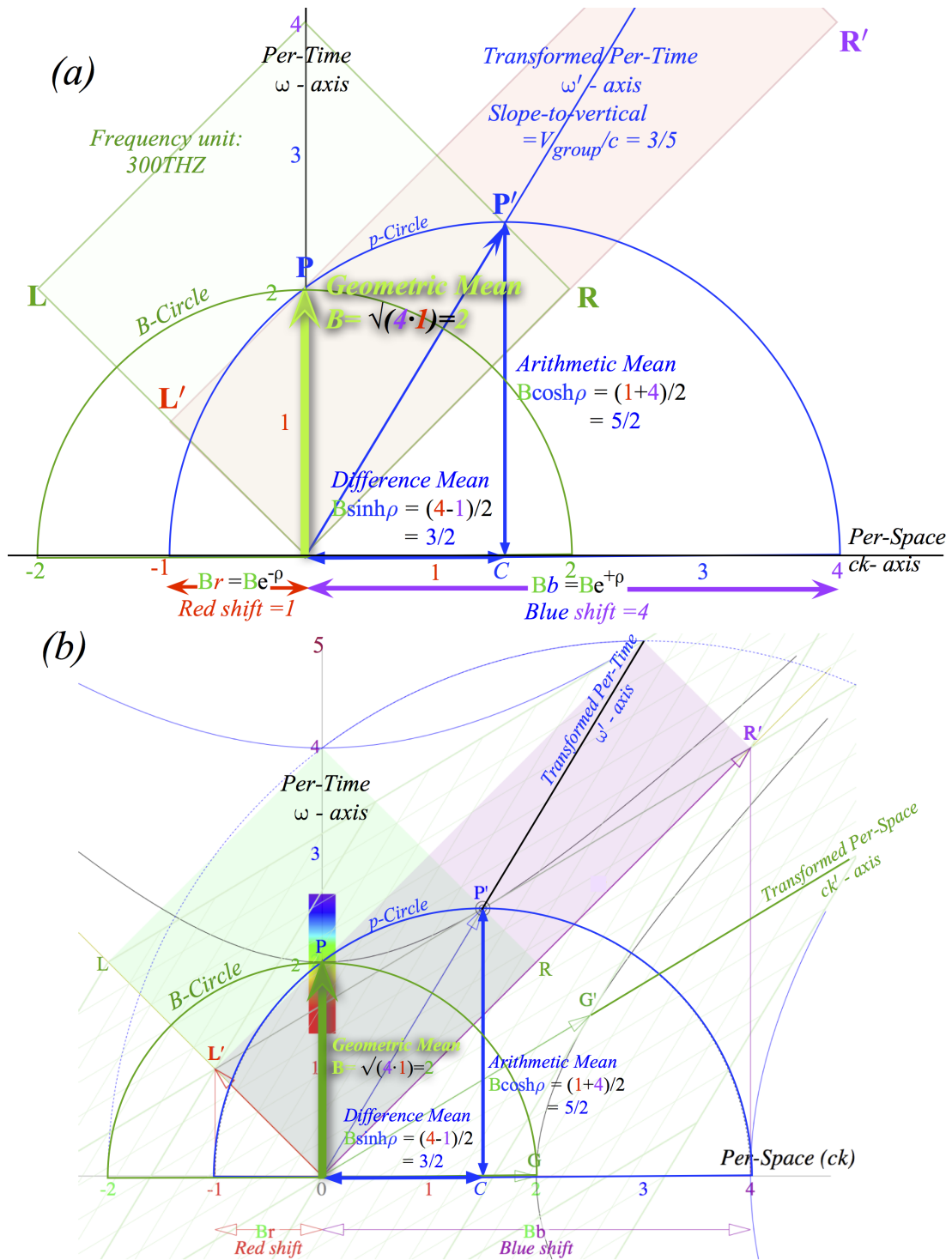


FIG. 12: (a) Thales-Euclid geometric and arithmetic means (b) Hyperbola construction step by circle radius CP' .

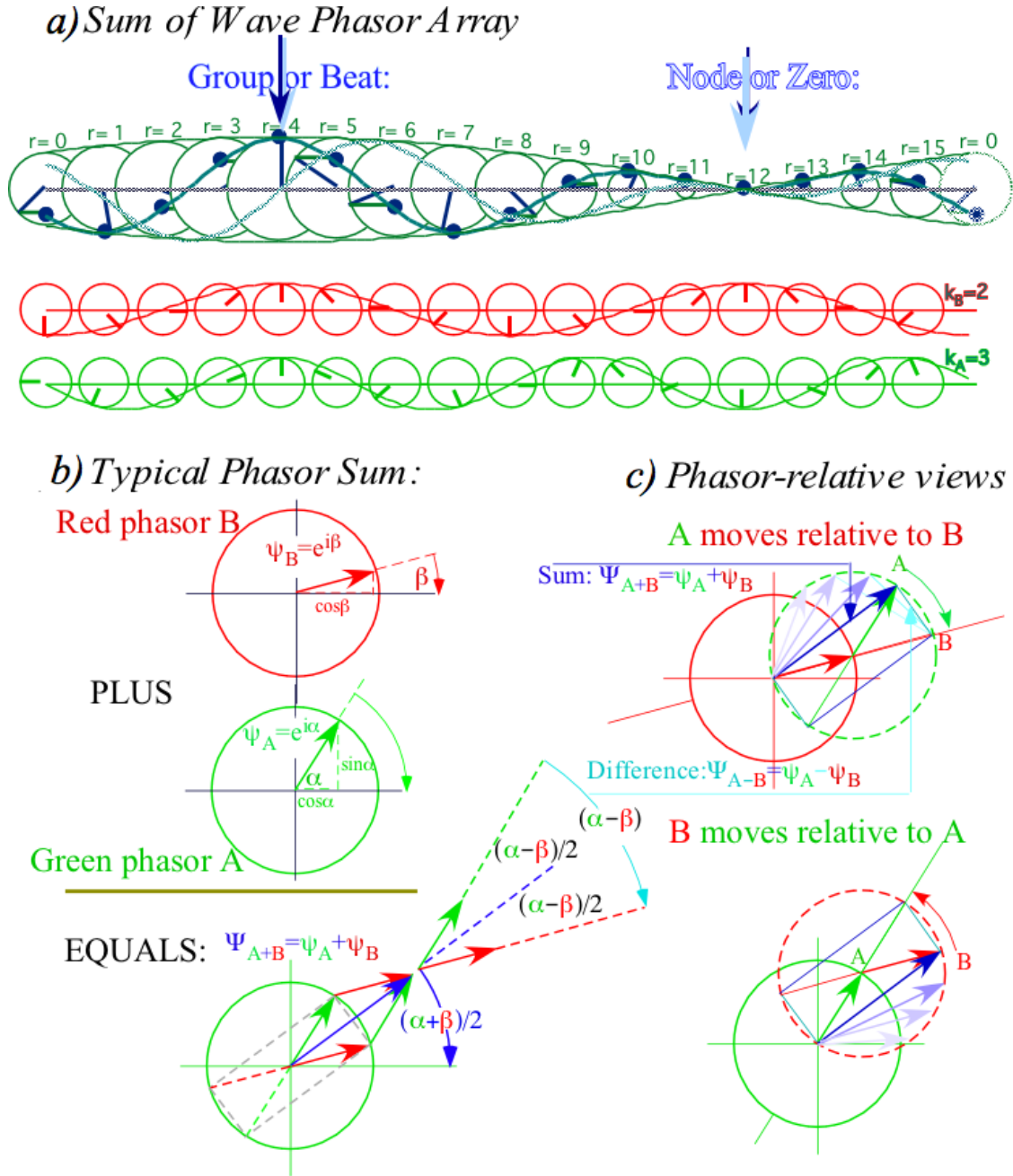


FIG. 13: (a) Sum $\Psi_{AB} = \Psi_A + \Psi_B$. (b) Sum of individual phasors. (c) Phasor A moves relative to B and vice-versa.

E. PW Sums of multiple CW harmonics and Doppler effects

Sums $\sum_{m=1}^n \cos mvt$ of n cosine waves (for $n=1,2,5,10$, and 50) are plotted on the left of Fig. 14 with a corresponding bandwidth $n \cdot v = \Delta v$ on the right. Each sum is a train of Pulse Waves (PW) with peaks at each crest of the fundamental ($n=1$) CW that have a decreasing

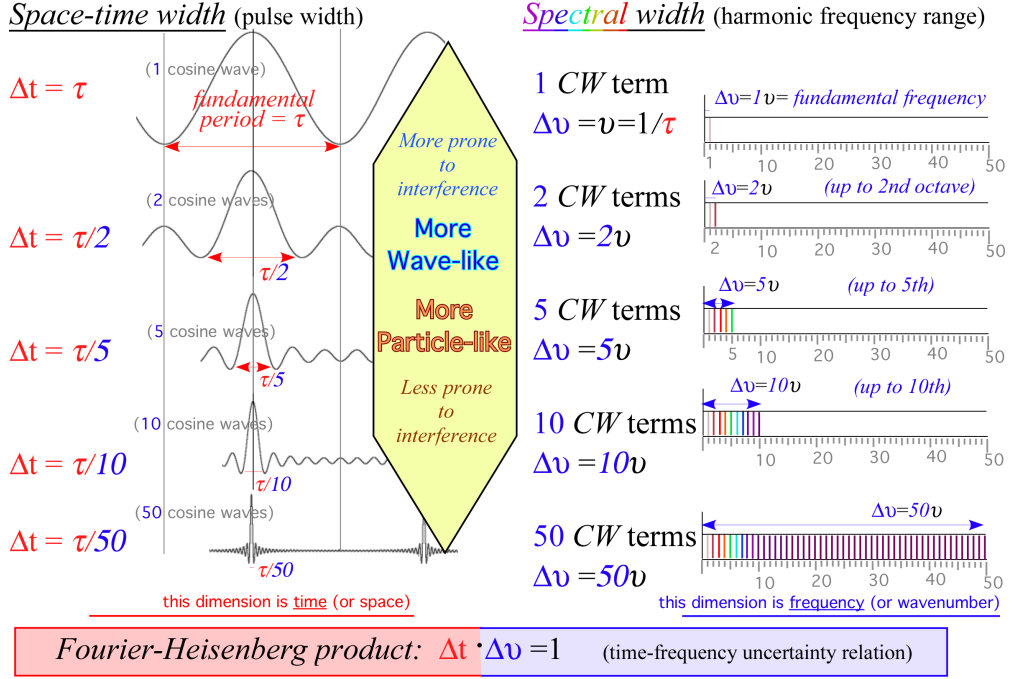


FIG. 14: Sums of $n=(1,2,5,10$ and $50)$ CW with “boxcar” harmonic spectrum

width Δt that is a fraction $\frac{1}{n}$ of the fundamental period τ . Meanwhile, the interval between crests (surrounding the fundamental trough points) has n wrinkles of decreasing ($\sim \frac{1}{n}$) amplitude. By defining bandwidth $\Delta\nu = n \cdot \nu = \frac{n}{\tau}$, we get a very simple uncertainty relation $\Delta t \cdot \Delta\nu = 1$. Laser jocks call a square-amplitude spectrum a “boxcar” spectrum. A boxcar wave has an annoying “ringing” due to its last $\cos nvt$ term lacking a following term to “beat” or destructively interfere its oscillation. Tapered amplitudes a_m suppress ringing by arranging to have the offending ringing end-term(s) have essentially zero amplitude.

$$\psi_{PW}^{\cos} = \sum_{m=1}^n a_m \cos mkx \quad \left[\text{taper: } a_m = e^{-m^2/a^2} \right] \quad \psi_{PW}^{\text{plane}} = \sum_{m=1}^n a_m e^{imk(x-ct)} \quad (26)$$

Tapered right-moving ($k=1$) plane-wave sums $\sum_{m=1}^n a_m e^{im(x-ct)}$ (in Fig. 15a) collide with left-moving sums $\sum_{m=1}^n a_m e^{im(x+ct)}$ (in Fig. 15c) to make a baseball-diamond lattice of PW (Pulse-Wave) paths in space-time that appears in Fig. 15b. Crests in 2-CW plot of Fig. 9 become PW peaks at baseline intersections that surround flat diamond areas in Fig. 15b where a CW trough would be in Fig. 9. As noted in Fig. 14 the high- n waves are more particle-like and cannot exhibit significant interference effects in regions where their n -components have destructively interfered their amplitudes away to near-zeros.

Only when their pulse peaks collide can there be right-moving and left-moving interference. Then all counter-propagating high- m -pairs of components try at once to make their own tiny square grids like those in Fig.9. The results are piled up square “bases” at each diamond intersection that would make a tall square pulse peak coming out of the page of Fig.15b below if it were plotted in 3D.

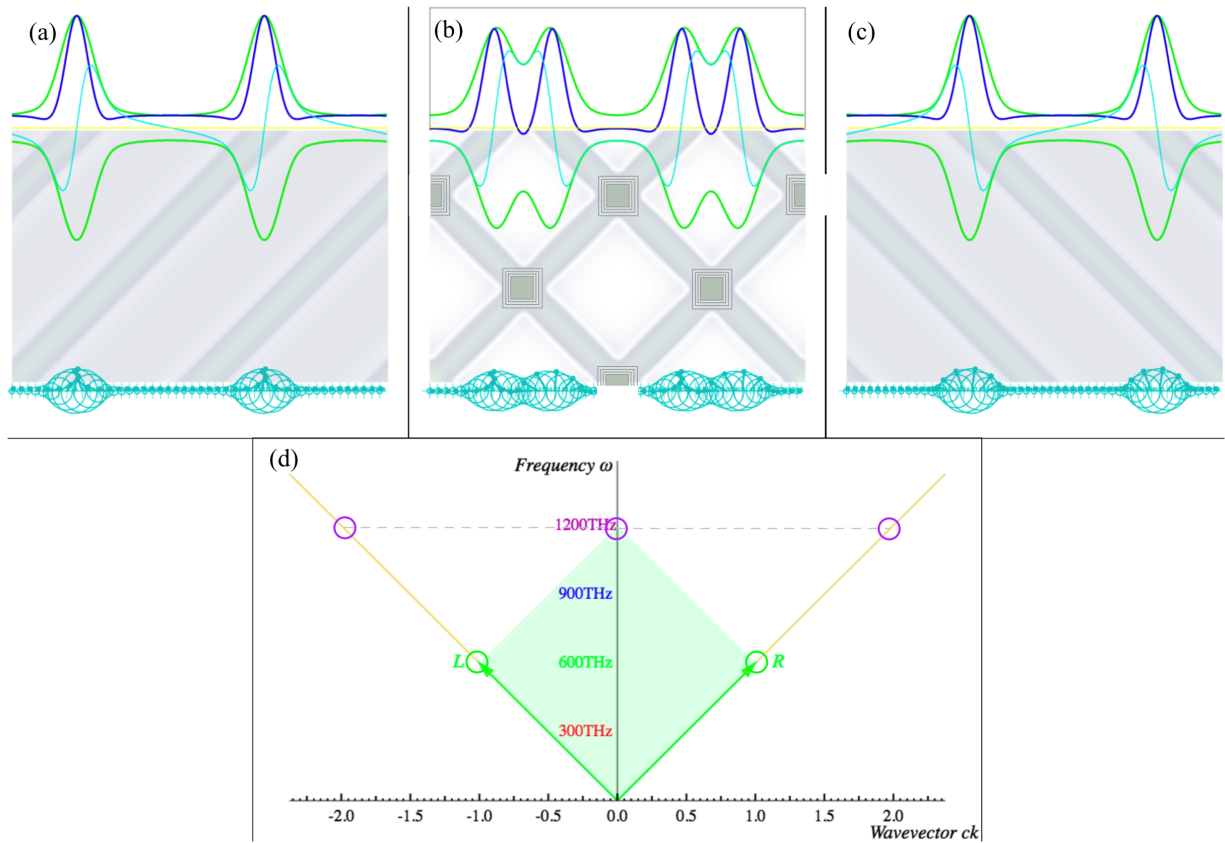


FIG. 15: (x, ct) -plots:(a-c)R&L moving PW $k=2,4,6,\dots$, (b)Sum:(a)+(c)

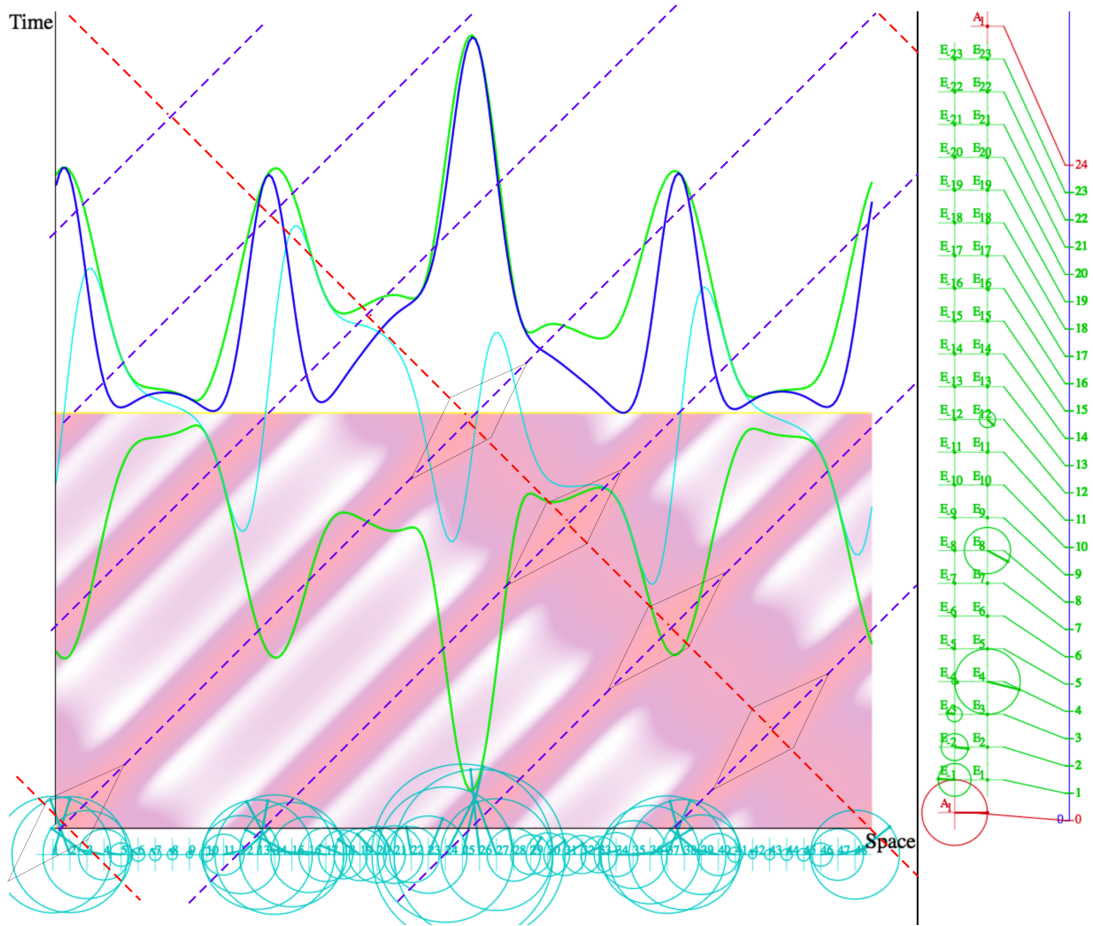


FIG. 16: Colliding PW of Fig. 15 as viewed in frame moving at $u=3c/5$.

Fig.16 is a Doppler shifted view of PW diamonds made into equal area rectangles framed by \mathbf{R}' and \mathbf{L}' paths drawn in Fig.10 and Fig.11a and sketched by dash-lines in Fig.16. The interference at each intersection of these paths should produce Minkowski rhombus structure that is a miniature of the rhombic space-time lattice cells in Fig.10.

As discussed in Chapter X the projection of wave grids to a moving observer requires up-tuning and de-tuning of both lasers' frequency and amplitude in order that they would be able to perceive a rest-frame grid that is Cartesian.

V. PROPERTIES AND APPLICATIONS OF RELAWAVITY GEOMETRY

The relawavity quantities q in Table I are dimensionless ratios q_B/q_A including 1-CW Doppler shifts (blue $b=e^\rho$ and red $r=1/b$) and 2-CW phase or group wave-velocity $V_{group}=1/V_{phase}$, wavelength λ , wavenumber $\kappa=1/\lambda$, wave-period, or wave-frequency $=1/\tau$, given for a frame moving at rapidity ρ_{AB} relative to a rest frame that starts with Alices value q_A that Bob records as q_B . Ratios are also functions of the conventional velocity parameter $\beta=u/c$ where $u=V_{group}$ is relative group velocity u_{AB} . Table II that follows this section includes the circular angle parameter σ that began the review of trigonometry. Here σ will serve to measure rotation of a laser beam transverse to Bob's rather than the longitudinal Doppler shift e^ρ he sees parallel to a beam. This σ is the stellar aberration angle and is the key parameter in a novel space-proper-time approach to relativity pioneered by Lewis Epstein²⁰. It is also useful in describing Transverse-Electric (TE) waveguide and cavity modes.

A. Space-proper-time plots and the stellar-aberration angle

Lewis C. Epstein²¹ developed a novel approach to space-time relativity that uses the transverse stellar aberration angle σ to define relative velocity by $u = c \sin\sigma$ as sketched in Fig. 17. This is in place of longitudinal Doppler definition $u = c \tanh\rho$ (16a) in terms of rapidity ρ given in (16a).

This alternative to Minkowski- (x, ct) -plots involves flipping proper-time definition (23) as follows into a Cartesian Pythagorean relation.

$$(c\tau)^2 = (ct')^2 - (x')^2 \Rightarrow (c\tau)^2 + (x')^2 = (ct')^2 \quad (27)$$

A Pythagorean geometry for space-proper-time or $(x, c\tau)$ -plots is shown by Fig. 18. There it is imagined all things travel at light-speed c including a stationary object ($x'=0$) that “moves” parallel to the $(c\tau)$ -axis. Moving object P is indicated by an vector (ct') that is inclined at aberration angle σ and also grows at rate c as given by (27) with $(x'=ct')$. Both the longitudinal parameter ρ for hyperbolic geometry and the transverse σ for circular geometry are useful and insightful. Applications to wave guide and cavity relawavity and quantum wave mechanics follow an application of ρ and σ geometric relations developed in

- (a) Fixed observer sees star directly overhead
 (b) Moving observer sees star shift angle σ in direction of \mathbf{u}

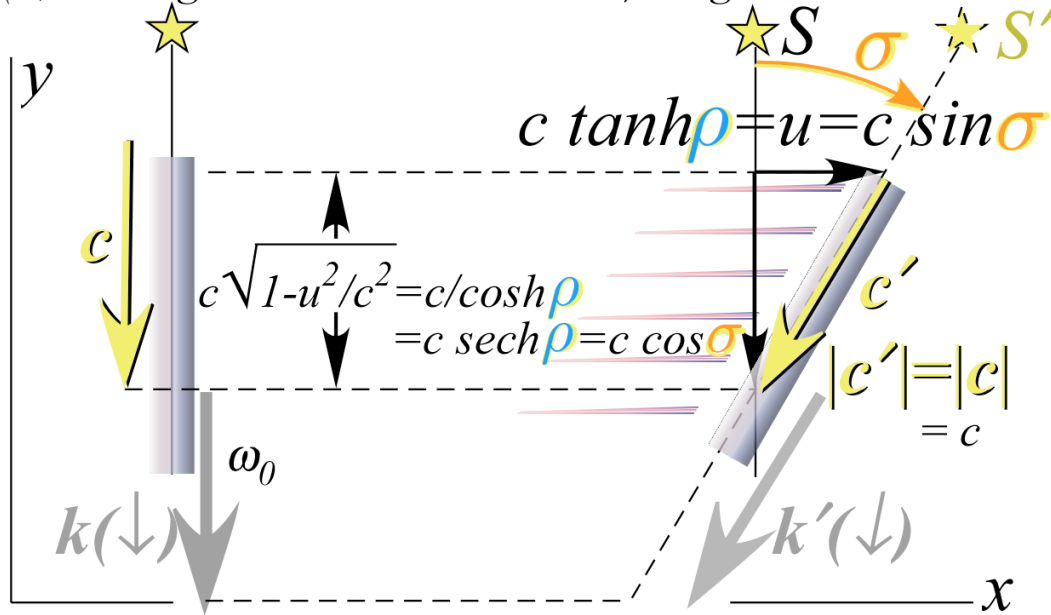


FIG. 17: Stellar aberration angle σ of light beam normal to direction of velocity \mathbf{u} .

Fig. 1 to Fig. 3. As group speed u becomes low ($u \ll c$) both ρ and σ converge on the old parameter $\beta = u/c$.

Proper time $c\tau$ vs. coordinate space x - (L. C. Epstein's "Cosmic Speedometer")

Particles P and P' have speed u in (x', ct') and speed c in $(x, c\tau)$

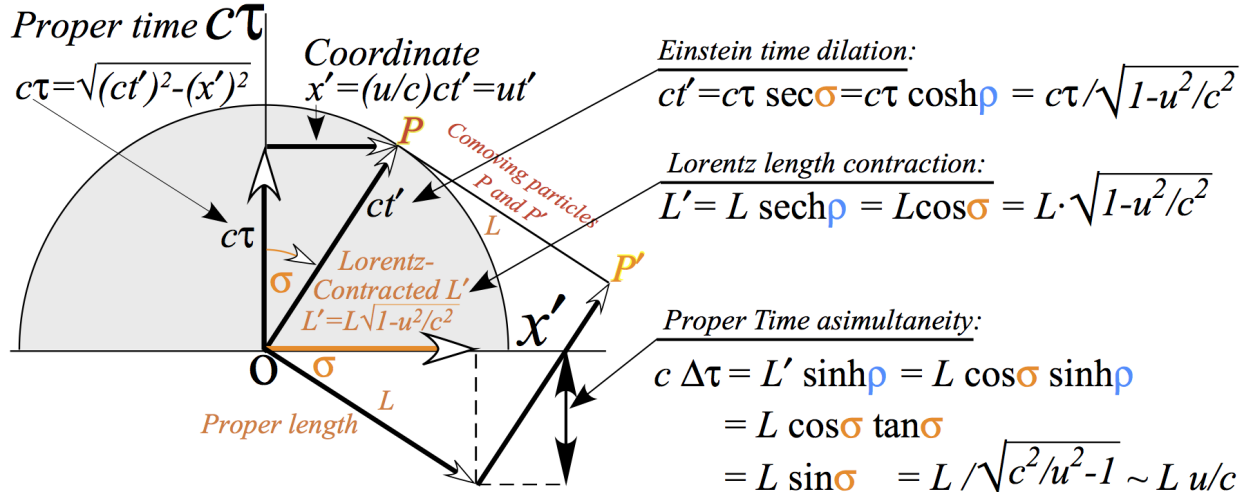


FIG. 18: Epstein space-proper- $c\tau$ geometry of relativistic effects in terms of ρ or σ .

Prime phase point \mathbf{P}' in Fig.19 at $(v, c\kappa) = B(\sinh \rho, \cosh \rho)$ is on Alice's v_A -axis \mathbf{OP}' of slope $\coth \rho$. \mathbf{P}' is a hyperbolic tangent point for line $\mathbf{LP}'\mathbf{R}$ of slope $\tanh \rho = |\mathbf{LL}'|/|\mathbf{L}'\mathbf{R}|$ with axis intercepts equal to $|\mathbf{QO}| = B\text{csch} \rho$ and $|\mathbf{AO}| = B\text{sech} \rho$. $\mathbf{P}'\mathbf{Q}$ parallels line \mathbf{OG}' of group $c\kappa_A$ -axis. Prime stellar point \mathbf{S}' at coordinates $(v, c\kappa) = (B\text{sech} \rho, \tanh \rho)$ defines stellar ray \mathbf{OS}' of slope $\text{csch} \rho$. \mathbf{S} is b -circle tangent point for line $\mathbf{C}'\mathbf{S}\mathbf{Y}$ having slope that is equal to $-\sinh \rho = -|\mathbf{C}'\mathbf{O}|/|\mathbf{OY}|$ with axis intercepts $|\mathbf{C}'\mathbf{O}| = B\cosh \rho$ and $|\mathbf{OY}| = B\coth \rho$. The ρ -functions relate to σ -functions in Fig.2 and Table II. (See plot in Fig.21.) Applications

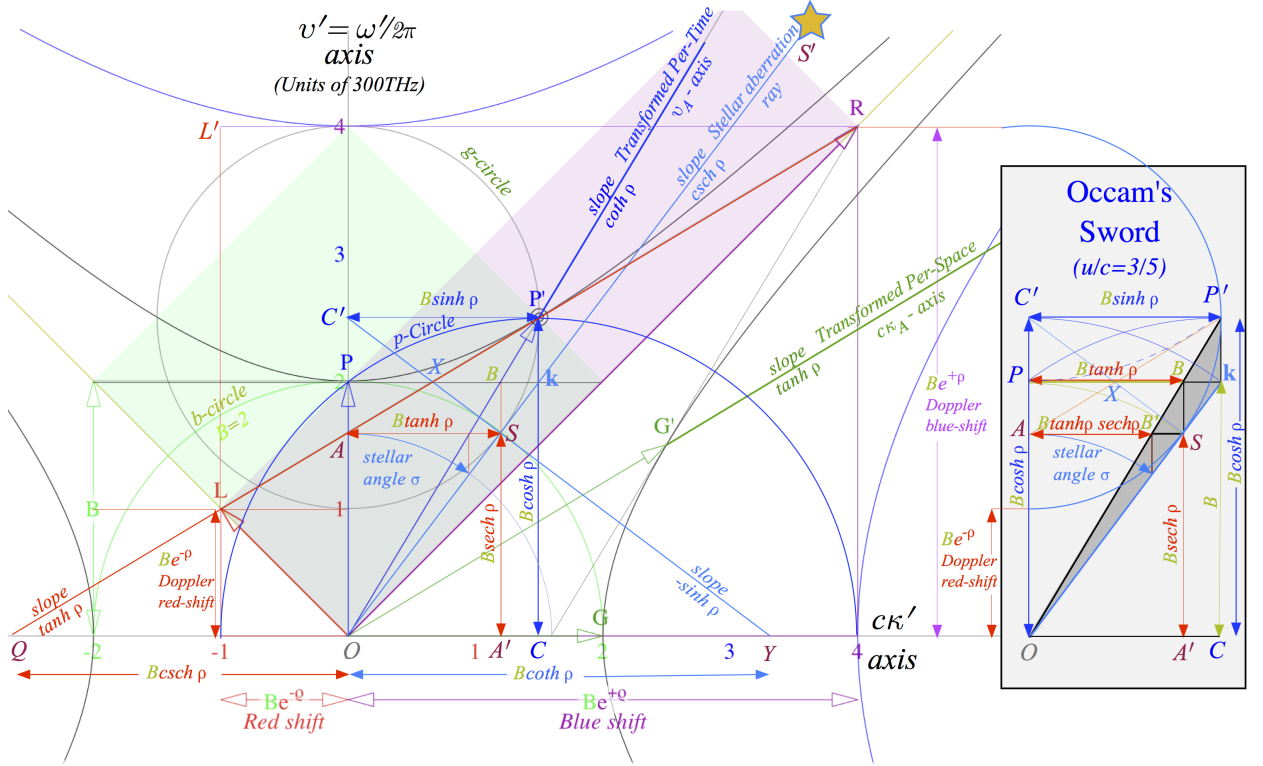


FIG. 19: Bob- $(v', c\kappa')$ -view of Alice- $(v_A, c\kappa_A)$ tangent geometry and (inset) Occam-Sword pattern relates σ , ρ , and v angles.

that follow use a pattern-recognition aid labeled Occam's Sword in Fig. 19(inset). It focuses mostly on geometry of $(\sin \Rightarrow \tan)$ and $(\cos \Rightarrow \sec)$ columns of Table II. The $(\cot \Rightarrow \csc)$ intercepts are outliers for low to moderate u/c values. The sword has a staircase whose steps belong to a $(\cosh \rho)^n$ -geometric series: $(B\cosh \rho, B, B\text{sech} \rho, \dots)$. Multiplying series by $\tanh \rho$ gives line- $(|\mathbf{C}'\mathbf{P}'| = B\sinh \rho)$, then line- $(|\mathbf{PB}| = B\tanh \rho)$, and lowest step- $(|\mathbf{AB}'| = B\tanh \rho \text{sech} \rho)$ in inset. Steps subtend a triple-cross- \mathbf{X} -point of tangents $\mathbf{C}'\mathbf{X}\mathbf{S}$, \mathbf{AXP}' , and b -baseline \mathbf{PXB} . Extensions of the tangents have κ -axis $(\cot \Rightarrow \csc)$ -intercepts on either side of the sword in

Fig. 19. The sword's leading \mathbf{k} -edge defines wavevectors for waveguides and for free-electron lasers and this makes them easier to analyze and visualize. At this point it might help to compare Fig. 19 to the elementary trig-map in Fig. 3.

1. TE-Waveguide geometry

Consider a sum of plane waves with wave-vectors $\mathbf{k}^{(+)}=(k\sin\sigma,+k\cos\sigma)=(k_x,k_y)$ pointing up in Fig. 20a and $\mathbf{k}^{(-)}=(k\sin\sigma,-k\cos\sigma)=(k_x,k_y)$ pointing down, each an angle $\pm\sigma$ relative to the y -axis in Fig 20.

$$E_z(\mathbf{r}, t) = e^{i(\mathbf{k}^{(+)}\cdot\mathbf{r}-\omega t)} + e^{i(\mathbf{k}^{(-)}\cdot\mathbf{r}-\omega t)} = e^{i(k_x\cdot x-\omega t)}[e^{ik_y\cdot y} + e^{-ik_y\cdot y}] \quad (28)$$

The result in xy -plane is a Transverse-Electric-(TE)-mode \mathbf{E} -field with plane-normal z -component E_z that vanishes on metallic floor and ceiling ($y=\pm Y/2$) of the waveguide.

$$E_z(\mathbf{r}, t)=e^{i(k_x\sin\sigma-\omega t)}2\cos(ky\cos\sigma)|_{y=\pm\frac{Y}{2}}=0 \quad \text{implies:} \quad k\frac{Y}{2}\cos\sigma=n\frac{\pi}{2} \quad (29)$$

Fig. 20 shows two cases of lowest ($n=1$) guide modes with Occam-sword geometry. Projection $Y\cos\sigma$ of floor-to-ceiling Y onto $\mathbf{k}^{(\pm)}$ -vectors is shown by right triangles at guide ends (29) to be $\frac{\pi}{k} = \frac{\lambda}{2}$, that is a half wave $\frac{\lambda}{2}$. Waveguide angle σ and dispersion function $v(\kappa)$ follows.

$$v = c\kappa = c\sqrt{\kappa_x^2 + \kappa_y^2} = c\sqrt{\kappa_x^2 + \kappa^2\cos^2\sigma} = \sqrt{c^2\kappa_x^2 + \left(\frac{c}{2Y}\right)^2} = \sqrt{c^2\kappa_x^2 + v_A^2} \quad (30)$$

Surprising insight into Fig. 20 waves results if we note it is what Bob sees if Alice and Carla point their $v_A=600\text{THz}$ 2-CW beam *across* Bob's x -line of motion at angle σ to y and not *along* x as in Fig. 9b. Bob can Doppler shift his wave-number κ_x and angle σ to zero and reduce frequency v in (30) to $v = v_A$.

Then Bob will be co-moving with Alice and Carla and see Alice's $\mathbf{k}^{(+)}$ -vector at zero aberration angle ($\sigma = 0$) if she is below Fig. 20 beaming straight up the y -axis. Meanwhile, Carla's $\mathbf{k}^{(-)}$ -vector points straight down. For ($\sigma = 0$) the wave given by (29) is a y -standing wave of wavelength $\lambda_A=2Y$ between Alice and Carla and not just a half-wave section ($Y=\frac{\lambda}{2}$) modeling a lowest mode of this xy -wave guide.

Ideally Alice and Carla's laser mode viewed along y looks like their x -standing wave in Fig. 9b or Fig. 10b and appears the same over its x -beam-width by having zero x -wave

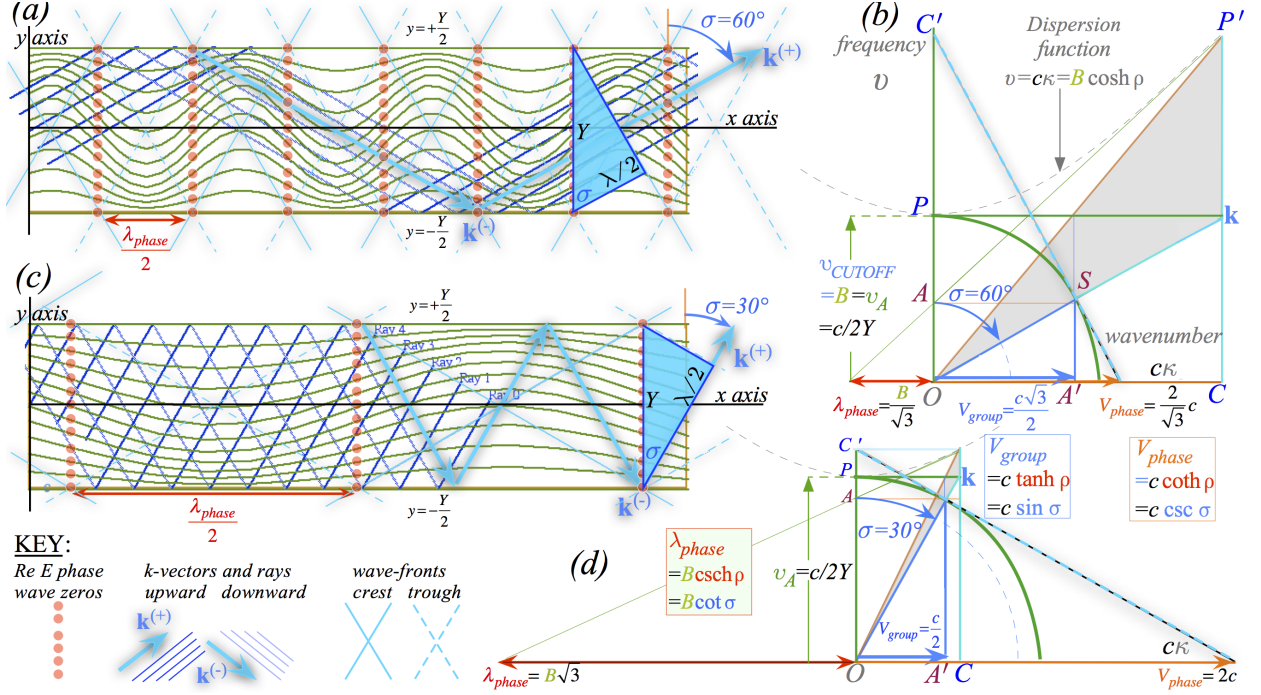


FIG. 20: TE-Waveguide and Occam sword geometry for stellar angle (a-b) $\sigma = 60^\circ$ and (c-d) $\sigma = 30^\circ$.

number $\kappa_x = \kappa_A \sin \sigma = 0$). Zero- κ_x or infinite x -wavelength ($\lambda_x = \lambda_A \csc \sigma = \infty$) is a flat-line wave parallel to the x -axis oscillating at Alice's (or Carla's) 600THz frequency v_A .

This x -flat wave is better known in wave guide theory as a *cut-off-frequency* mode where the cut-off-frequency $v_{\text{CUTOFF}} = \frac{c}{2Y} = v_A$ is the lower bound to frequency that can enter a waveguide of width Y . In Fig.20b it corresponds to dispersion function bottom point B (or P) that is well separated from its phase point P' in the upper left of the figure. That separation $|\mathbf{OC}| = B \sinh \rho = B \tan \sigma$ gives a mode in Fig.20a that is more robust than the near-cutoff mode in Fig. 20c having less $|\mathbf{OC}|$ and a more 'bouncy' \mathbf{k} -vector in Fig.20c-d.

The $\tan \sigma$ -column of Table II represents the phase wave-number ratio $\kappa_{\text{phase}}/\kappa_A$ of Bob's κ_{phase} to κ_A that Alice and Carla claim is their output. Later it is shown that $|\mathbf{OC}| = \kappa_x$ is mode wave *momentum* while vertical interval $|\mathbf{CP}'| = B \cosh \rho = B \sec \sigma = v_{\text{phase}}$ or phase frequency ratio v_{phase}/v_A in Table II correspond to mode carrier wave *energy*. These determine wave robustness and phase velocity V_{phase}/c is equal to their per-space-time ratio $v_{\text{phase}}/\kappa_{\text{phase}}$ or their space-time ratio $\lambda_{\text{phase}}/\tau_{\text{phase}}$.

The importance of waveguide phase or carrier behavior is matched by that of group or

signal wave dynamics. Each has six of twelve variables listed in Table II. Matching phase velocity $V_{phase}/c = \coth\rho = \csc\sigma$ is reciprocal to $V_{group}/c = \tanh\rho = \sin\sigma$. Both are indicated by arrow lengths at the base of Occam Sword plots in Fig. 20b or Fig. 20d. The latter has V_{group} much lower than V_{phase} while the former has both closing in on light speed c .

Group velocity V_{group} equals projection $c \sin\sigma$ of $c\hat{\mathbf{k}}$ -vector onto the waveguide x-axis. One may imagine a signal bouncing off guide floor or ceiling riding on the \mathbf{k} -vectors normal to phase wavefronts moving at speed c along $\mathbf{k}^{(+)}$ or $\mathbf{k}^{(-)}$ in Fig. 20a or Fig. 20c. So a signal wastes time bouncing around the guide x -axis while the phase crests proceed via a greater speed $c \csc\sigma$. A signal may be imagined as an extra wrinkle in symmetry of identical wave crests due to lately added Fourier components limited by envelope group velocity as an established underlying phase maintains Evenson's c -lockstep. Per-space-time $(v, c\kappa_x)$ geometry of Fig. 20b or Fig. 20d rules that of space-space (x, y) in Fig. 20a or Fig. 20c.

2. Wave parameter variation with group velocity

As relative group velocity u/c or rapidity ρ grows, so do most of the eight wave-ratio variables listed in Table II with some approaching infinity while others approach zero. Fig. 21 shows a plot of those eight quantities versus group velocity ($u/c = V_{group}/c$) with their values for $u/c = 3/5$ appearing mid-plot in the order listed in Table II.

There near $u/c = 3/5 = 0.6$, the function pair $\operatorname{csch}\rho$ and $\operatorname{cosh}\rho$ and pair $\operatorname{sech}\rho$ and $\sinh\rho$ are close to their respective crossing points one above the other on the vertical line $u/c = G_-$ where the sub-unit Golden Mean is $G_- = \frac{\sqrt{5}-1}{2} = 0.618\dots$ is a root pair with $G_+ = \frac{\sqrt{5}+1}{2} = 1.618\dots$

The sech - \sinh pair cross at the Golden Root $\sqrt{G_-} = 0.7862\dots$ and csch - \cosh pair cross at inverse root $\sqrt{G_+} = 1/\sqrt{G_-} = 1.272\dots$ of G_+ . The $\operatorname{csch}\rho$ and $\tanh\rho$ pair cross at plot point $(\frac{u}{c} = \sqrt{G_-}, y = \sqrt{G_-})$. The \sinh - \coth pair cross at $(\frac{u}{c} = \sqrt{G_-}, y = \sqrt{G_+})$.

Between the "Golden" intersections are three more crossing points on the vertical line $\frac{u}{c} = x = \frac{1}{\sqrt{2}}$. They are sech - \tanh at $y = \frac{1}{\sqrt{2}}$, csch - \sinh at $y=1$, and cosh - \coth at $y = \sqrt{2}$. Crossings correspond to a singular case of symmetry in a trigonometric map like Fig. 19.

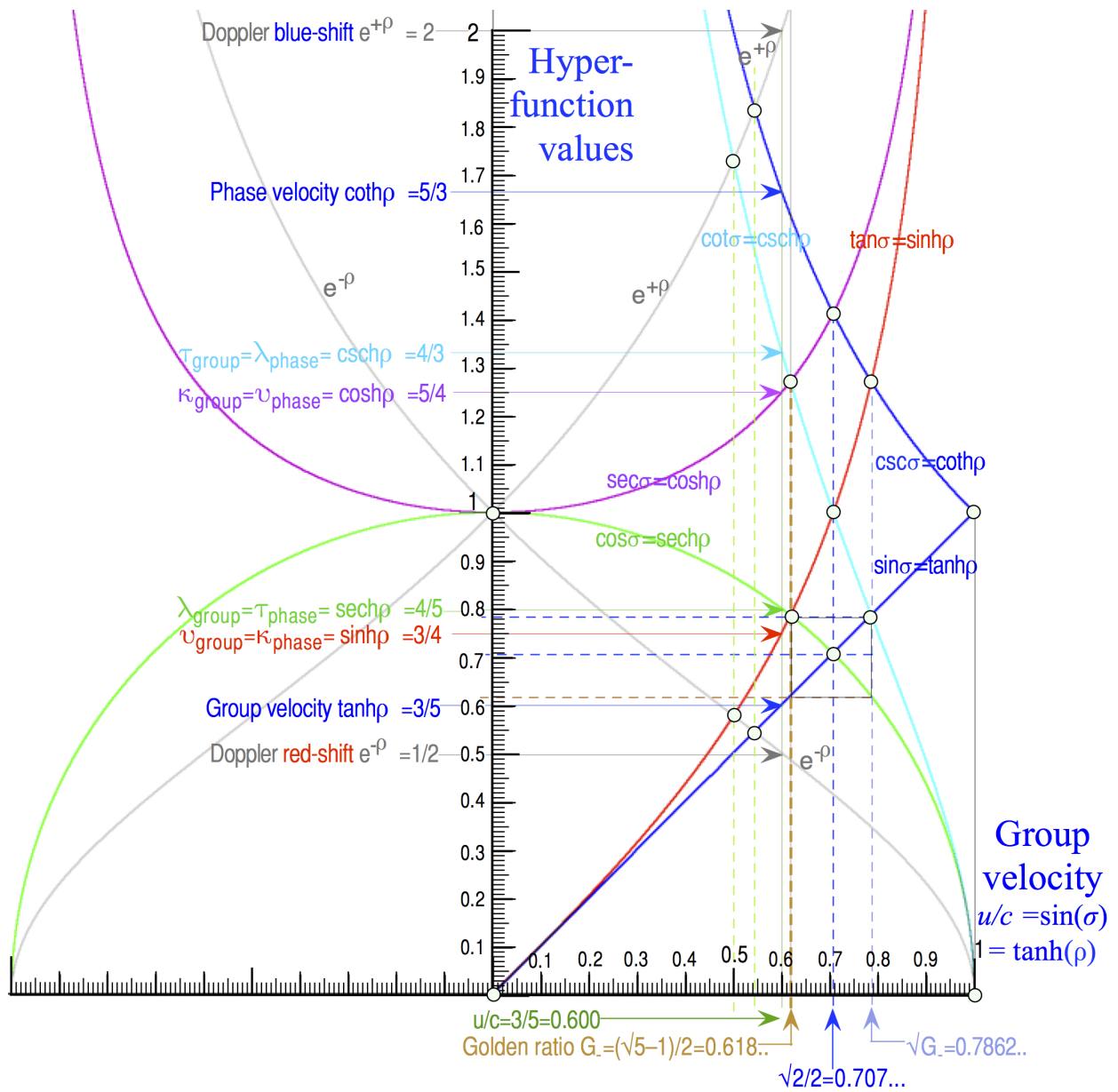


FIG. 21: Plot of Table II values versus group velocity u/c . (List is labeled for $u/c = 3/5$.)

3. Table II - Relativity ratios versus rapidity- ρ , guide angle- σ , and $\beta=u/c$

<i>group</i>	$b_{RED}^{Doppler}$	$\frac{V_{group}}{c}$	$\frac{v_{group}}{v_A}$	$\frac{\lambda_{group}}{\lambda_A}$	$\frac{\kappa_{group}}{\kappa_A}$	$\frac{\tau_{group}}{\tau_A}$	$\frac{c}{V_{group}}$	$b_{BLUE}^{Doppler}$
<i>phase</i>	$\frac{1}{b_{BLUE}^{Doppler}}$	$\frac{c}{V_{phase}}$	$\frac{\kappa_{phase}}{\kappa_A}$	$\frac{\tau_{phase}}{\tau_A}$	$\frac{v_{phase}}{v_A}$	$\frac{\lambda_{phase}}{\lambda_A}$	$\frac{V_{phase}}{c}$	$\frac{1}{b_{RED}^{Doppler}}$
<i>rapidity</i> ρ	$e^{-\rho}$	$\tanh \rho$	$\sinh \rho$	$\operatorname{sech} \rho$	$\cosh \rho$	$\operatorname{csch} \rho$	$\operatorname{coth} \rho$	$e^{+\rho}$
<i>stellar</i> ∇ <i>angle</i> σ	$1/e^{+\rho}$	$\sin \sigma$	$\tan \sigma$	$\cos \sigma$	$\sec \sigma$	$\cot \sigma$	$\csc \sigma$	$1/e^{-\rho}$
$\beta \equiv \frac{u}{c}$	$\sqrt{\frac{1-\beta}{1+\beta}}$	$\frac{\beta}{1}$	$\frac{1}{\sqrt{\beta^2-1}}$	$\frac{\sqrt{1-\beta^2}}{1}$	$\frac{1}{\sqrt{1-\beta^2}}$	$\frac{\sqrt{\beta^2-1}}{1}$	$\frac{1}{\beta}$	$\sqrt{\frac{1+\beta}{1-\beta}}$
<i>value for</i> $\beta=3/5$	$\frac{1}{2}=0.5$	$\frac{3}{5}=0.6$	$\frac{3}{4}=0.75$	$\frac{4}{5}=0.80$	$\frac{5}{4}=1.25$	$\frac{4}{3}=1.33$	$\frac{5}{3}=1.67$	$\frac{2}{1}=2.0$

TABLE II: Includes rapidity- ρ and Stellar angle- σ parameters

VI. RELATIVITY GIVES BASIC WAVE MECHANICS OF MATTER

Since the last century, fundamental developments of quantum mechanics have relied on concepts from advanced classical mechanics of Lagrange, Hamilton, Legendre, Jacobi, and Poincare that were developed mostly in the preceding(19th) century. The latter contain a formidable web of formalism using ecclesiastical terms such as *canonical* that once implied higher levels of truthiness, but for modern physics students, they mean not so much.

Below is a simpler approach that connects wave geometry of Sec. IV to 16th through 18th century mechanics of Galileo, Kepler, and Newton and then derives mechanics fundamentals for the 20th and 21st centuries. It also clarifies some 19th century concepts that are often explained poorly or not at all. This includes Legendre contact transformations, canonical momentum, Poincare invariant action, and Hamilton-Jacobi equations. Understanding of these difficult classical ideas and connections is helped by wave geometry or *relawavity*.

2-CW geometry of Fig. 19 has hyperbolic coordinates of phase frequency $v_{phase}=B\cosh\rho$ and c -scaled wave number $c\kappa_{phase}=B\sinh\rho$ with slope equal to group velocity $V_{group}/c=u/c=\tanh\rho$. Each depends on rapidity ρ that approaches u/c for Galilean-Newtonian speeds $u\ll c$.

$$\begin{aligned} v_{phase} &= \cosh \rho \approx B + \frac{1}{2}B\rho^2 & (\text{for } u \ll c) \\ c\kappa_{phase} &= \sinh \rho \approx B\rho & (\text{for } u \ll c) \\ u/c &= \tanh \rho \approx \rho & (\text{for } u \ll c) \end{aligned} \quad (31)$$

At these low speeds κ_{phase} and v_{phase} are functions of group velocity $u=c\rho$ or $u^2=c^2\rho^2$. The hyperbolic base coefficient B has frequency units ($1Hz=1s^{-1}$) of v_{phase} and $c\kappa_{phase}$ so B/c^2 multiplies u^2 and u .

$$v_{phase} \approx B + \frac{1}{2}[B/c^2]u^2 \quad \Leftarrow \text{for } (u \ll c) \Rightarrow \quad \kappa_{phase} \approx [B/c^2]u \quad (32)$$

From freshman physics is recalled kinetic energy $KE=const.+ \frac{1}{2} Mu^2$ and Galilean momentum $p=Mu$. One *Joule·s* scale factor $h=Mc^2/B$ gives v_{phase} energy units and κ_{phase} momentum units. Then these wave coordinates give classical KE and p formulas. But, an annoying (and large) constant Mc^2 is added to KE !

$$hv_{phase} \approx Mc^2 + \frac{1}{2}Mu^2 \quad \Leftarrow \text{for } (u \ll c) \Rightarrow \quad h\kappa_{phase} \approx Mu \quad (33)$$

One may ask, “Is this just a lucky coincidence?”

The answer involves the base or bottom value $B=v_A$ of Alice’s frequency hyperbola. It is also Bob’s bottom due to hyperbola invariance to ELT. The constant $const.=hB=hv_A=Mc^2$ may be the most famous formula in physics. Here it is Einstein’s rest-mass-energy equation. It is an add-on to Newton’s kinetic energy $\frac{1}{2}Mu^2$ that is perhaps the *second* most famous physics formula. This add-on does not contradict Newton’s result. Physical effects depend only on *difference* or *change* of energy so any add-on constant (*const.*) has no observable effect. The question of false coincidence criticizes (33) for Galilean-Newtonian formulas valid only at low velocity ($u\ll c$) and low ρ . The approximate v_{phase} and κ_{phase} in (33) need to be replaced by Table 2 formulas $v_{phase} = B\cosh\rho$ and $c\kappa_{phase} = B\sinh\rho$ that hold for *all* ρ .

$$\begin{aligned} E = hv_{phase} = Mc^2 \cosh \rho & \quad \Leftarrow \text{for all } \rho \Rightarrow & \quad p = h\kappa_{phase} = Mc \sinh \rho \\ & = \frac{Mc^2}{\sqrt{1 - u^2/c^2}} & \quad \Leftarrow \text{for } |u| < c \Rightarrow & \quad = \frac{Mu}{\sqrt{1 - u^2/c^2}} \end{aligned} \quad (34)$$

The old-fashioned $\beta=u/c$ form of $\cosh\rho$ (Table 2) is Einstein²² 1905 total energy formula. Later in 1923, DeBroglie gives wave momentum formula²³ $p = \hbar k = h\kappa$ that has a $\beta=u/c$ form for $\sinh\rho$, too. Three lines above derive both ρ -forms from Table II. This allows physics students to enjoy one-button-press calculator-recall as well as the geometric and algebraic elegance of relativity discussed below.

Underlying (34) is considerable physics and mystery of “scale factor” h (or $\hbar \equiv h/2\pi$) the Planck constant $h=6.62607\cdot 10^{-34}$ Joule·sec that appears in his cavity energy axiom $E_N=hNv$. Thus (34) gives just the lowest quantum level ($N=1$) of Planck’s axiom²⁴. (Modern form $E_N=N\omega$ has angular frequency $\omega=2\pi v$ and angular $=1.05\cdot 10^{-34}$ Js.) A quick-fix replaces h with hN , but underlying quantum oscillator theory of electromagnetic cavity waves still needs to be discussed later in Sec. X.

So far, the only axioms needed by SR results (34) are Evenson’s (*All colors go c!*) and time reversal symmetry following Fig. 7 and Fig. 8. These involve space, time, frequency and phase factors of plane light waves that are sufficient to develop the special relativity theory. But this phase approach has so far ignored amplitude factor A of light wave $\Psi = Ae^{i(\mathbf{k}\cdot\mathbf{r}-\omega t)}$. While phase factor $e^{i(\mathbf{k}\cdot\mathbf{r}-\omega t)}$ describes the *quality* aspects of the light, an amplitude factor A describes the *quantity* of light, or more to the point, an average number N of *quanta* or *photons* in a wave having the N factor of Planck’s axiom. Raising N raises overall phase frequency Nv_{phase} and in proportion, both total energy hNv_{phase} and total wave *quantum-mass* $M_N = (hNv_{phase})/c^2$. (As seen below, this “light-weight” is tiny unless N

is astronomical.)

The logical efficiency of optical axioms leading to (34) sheds some light on the three of the most logically opaque concepts of physics, namely energy, momentum and mass by expressing them as phase frequency ν (inverse time τ) and wavenumber κ (inverse length λ). Perhaps, the terms *energy* and *momentum* could someday go the way of *phlogiston*!

A. What *is* energy?

Once I asked a professor lecturing on energy, “What is *Energy*?” He replied, “It measures ability to do *Work*.” So, I asked, “What is *Work*?” He replied, “Well, it’s *Energy*, of course!”

Probably, he would give the same circular logic if asked about *momentum*, another *sine qua non* of basic physics. A favorite flippant response to E and p questions is that momentum is the “*Bang*” and energy is the *\$Buck\$* that pays for it. ($\$1.00=10kWhr$ is close to national average.) This makes sense given an (unfortunate) U.S expression “Get more bang for your buck!” but only on the 4th of July.

Wave energy and momentum results (34) defeat such circular logic by showing how energy E is proportional to temporal frequency (ν_{phase} waves per second) and momentum p_α is proportional spatial frequency (κ_{phase} waves per meter in direction α). One should note the ratio of momentum p and energy E in (34) is $\frac{cp}{E} = \frac{ck}{\omega} = \frac{u}{c}$. It is a wave velocity relation for any scale-factor h (or hN).

The answer in (34) for wave energy inside Alice’s laser cavity is a product of her quantum tick-rate $\nu_{phase}=\nu_A=600THz$, scale factor h (actually hN), and Einstein dilation factor $\cosh\rho$ that is $\cosh 0=1$ for her and $\cosh\rho=\frac{5}{4}$ for Bob in Fig. 10b. Bob might complain about her $\frac{4}{5}$ -shortened wavelength $\lambda_{group} = (\frac{1}{2}\mu m)sech\rho = \frac{1}{2}\frac{4}{5}\mu m$ instead of complimenting her for $\frac{5}{4}$ more wave energy. (When you can’t say something nice...) Bob may not see her considerable increase of momentum from zero ($\sinh 0=0$) to

$$p = hN\kappa_{phase} = hN\kappa_A \sinh \rho = hN\frac{\nu_A}{c}\frac{3}{4}$$

He could be excused for overlooking such a tiny momentum. (p has a $\frac{1}{c}$ -factor that E lacks.)

$$E = hN\nu_A \cosh \rho = hN\nu_A\frac{5}{4}$$

A most remarkable thing about (energy, momentum) $\propto (\nu_{phase}, \kappa_{phase})$ relations (34) (now

with hN in for h) and the Alice-Bob story is that (34) applies not just to Alice's light wave but also to its laser cavity frame. (Recall discussion after Fig. 11.) In fact *any* mass M (including Alice and Bob themselves) is made of waves with an internal "heartbeat" frequency $v_{phase}=Mc^2/Nh$ that is *incredibly* fast due to the c^2 -factor and tiny Planck- h divisor. Also, Alice's light wave with $v_{phase}=v_A$ has a mass $M_A = Nhv_A/c^2$ that is *incredibly* tiny here due to *both* a tiny Planck- h factor and enormous c^2 -divisor.

1. *What's the matter with energy?*

Evenson axioms of optical dispersion and time symmetry imply a 2-CW light geometry that leads directly to exact mass-energy-momentum and frequency relations (34) with low-speed approximations (33). A light wave with rest mass and rest energy proportional to a proper invariant phase frequency

$$v_{phase} = v_A = v'_A$$

is effectively a quantum matter wave. Its phase frequency gives its intrinsic rest mass.

$$M_{A_N} = Nhv_A/c^2$$

In so doing, concepts of mass or matter lose classical permanence and become fungible. We define three types of mass M_{rest} , M_{mom} , and M_{eff} distinguished by their dependence on ρ or velocity u . The first is $M_{rest}=M_{A_N}$. The other two approach M_{rest} at low $u \ll c$. Einstein rest mass M_{A_N} is invariant to ρ . It labels a hyperbola with a bottom base level B .

$$E_N(\rho = 0) = hB = M_{A_N}c^2$$

This label is respected by all observers including Alice and Bob. Each mode A of Alice's cavity has a stack of $N=1,2,3,\dots$ hyperbolas, one for each quantum number N -value.

$$\begin{aligned} E_N^2 &= (hNv_A)^2 = (M_{A_N}c^2)^2 \cosh^2 \rho = (M_{A_N}c^2)^2 (1 + \sinh^2 \rho) \\ &= (M_{A_N}c^2)^2 + (cp_N)^2 \end{aligned} \quad (35)$$

(E, cp) -space hyperbola $E = \sqrt{(Mc^2)^2 + (cp)^2}$ in Fig. 22 is a plot of an exact Einstein-Planck matter wave dispersion (34). The inset is a plot of approximation (32) for low p and $u \ll c$. Difficulties of this *Bohr*²⁵-*Schrodinger*²⁶ *approximation* are discussed later.

The second type of mass M_{mom} is *momentum-mass* defined by ratio p/u of relativistic momentum $p=Mc \sinh$ from (34) with group velocity $u=c \tanh\rho$. M_{mom} satisfies Galileo's old definition $p=M_{mom} u$, but now using the newly defined relativistic wave quantities.

$$\begin{aligned} \frac{p}{u} &\equiv M_{mom} = \frac{M_{rest}c}{u} \sinh \rho = M_{rest} \cosh \rho \xrightarrow{u \rightarrow c} M_{rest}e^\rho/2 \\ &= \frac{M_{rest}}{\sqrt{1-u^2/c^2}} \xrightarrow{u \ll c} M_{rest} \end{aligned} \quad (36)$$

The third type of mass M_{eff} is *effective-mass* defined by ratio dp/du of *change* of momentum $p=Mc \sinh\rho$ from (34) with *change* of group velocity $du = c \operatorname{sech}^2\rho d\rho$. M_{eff} satisfies Newton's quite old definition $F=M_{eff} a$, but now using relativistic wave quantities.

$$\frac{F}{a} \equiv M_{eff} \equiv \frac{dp}{du} = \frac{dp}{d\rho} \Big/ \frac{d\rho}{du} = M_{rest}c \cosh \rho / c \operatorname{sech}^2\rho = M_{rest} \cosh^3\rho \quad (37)$$

Another derivation of M_{eff} uses group velocity $V_{group} = \frac{dv}{d\kappa} = u$ as the independent variable.

$$\begin{aligned} \frac{F}{a} &\equiv M_{eff} \equiv \frac{dp}{du} = \frac{hd\kappa}{dV_{group}} = h \Big/ \frac{d}{d\kappa} \frac{dv}{d\kappa} = h \Big/ \frac{d^2v}{d\kappa^2} \\ &= M_{rest} \Big/ (1-u^2/c^2)^{3/2} \xrightarrow{u \ll c} M_{rest} \end{aligned} \quad (38)$$

Group velocity and its tangent geometry is a crucial but hidden part of the matter wave theory. Physicists tend to commit to memory a derivative formula $\frac{dv}{d\kappa} = \frac{d\omega}{dk}$ for group velocity and forget $\frac{\Delta v}{\Delta\kappa} = \frac{\Delta\omega}{\Delta k}$ that is a finite-difference formula from which it is derived. This may give wrong results since the latter is *exact* for discrete frequency spectra while the former may be ill-defined. The wave Minkowski coordinate geometry starts with half-difference ratios to give V_{group} in primary u -formulae (15) and (16).

$$V'_{group}/c = \frac{\Delta v}{c\Delta\kappa} = \frac{v_R - v_L}{v_R + v_L} = \frac{e^\rho - e^{-\rho}}{e^\rho + e^{-\rho}} = \tanh \rho \quad (39)$$

What follows in Fig. 10 through Fig. 12 and Fig. 19 is based entirely upon the more reliable finite-difference definition $\frac{\Delta v}{\Delta\kappa} = \frac{\Delta\omega}{\Delta k}$ that gives exactly desired slope.

Nevertheless, Nature is kind to derivative definition $\frac{dv}{d\kappa} = \frac{d\omega}{dk}$ as seen in Fig. 19. There hyperbolic tangent slope of line **RL** with altitude $\Delta v = v_R - v_L$ and base $\Delta\kappa = \kappa_R - \kappa_L$ has a finite-difference slope exactly equal to the derivative of the hyperbola at tangent point **P'** on phase velocity line **OP'**. Geometry of Doppler action (39) is at play. That slope $\frac{dv}{d\kappa} = \frac{d\omega}{dk}$ equals $V_{group} = u$ and is the velocity of Alice relative to Bob. It is also related to the momentum/energy ratio $\frac{cp}{E} = \frac{ck}{\omega} = \frac{u}{c}$ noted before.

$$V_{group} = u = \frac{\Delta v}{\Delta\kappa} = \frac{dv}{d\kappa} = \frac{d\omega}{dk} = \frac{dE}{dp} = \frac{c^2 p}{E} \quad (40)$$

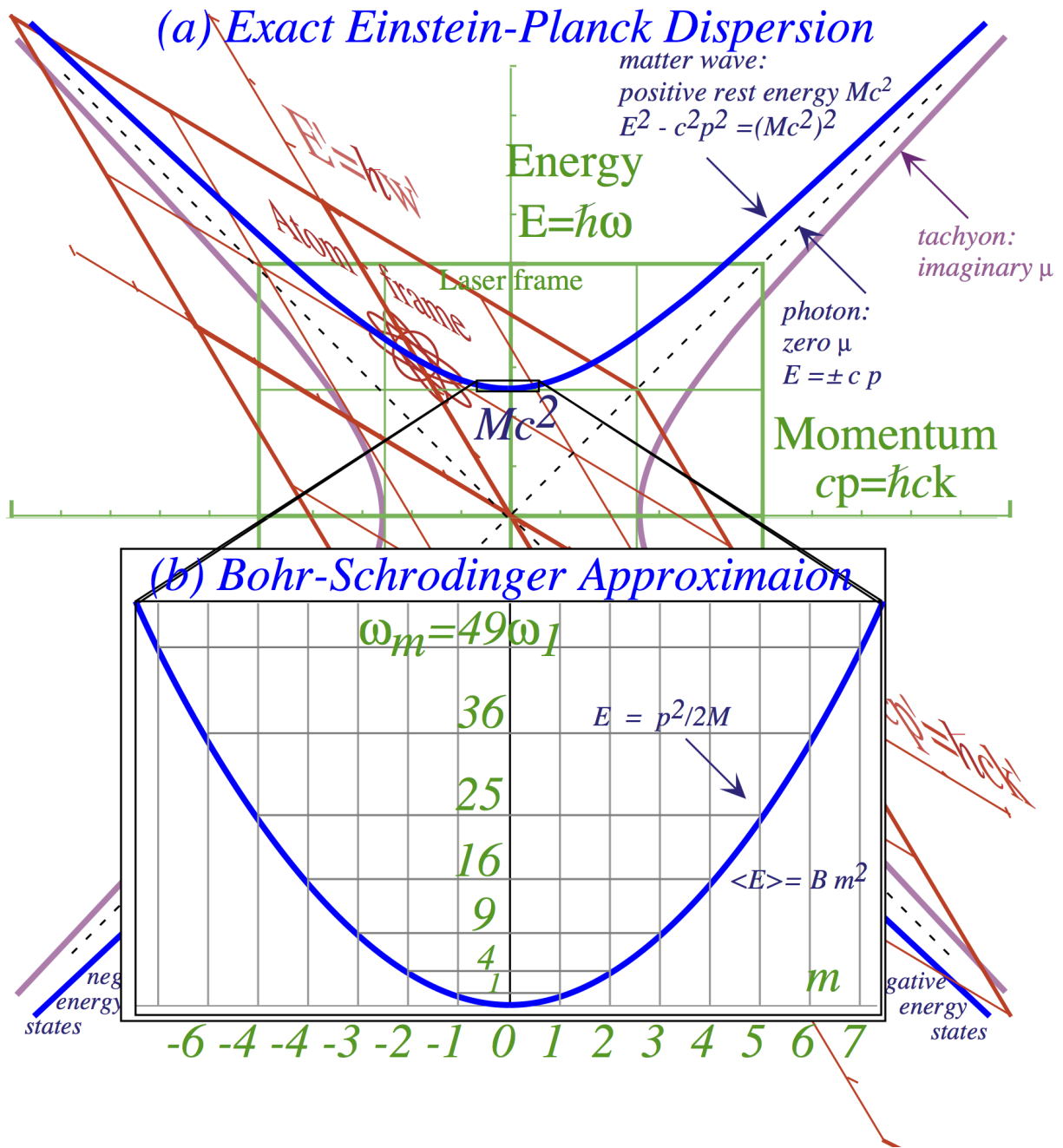


FIG. 22: (a) Einstein-Planck energy-momentum dispersion (b) Bohr-Schrodinger approximation

As slope $\frac{dv}{d\kappa} = u$ of dispersion hyperbola $v(\kappa)$ affects velocity u and relations with momentum p , so does curvature $\frac{d^2v}{d\kappa^2}$ affect acceleration a and its relation to force F or momentum time rate of change $\frac{dp}{dt}$ in the effective-mass M_{eff} equations (37) and (38). One is inclined to regard M_{eff} as a quantum mechanical result since it is a product of Planck constant h with

inverse $\frac{d^2v}{d\kappa^2}$ the approximate *Radius of Curvature* $RoC=1/\frac{d^2v}{d\kappa^2}$ of dispersion function $v(\kappa)$. Geometry of a dispersion hyperbola $v = v_A \cosh \rho$ is such that its bottom ($\rho = 0 = u$) radius of curvature RoC equals the rest frequency $v_A = M_{rest}c^2/h$ that is labeled as the *b-circle* radius B in Fig. 19. Hyperbola curvature decreases as ρ increases, and so its RoC and M_{eff} grow according to (53) and (45) in proportion to exponential $e^{3\rho}$ as velocity u approaches c , three times faster than the e^ρ for high- ρ growth of momentum mass M_{mom} in (36).

2. How light is light?

Since 1-CW dispersion $v = \pm c\kappa$ is flat, its RoC and photon effective mass are infinite $M_{eff}^\gamma = \infty$. This is consistent with the Evenson's axiom prohibiting c -acceleration. (Pure colors *always* go c .) The other extreme is photon rest mass which is zero $M_{rest}^\gamma = 0$. Between these extremes, photon momentum-mass M_{mom}^γ depends on CW color or frequency v .

$$\begin{aligned}
 (a) \gamma - \text{rest mass: } M_{rest}^\gamma &= 0, \\
 (b) \gamma - \text{momentum mass: } M_{mom}^\gamma &= \frac{p}{c} = \frac{h\kappa}{c} = \frac{hv}{c^2} \\
 (c) \gamma - \text{effective mass: } M_{eff}^\gamma &= \infty.
 \end{aligned} \tag{41}$$

Newton's *Optics* text he rejects the wave nature of light in favor of a corpuscular one.

He described interference effects as light's "fits". Perhaps, light having three mass values in (40) would, for Newton, verify its schizophrenic insanity. Also, the fact that 2-CW 600THz cavity momentum \mathbf{p} must average to zero while each photon adds a tiny mass M_{mom}^γ , might support his corpuscular view.

$$M_{mom}^\gamma = \frac{hv}{c^2} = v(7.4 \cdot 10^{-51})kg \cdot s = 4.4 \cdot 10^{-36}kg \quad (\text{for: } v = 600\text{THz})$$

A 1-CW state has zero M_{rest}^γ , but 1-photon momentum (34) is a non-zero quantity $p^\gamma = M_{mom}^\gamma c$.

$$p^\gamma = h\kappa = \frac{hv}{c} = v(2.2 \cdot 10^{-42})kg \cdot m = 1.3 \cdot 10^{-27}kg \cdot m \cdot s^{-1} \quad (\text{for: } v = 600\text{THz})$$

In the form Galileo's $p^\gamma = M_{mom}^\gamma c$ is exact for light. It is another of "Galilean Revenge" like the exact Galilean addition (Fig.8) of rapidity ρ and of phase angular velocity ω (Fig. 9).

Photons are light! With numbers so tiny it is a wonder relativistic or quantum effects were ever noticed. That is so, unless the photon quantum number N is huge as in thermonuclear blast²⁷ or a star²⁸. Then light can be mega-tons.

VII. RELAWAVITY GEOMETRY OF HAMILTONIANS AND LAGRANGIAN

The 2-CW matter-wave in Fig.9 has a rest frame with origin $x' = 0$ and $k' = 0 = k_{phase}$ where the invariant phase function $\Phi = kx - \omega t = k'x' - \omega't'$ reduces to $\Phi = 0 - \varpi\tau$, a product of its proper or base frequency $B = \varpi = Mc^2/\hbar$ defined after (33) with proper time $t=\tau$ defined by (23). The (x,t) -differential of phase is reduced as well to a similar negative mass-frequency (ω)-term.

$$d\Phi = kdx - \omega dt = 0 \cdot 0 - \frac{Mc^2}{\hbar} d\tau \equiv -\varpi d\tau \quad (42)$$

A proper-time interval $d\tau$ dilates to ρ -moving frame time interval dt by Einstein dilation relations.

$$dt = \frac{d\tau}{\sqrt{1 - u^2/c^2}} = d\tau \cosh \rho \quad \Leftrightarrow \quad d\tau = dt \sqrt{1 - u^2/c^2} = dt \operatorname{sech} \rho \quad (43)$$

One of the interesting tales of modern physics is the first meeting²⁹ between Dirac³⁰ and the younger Richard Feynman³¹. Both had been working on aspects of quantum phase and classical Lagrangian mechanics. Dirac mused about some formulas in one of his papers that showed similarities between a Lagrangian function and quantum phase. Feynman said abruptly, “That’s because the Lagrangian *is* quantum phase!” That was a fairly radical bit of insight for the time. It deserves to have its geometry clarified.

A. Phase and action related to Lagrangian and Hamiltonian functions

Feynman’s observation has to have some units adjusted since Lagrangian L has *Joule* units of energy while phase Φ is a dimensionless invariant. A quantity S called *Action* is quantum phase Φ scaled by Planck’s angular constant $\hbar = \frac{h}{2\pi} = 1.05 \cdot 10^{-34} J \cdot s$ that is defined by the following time integral of L .

$$S \equiv \hbar \Phi \equiv \int L dt \quad \text{where:} \quad \hbar \equiv \frac{h}{2\pi} = 1.05 \cdot 10^{-34} \text{ Joule} \cdot \text{Second} \quad (44)$$

Differentials of action and phase (41) with time (42) combine to re-express Ldt .

$$dS \equiv Ldt = \hbar d\Phi = -Mc^2 d\tau = -Mc^2 \sqrt{1 - u^2/c^2} \cdot dt = -Mc^2 dt \operatorname{sech} \rho \quad (45)$$

From ρ -frame time derivative $dt/d\tau$ (41) arises the Lagrangian in terms of rapidity ρ or stellar angle σ .

$$L = -Mc^2 \sqrt{1 - u^2/c^2} = -Mc^2 \operatorname{sech} \rho = -Mc^2 \cos \sigma \quad (46)$$

Table II supplies identity $\text{sech}\rho = \cos\sigma$ for L in (45) and $\tanh\rho = \sin\sigma$ for group velocity u .

$$u \equiv V_{group} = c \tanh \rho = c \sin \sigma \quad (47)$$

A classical convention has Lagrangian L be explicit function of velocity. This is consistent with the low- $\rho \cong \frac{u}{c}$ approximation to Lagrangian (45) that recovers the Newtonian $KE = \frac{1}{2}Mu^2$ term in (33).

$$L = -Mc^2 \sqrt{1 - u^2/c^2} \xrightarrow{u \ll c} -Mc^2 + \frac{1}{2}Mu^2 + \dots \quad (48)$$

A following discussion of explicit functionality for Hamiltonian $H(p)$ and Lagrangian $L(u)$ involves the geometry of Legendre contact transformation depicted in Fig. 23a-b below and a Fig. 24 that follows.

B. Hamiltonian, Poincare invariants, and Legendre contact transformation

The invariant phase differential (41) with an \hbar -factor as in (44) is a key relation.

$$dS \equiv Ldt \equiv \hbar d\Phi = \hbar k dx - \hbar \omega dt \quad (49)$$

Energy $E = \hbar \omega_{phase} = \hbar \omega = H$ and momentum $p = \hbar \kappa_{phase} = \hbar k$ from (34) for $N=1$ are used.

$$dS \equiv Ldt \equiv \hbar d\Phi = p dx - Hdt \quad \Rightarrow \quad L = p \frac{dx}{dt} - H = p\dot{x} - H \quad (50)$$

Here energy E is identified with Hamiltonian function H . Results include the classical *Poincare differential invariant* $Ldt=pdx-Hdt$ and the *Legendre transform* $L=pu-H$ between Lagrangian L and Hamiltonian H . Remarkably, it shows L/Mc^2 is the negative reciprocal of H/Mc^2 .

$$H = \hbar \omega = Mc^2 \cosh \rho = Mc^2 \sec \sigma = \frac{Mc^2}{\sqrt{1 - u^2/c^2}} \quad (51a)$$

$$L = \hbar \dot{\Phi} = -Mc^2 \text{sech}\rho = -Mc^2 \cos \sigma = -Mc^2 \sqrt{1 - u^2/c^2} \quad (51b)$$

Except for a (-)sign, H and L are co-inverse (cos,sec)-cousin functions (mid-columns of Table II). So are Einstein t -dilation and Lorentz x -contraction, respectively. H is explicit function of momentum p and L is explicit function of velocity u . So are u and p a 1st *cousin* (sin,tan) pair in Table II. Group velocity is $u \equiv V_{group} = c \tanh \rho = c \sin \sigma$. Momentum follows.

$$cp = \hbar ck = Mc^2 \sinh \rho = Mc^2 \tan \sigma = \frac{Mc u}{\sqrt{1 - u^2/c^2}} \quad (52)$$

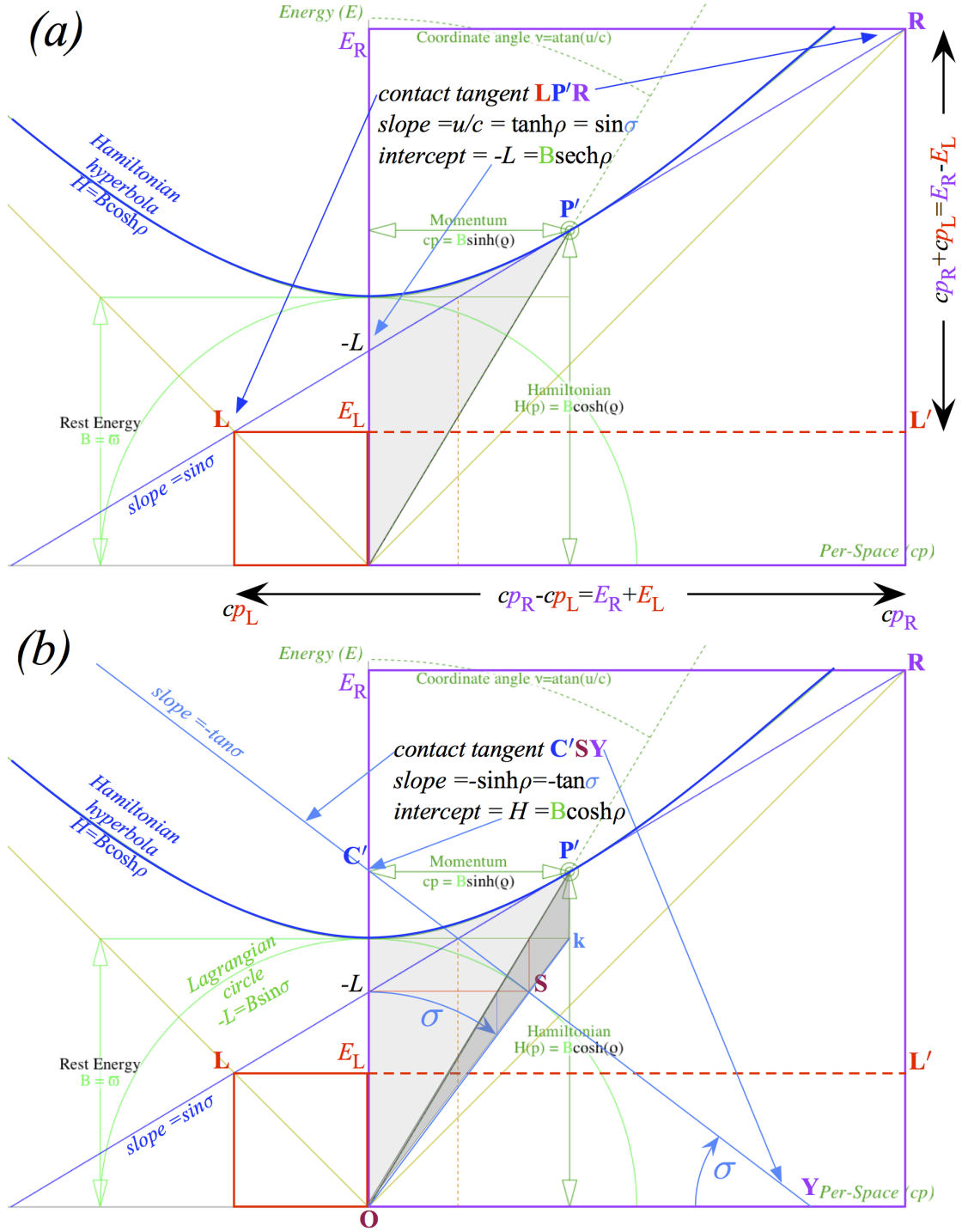


FIG. 23: (a) Slope,intercept($u/c,-L$) of $H(p)$ -tangent LP' give (u,L) point S on $L(u)$ -circle.
(b) Slope,intercept (cp,H) of $L(u)$ -tangent $C'S$ give (p,H) point P' on $H(p)$ -hyperbola.

Legendre contact transformation $H(cp) = pu - L = cpu/c - L$ uses slope u/c and intercept $-L$ of tangent line LR contacting H -hyperbola in Fig. 23a to locate contact point $L(u)$ of

Lagrangian plot. Inverse Legendre contact transformation $L(u)=pu-H$ uses slope p and intercept H of stellar tangent line **CSY** contacting the L -circle in Fig.23b to locate point $H(p)$ of Hamiltonian plot. This construction is further clarified by separate plots of $H(p)$ in Fig.24a and $L(u)$ in Fig.24b.

Tangent contact transformation is a concept based upon wave properties and goes back to the Huygens and Hamilton principles discussed below. The basics of this lie in construction of space-time (x,ct) wave-grids given frequency-**k**-vectors (ν,ck) like **P'** and **G'** in Fig.10. Each **P'** or **G'** coordinate pair (ν,ck) determines lines with speed ν/κ and t -intercept spacing $\tau=1/\nu$ on ct -axis while x -intercept spacing is $\lambda=1/\kappa$ on x -axis. These phase and group grid lines make Minkowski zero-line coordinates.

This geometry applies as well to energy-momentum $(E,cp)=h(\nu,ck)=(\omega,ck)$ spaces. Functional dependence of wave grid spacing and slopes determines classical variables, equations of motion, as well as functional *non*-dependence. For example, Lagrangian L is an explicit function of velocity u but *not* momentum p , that is, $\frac{\partial L}{\partial p} = 0$. Hamiltonian H is explicit function of momentum p but *not* velocity u , that is, $\frac{\partial H}{\partial u} = 0$. Such 0^{th} -equations combined with $L=pu-H$ give 1^{st} -Hamilton and 1^{st} -Lagrange equations.

$$0 = \frac{\partial L}{\partial p} = \frac{\partial}{\partial p}(pu - H) \Rightarrow u = \frac{\partial H}{\partial p} \quad \left(\begin{array}{l} \text{Hamilton's} \\ 1^{st} \text{ equation} \end{array} \right) \quad (53a)$$

$$0 = \frac{\partial H}{\partial u} = \frac{\partial}{\partial u}(pu - L) \Rightarrow p = \frac{\partial L}{\partial u} \quad \left(\begin{array}{l} \text{Lagrange} \\ 1^{st} \text{ equation} \end{array} \right) \quad (53b)$$

In Fig.23a slope of $H(p)$ -hyperbola at tangent point **P'** is group velocity $u/c=\tanh\rho=\sin\sigma=3/5$.

In Fig.23b slope of $-L(u)$ -circle at tangent point **S** is momentum $cp =B\sinh\rho =B\tan\sigma =(\text{Mc}^2)^{3/4}$ with a minus (-) sign. This minus sign in (50b) for Lagrangian $L=-\text{Mc}^2 \cos\sigma$, for example, is a result of (-) in basic phase $(kx-\omega t)$ and phasor conventions. (We like clocks to turn clockwise(\curvearrowright), too)

For a low- $(\rho \approx u/c)$ approximate Lagrangian (47), one may drop the $-\text{Mc}^2$ term and just keep the Newtonian kinetic energy term $(\frac{1}{2}Mu^2)$ that is equal to the corresponding kinetic term $(p^2/2M)$ in the approximate Hamiltonian. Of course, $p^2/2M$ reduces to $\frac{1}{2}Mu^2$ if approximate momentum $p=Mu$ is used, so students are well to ask, “Why are we so fussy about having only momentum p -dependence of H and only velocity u -dependence of L ?”

It is true that Hamiltonian $H(p)$ hyperbola minimum in Fig. 23 and Fig. 24a are nearly identical to the Lagrangian $L(u)$ circle minimum in Fig. 23b that lies below Fig. 24b. There

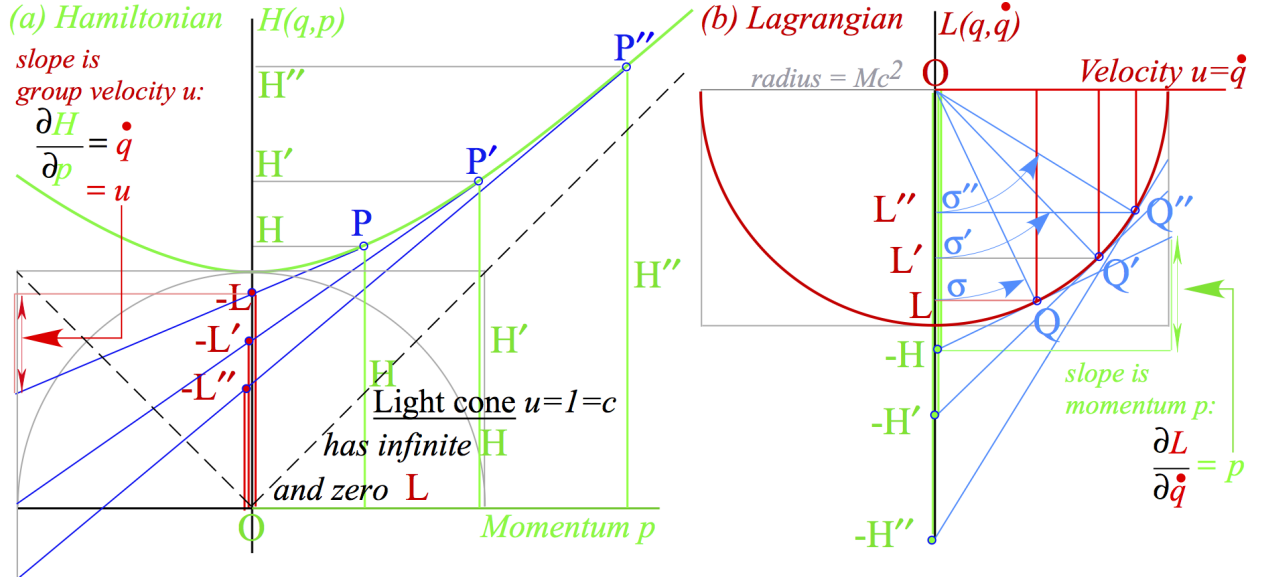


FIG. 24: Relativistic Legendre contact transformation between (a) Hamiltonian $H(p)$ (b) Lagrangian $L(u)$.

both curves are nearly parabolic. But, at higher speeds the Lagrangian $L(u)$ approaches zero precipitously as stellar angle σ approaches $\pi/2$ and velocity u approaches c . Meanwhile, Hamiltonian $H(p) = B \cosh \rho$ and its momentum $p = B \sinh \rho$ each approach $Be^\rho/2$ as rapidity ρ grows without bound.

So it should be clear that hyperbolic “Country-cousin” functions involving rapidity ρ and momentum p must share a Hamiltonian with infinite horizon, while circular “City-cousin” functions of the very restricted stellar angle $-\pi < \sigma < \pi$ and velocity $-c < u < c$ must share a localized Lagrangian that is the keeper of quantum phase.

The third (csc,cot)-cousin pair $\lambda_{phase} = B \csc \rho = B \cot \sigma$ and $V_{phase} = B \coth \rho = B \csc \sigma$ from Table II do not appear in any discussions of classical correspondence. Instead, these describe the phase part or “quantum guts” of a 2-CW internal structure, and as such were nonexistent for 19-century classicists, and one might add, still today a bit sketchy and hard to observe. Now that v_{phase} is seen as the heartbeat of quantum physics one may note DeBroglie wavelength λ_{phase} and velocity V_{phase} in Fig. 25 at the lower edges of geometric constructions just inside the Doppler blue shift ($b=e^\rho$)-bottom line of the **R** box.

One may compare Fig. 25 to Trigonometry Maps (TM) in Fig. 3 that share points $\mathbf{P} = \frac{1}{2}(\mathbf{R} + \mathbf{L})$ and $\mathbf{G} = \frac{1}{2}(\mathbf{R} - \mathbf{L})$. Fig. 3 exhibits fundamental and ancient geometry with trian-

gular relations that have fundamental roles in Fig. 25 in describing a *relativity* of relativistic quantum mechanics.

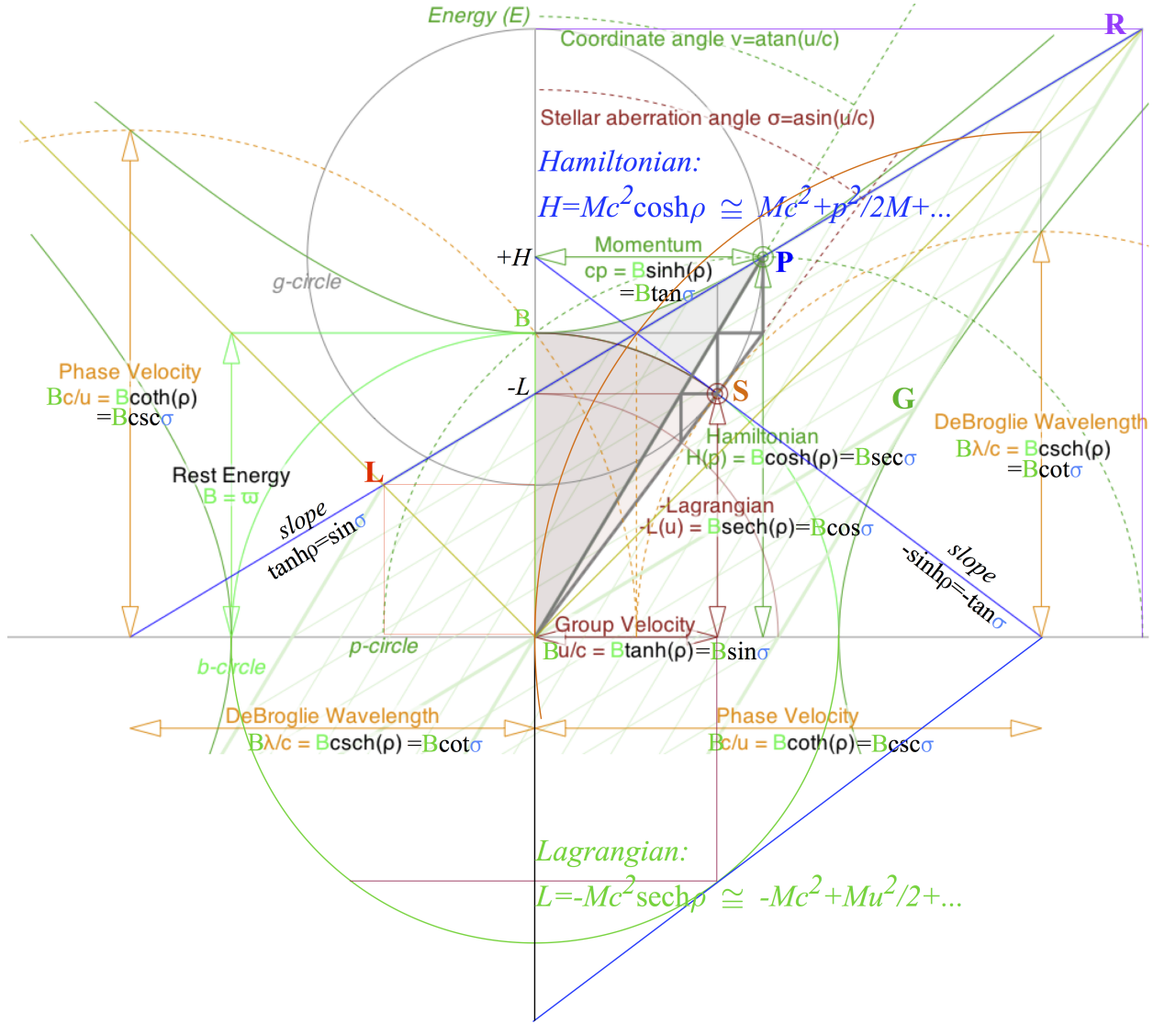


FIG. 25: Geometric elements of positive-energy relativistic quantum mechanics.

C. Hamilton-Jacobi quantization

Invariant phase Φ or action S differential (48) and (49) are integrable under certain conditions.

$$dS \equiv Ldt \equiv \hbar d\Phi = pdx - Hdt = \hbar kdx - \hbar \omega dt \quad (54)$$

Then each coefficient of a differential term dq in dS should be a corresponding partial derivative $\frac{\partial S}{\partial q}$.

$$\frac{\partial S}{\partial x} = p, \quad \frac{\partial S}{\partial t} = -H. \quad (55)$$

These are known as *Hamilton-Jacobi equations* for the phase action function S . Classical *HJ*-action theory was intended to analyze families of trajectories (PW or particle paths). Dirac and Feynman related this to matter-wave mechanics (CW phase paths) by proposing approximate semi-classical wavefunction Ψ based on Lagrangian action $S=\Phi$ in its phase.

$$\Psi \approx e^{i\Phi} = e^{iS/\hbar} = e^{i \int L dt/\hbar} \quad (56)$$

Approximation symbol (\approx) indicates that phase but not amplitude is expected to vary here. The *HJ* form $\frac{\partial S}{\partial x} = p$ turns x -derivative of Ψ into standard quantum \mathbf{p} -operator form $\mathbf{p} = \frac{\hbar}{i} \frac{\partial}{\partial x}$.

$$\frac{\partial}{\partial x} \Psi \approx \frac{i}{\hbar} \frac{\partial S}{\partial x} e^{iS/\hbar} = \frac{i}{\hbar} p \Psi \quad \Rightarrow \quad \frac{\hbar}{i} \frac{\partial}{\partial x} \Psi = \mathbf{p} \Psi \quad (57a)$$

The *HJ* form $\frac{\partial S}{\partial t} = -H$ turns t -derivative of Ψ similarly into Hamiltonian operator $\mathbf{H} = \hbar i \frac{\partial}{\partial t}$.

$$\frac{\partial}{\partial t} \Psi \approx \frac{i}{\hbar} \frac{\partial S}{\partial t} e^{iS/\hbar} = -\frac{i}{\hbar} \mathbf{H} \Psi \quad \Rightarrow \quad i\hbar \frac{\partial}{\partial t} \Psi = \mathbf{H} \Psi \quad (57b)$$

Action integral $S = \int L dt$ is to be minimized. Feynman's interpretation of this is depicted in Fig.26. Any mass M appears to fly so that its phase proper time τ is maximized. The proper mass-energy frequency $\omega = Mc^2/\hbar$ is constant for a mass M . Minimizing $-\varpi\tau$ is thus the same as maximizing $+\tau$. Clocks near light cone tick slowly compared ones near max- τ . Those on light cone do not tick!

One may explain how a flying mass finds and follows its max- τ path by imagining it is first a wave that could spread Huygen's wavelets out over many paths. But, an interference of Huygen wavelets favors stationary and extreme phase. This quickly builds constructive interference in the stationary phase regions where the the fastest possible clock path lies. Nearby paths contain a continuum of non-extreme or non-stationary wavelet phase that interfere *destructively* to crush wave amplitude off the well-beaten max- τ path as sketched in Fig.27.

The very "best" are so-called stationary-phase rays that are extremes in phase and thereby satisfy Hamilton's Least-Action Principle requiring that $S = \int L dt$ is minimum for "true" classical trajectories. This in turn enforces Poincare invariance by eliminating, by

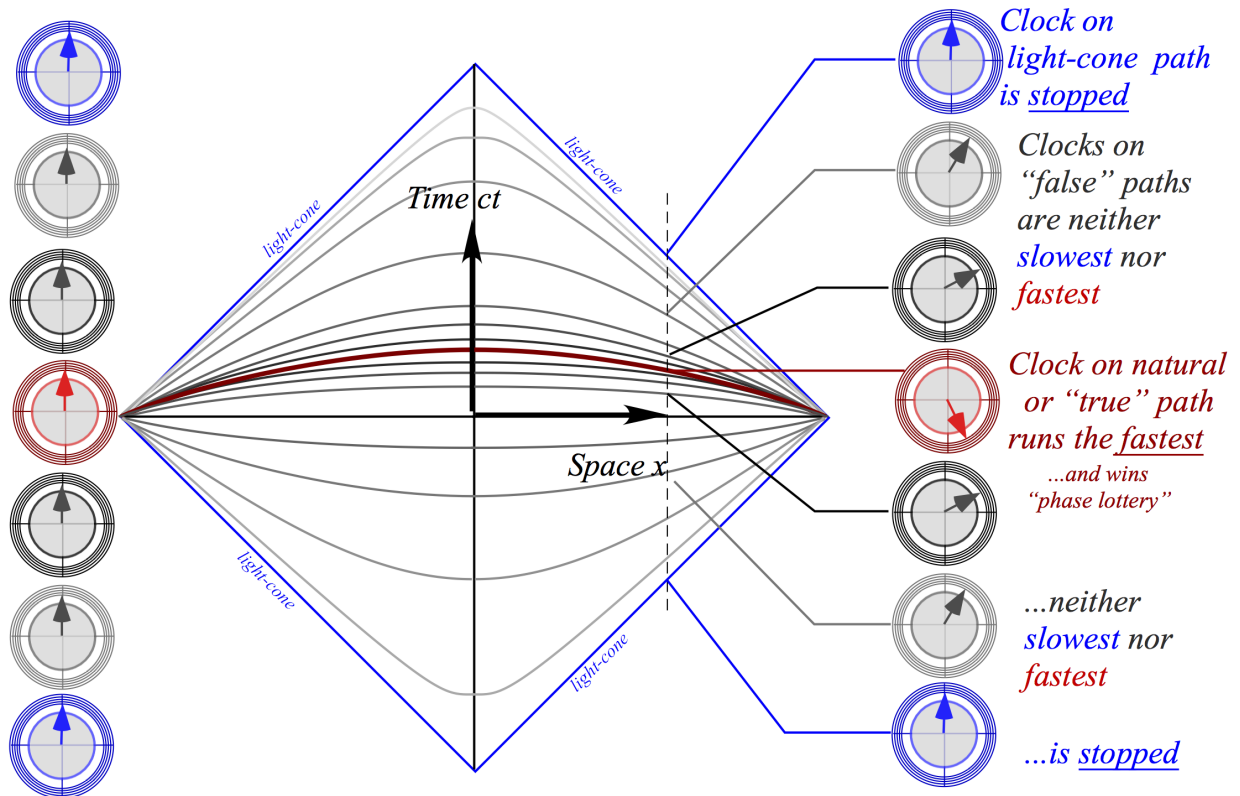


FIG. 26: Feynman’s flying clock contest winner has the greatest advance of time.

de-phasing, any “false” or non-classical paths because they do not have an invariant (and thereby stationary) phase. So “bad rays” cancel each other in a cacophonous mish-mash of mismatched phases.

Each Huygen wavelet in Fig. 27 is tangent to the next wavefront being produced. That contact point is precisely on a ray or true classical trajectory path of minimum action and on the resulting “best” wavefront. Time evolution from any wavefront to the next is thus a contact transformation between two wavefronts described by this geometry of Huygens Principle.

Thus a Newtonian clockwork-world appears to be the perennial cosmic gambling-house winner in a kind of wave dynamical lottery on an underlying wave fabric. Einstein’s God may not play dice³², but some persistently wavelike entities seem to be gaming at enormous Mc^2/\hbar -rates down in the cellar! And in so doing, geometric order is created out of chaos.

It is ironic that Evenson and other metrologists have made the greatest advances of precision in human history, not with metal bars or ironclad classical mechanics, but by

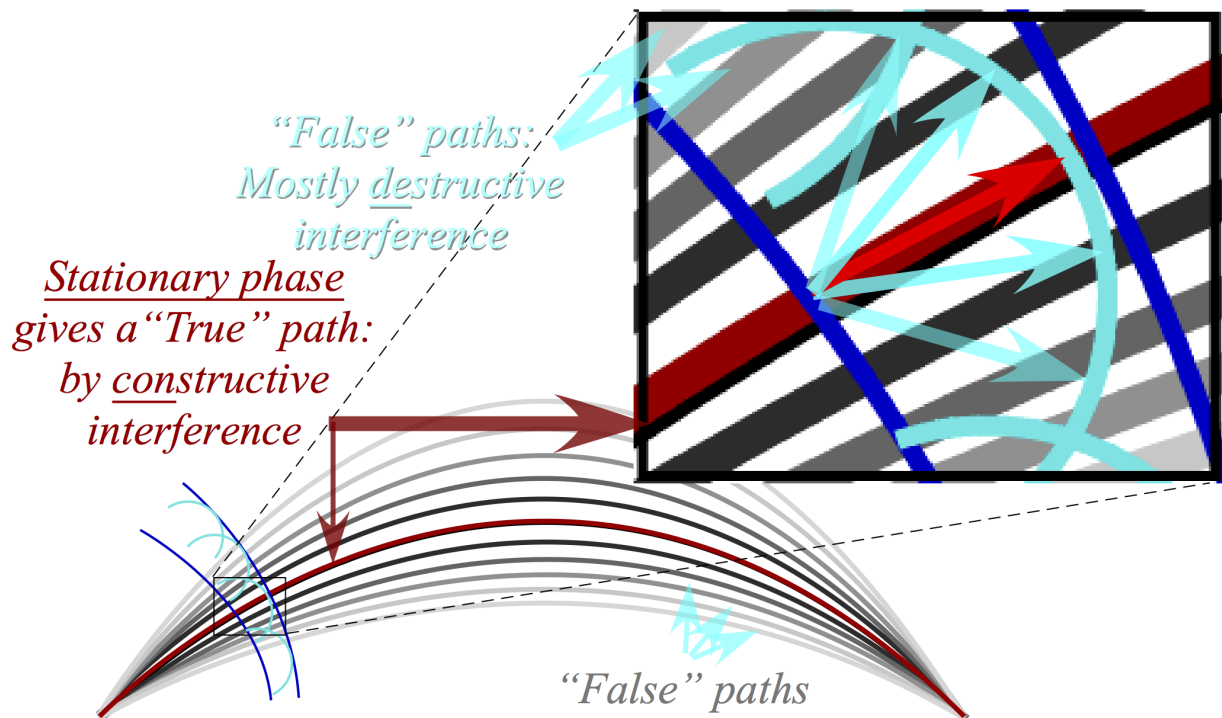


FIG. 27: Quantum waves interfere constructively on “True” path but mostly cancel elsewhere.

using the most ethereal and dicey stuff in the universe, light waves. This motivates a view of classical matter or particle mechanics that is more simply and elegantly done by its relation to light and its built-in relativity, resonance, and quantization that occurs when waves are subject to boundary conditions or otherwise confined. While Newton was grouching about “fits” of light, perhaps his crazy stuff was just trying to tell him something!

Derivation of quantum phenomena using a classical particle paradigm seems as silly now as deriving Newtonian results from an Aristotelian paradigm. It now seems much more likely that particles are made by waves, optical or otherwise, rather than vice versa as Newton believed. Also, CW trumps PW as CW axioms of Evenson (*All colors go c.*) and Doppler time-reversal ($r=1/b$) can easily derive Lorentz-Einstein-Minkowski algebra and geometry summarized in Table II and re-derive exact relations (34) for relativity and quantum wave mechanics using geometry summarized in Fig. 25.

VIII. RELAWAVITY GEOMETRY OF QUANTUM TRANSITIONS

Preceding theory uses combinations of states $|N, \mathbf{k}_n, \omega\rangle$ or wavefunctions $\Psi_{N, \mathbf{k}, \omega} = A_N e^{i(\mathbf{k} \cdot \mathbf{r} - \omega t)}$ of an ideal optical cavity that are quantized by quantum mode numbers n for phase and photon numbers N for amplitude. This leads to geometry of elementary quantum transitions that involve change or transition of one such state into another. Such a discussion begins with symmetry and related conservation rules that restrict such transitions.

A. Symmetry and conservation principles

In Newtonian mechanics the first law or axiom is one of momentum conservation. Such physical axioms, by definition, have only experimental proof or justification. Logical proof or disproof is possible only if an older theory like classical mechanics becomes undermined by a more general theory like relativity or quantum mechanics having finer axioms. Then an older axiom might be proved using newer and more basic axioms, or else it might be disproved or reduced to an approximate or conditional result.

Patient teachers respect critically thinking students having doubt about the classical momentum conservation law. Indeed, How *does* Nature avoid losing even the tiniest bit of a momentum current however large it may be? This seems miraculous as does conservation of energy, though the latter is a provable result of the former given time reversal symmetry.

So it provides pedagogical relief to unite momentum and energy conservation rules in the wave nature of light seemingly shared by all matter. Newton's momentum axiom replaced by Evenson CW axiom gives Einsein-Planck-DeBroglie results (34) that match momentum \mathbf{p} to phase wavenumber vector $\kappa = \mathbf{k}/2\pi$ scaled in h or Nh units while doing the same to energy E and phase frequency ν .

A rough statement of how CW axioms undermine or “prove” \mathbf{p} -or- E conservation axioms is that their conservation is required by wave coherence and so $\mathbf{p} = h\kappa$ and $E = h\nu$ must be conserved, too. However, this oversimplifies deeper concepts of symmetry logic, a kind of “grown-up” geometry.

CW axioms are symmetry principles due to the Lorentz-Poincare isotropy of space-time. That invokes invariance to a translation $\mathbf{T}(\vec{\delta}, \tau)$ that has plane wave eigenfunctions $\Psi_{k, \omega} = A e^{i(kx - \omega t)}$ and eigenstates $|\Psi_{k, \omega}\rangle$ with roots-of-unity eigenvalues $e^{i(k \cdot \delta - \omega \cdot \tau)}$ as in the bra-ket

relations below.

$$\mathbf{T}(\delta, \tau) |\Psi_{k, \omega}\rangle = e^{i(k \cdot \delta - \omega \cdot \tau)} |\Psi_{k, \omega}\rangle, \quad \langle \Psi_{k, \omega} | \mathbf{T}^\dagger(\delta, \tau) = \langle \Psi_{k, \omega} | e^{-i(k \cdot \delta - \omega \cdot \tau)}. \quad (58)$$

The relations apply also to N -factor (or " N -particle") states $\Psi_{K, \Omega} = \Psi_{k_1, \omega_1} \Psi_{k_2, \omega_2} \cdots \Psi_{k_N, \omega_N}$ where exponents add $S = \int L dt$ -values of each constituent to a total \mathbf{K} -vector $K = k_1 + k_2 + \dots + k_N$ with a total frequency $\Omega = \omega_1 + \omega_2 + \dots + \omega_N$ to give the $\mathbf{T}(\vec{\delta}, \tau)$ -eigenvalue in exponential form $e^{i(K \cdot \delta - \Omega \cdot \tau)}$.

\mathbf{T} -symmetry requires quantum time evolution operator \mathbf{U} not be affected by \mathbf{T} movement. This means $\mathbf{U} = \mathbf{T} \mathbf{U} \mathbf{T}^\dagger$ and \mathbf{U} commute with \mathbf{T} ($\mathbf{U} \mathbf{T} = \mathbf{T} \mathbf{U}$ for any \mathbf{T}). So transition matrix $\langle \Psi_{K', \Omega'} | \mathbf{U} | \Psi_{K, \Omega} \rangle$ equals $\langle \Psi_{K', \Omega'} | \mathbf{T} \mathbf{U} \mathbf{T}^\dagger | \Psi_{K, \Omega} \rangle$, and relations ((57)) yield (K, Ω) conservation rules: $(K', \Omega') = (K, \Omega)$.

$$\begin{aligned} \langle \Psi'_{K', \Omega'} | \mathbf{U} | \Psi_{K, \Omega} \rangle &= \langle \Psi'_{K', \Omega'} | \mathbf{T}^\dagger(\delta, \tau) \mathbf{U} \mathbf{T}(\delta, \tau) | \Psi_{K, \Omega} \rangle \quad (\text{if } \mathbf{U} \mathbf{T} = \mathbf{T} \mathbf{U} \text{ for all } \delta \text{ and } \tau) \\ &= e^{-i(K' \cdot \delta - \Omega' \cdot \tau)} e^{i(K \cdot \delta - \Omega \cdot \tau)} \langle \Psi'_{K', \Omega'} | \mathbf{U} | \Psi_{K, \Omega} \rangle = 0 \text{ unless } : K' = K \text{ and } : \Omega' = \Omega \end{aligned} \quad (59)$$

\mathbf{T} -symmetry implies total energy $E = \hbar \Omega$ and total momentum $\mathbf{P} = \hbar \mathbf{K}$ conservation for ideal CW states.

However, laboratory CW have momentum uncertainty $\Delta k = 1/\Delta x$ due to finite beam size Δx and energy uncertainty $\Delta E = \Delta \omega = 1/\Delta \tau$ due to finite lifetime $\Delta \tau$. Newton's 1st-law is verified only to the extent that lifetime or beam-width accommodates greater numbers of wavelengths or wave periods.

B. Single-photon transitions and Feynman diagram geometry

The geometric analysis of photon-affiliated transitions begins with the simple Doppler shifted or Lorentz transformed "baseball-diamond" geometry shown in Fig. 28. Most figures showing this geometry so far, including Fig. 19, Fig. 12 and the original Fig. 10, are drawn for velocity $u/c = 3/5$ or Doppler shift $b = 2$. Here, Fig. 28 uses odd values $b = 3/2$ or $u/c = 5/13$ to avoid distracting crossings found in Fig. 21 level plot. The Planck-Einstein-DeBroglie relation (34) is labeled by *energy* $E = \hbar \Omega$ plotted versus c -scaled momentum $cp = \hbar k$ so that both have the same dimensions of energy.

1. *Photon transitions obey rocket-science formula*

Tiny photon momentum $p=k$ needs a c -factor to show up in plots. Also, Fig. 28 is bisected by a wavy right-angle **HPK** inscribed in a g -circle that represents photon (ω, ck) -vectors connecting levels of high-state $|\omega_h\rangle$ at rest frequency $\omega_h=3$, middle-state $|\omega_m\rangle$ at $\omega_{mm}=2$, and low-state $|\omega_\ell\rangle$ at $\omega=4/3$. Each frequency relates to one above it (or below it) by blue-shift factor $e^{+\rho}=3/2$ (or red-shift factor $e^{-\rho}=2/3$). Thus the middle frequency $\omega_m=2$ is the geometric mean $\omega_m = \sqrt{\omega_h\omega_\ell}$ of those above and below.

$$3 = \omega_h = e^{+\rho}\omega_m \quad 2 = \omega_m = e^{+\rho}\omega_\ell \quad \frac{4}{3} = \omega_\ell = e^{-\rho}\omega_m = e^{-2\rho}\omega_h \quad (60)$$

Wavy segment **HP'** represents a photon of energy $\hbar\Omega_{HP'} = \hbar\omega_m \sinh \rho$ that would be emitted in a transition from a stationary mass $M_H = \hbar\omega_h/c^2$ at point **H** to a mass $M_P = \hbar\omega_m/c^2$ moving with rapidity ρ at point **P'**. Implicit in Fig. 28 is the choice of right-to-left direction for the outgoing photon momentum $cp = -\hbar\omega_m \sinh \rho$ recoiling left-to-right by just enough to conserve momentum as (58) requires. Mass M_H loses energy (frequency) equal to momentum (wavevector) of outgoing photon. Since M_H is initially stationary, it must lose energy by reducing rest-mass from M_H to M_P by Doppler shift ratio $e^{+\rho}$.

$$\frac{M_H}{M_P} = \frac{\omega_h}{\omega_m} = e^\rho \quad (61)$$

A rest mass formula results for recoil rapidity ρ with a simple low- ρ ($\rho \approx u/c$)-approximation.

$$\rho = \ln \frac{M_H}{M_P} \xrightarrow{\rho \rightarrow \frac{u}{c}} u = c \ln \frac{M_H}{M_P} \quad (62)$$

Interestingly, this quantum recoil formula is reminiscent of a famous rocket formula.

$$V_{burnout} = c_{exhaust} \ln \frac{M_{initial}}{M_{final}} \quad (63)$$

One might recall a popular expression, ‘‘This isn’t rocket science!’’ Usual notions are that quantum transitions are infinite discrete ‘‘jumps’’ with emitted (or absorbed) photons acting like bullets. This appears wrong-headed in light of a more complete relativistic picture of an atom or nucleus in (61). It gradually exhales its mass like a rocket with an optical exhaust velocity of c .

One may also recall classical Lorentz resonance models of atomic transitions. Lorentz of ELT did non-relativistic theory to show atoms undergo over 10^5 oscillations during decay

to a stationary mass M_K . Lowest energy level $\omega_l = M_K c^2$ in Fig. 29 has frequency $\omega_l = 4/3$ and zero momentum due to its leftward recoil from rightward emitted photon.

Feynman diagrams in right-hand inset panels of Fig. 29 are scale models of photon energy-momentum \mathbf{k}_{ab} -vectors emitted from head of initial mass- M_A, \mathbf{K}_A -vector on the tail point of recoiling mass- M_B, \mathbf{K}_B -vector. One may imagine per-space-time (ω, k) diagrams as space-time (x, ct) mass and photon tracks due to Fourier reciprocity demonstrated in Fig. 10 and Fig. 11. Also \mathbf{K} -vectors rearrange into head-to-tail zero-sum triangles representing energy-momentum conservation demanded by (58).

2. Geometric level and transition sequences

Level sequence $\{\dots, \omega_l, \omega_m, \omega_h, \dots\}$ in (59) is part of an infinite geometric series having blue-shift ratio $b=e^{+\rho} = 3/2$ or red-shift ratio $r=e^{-\rho} = 2/3$ ranging from 0 to ∞ . The energy $E_m = \omega_m$ or frequency ω_m value labeling hyperbola- ω_m may be scaled to give an infinite sequence based on ratio $b^1 = 3/2 = r^{-1}$.

$$\{\dots, r^2\omega_m, r^1\omega_m, r^0\omega_m, b^1\omega_m, b^2\omega_m, b^3\omega_m, \dots, b^q\omega_m, \dots\} \quad (65)$$

This labels a geometric sequence stack of hyperbolas shown in Fig. 30. Meanwhile, rapidity $\rho = \ln \frac{3}{2}$ labeling velocity line- $(u/c=5/13)$ is boosted through a sequence of ρ_p -values $\{\dots, -2\rho, -\rho, 0, 2\rho, 3\rho, \dots, p\rho, \dots\}$ and defines p -points of momentum $(p_{p,q} = b^q\omega_m \sinh \rho_p)$ (where: $\rho_p = p \cdot \rho$) on each $b^q\omega_m$ -hyperbola.

The result is a lattice in Fig. 30 of transition points $P_{p,q} = (cp_{p,q}, E_q)$ that are scaling- and Lorentz-boost-equivalent to the point $P = P_{0,0}$ at the center of Fig. 28 and Fig. 29 or else the point $P' = P_{1,0}$ that is the center of transitions in those figures. Choice of origin is quite arbitrary in a symmetry manifold defined by group operations. The $\pm 45^\circ$ -light-cone boundaries and their intersection $(cp, E) = (0, 0)$ lie outside of this open set of $P_{p,q}$ points. The choice of the base Doppler ratio $b = e^{+\rho}$ is also arbitrary and may be irrational. However, a rational b guarantees all 16 functions in Table II are also rational. The lattice in Fig. 30 may be viewed at $\pm 45^\circ$ as a quasi-Cartesian grid of lines. Each line is positioned according to rest-frequency power $\omega_m e^{q\rho}$ at its meeting point on the vertical ω -axis (or 2^{nd} -base of a Doppler baseball diamond) as shown in Fig 27. The $+45^\circ$ R -axis (1st-baseline) is marked-off by sequence $\omega_R = \omega_m e^{R\rho}$ ($R = -2, -1, 0, 1, 2, \dots$) and the -45° L -axis (3rd-baseline) is marked-off by

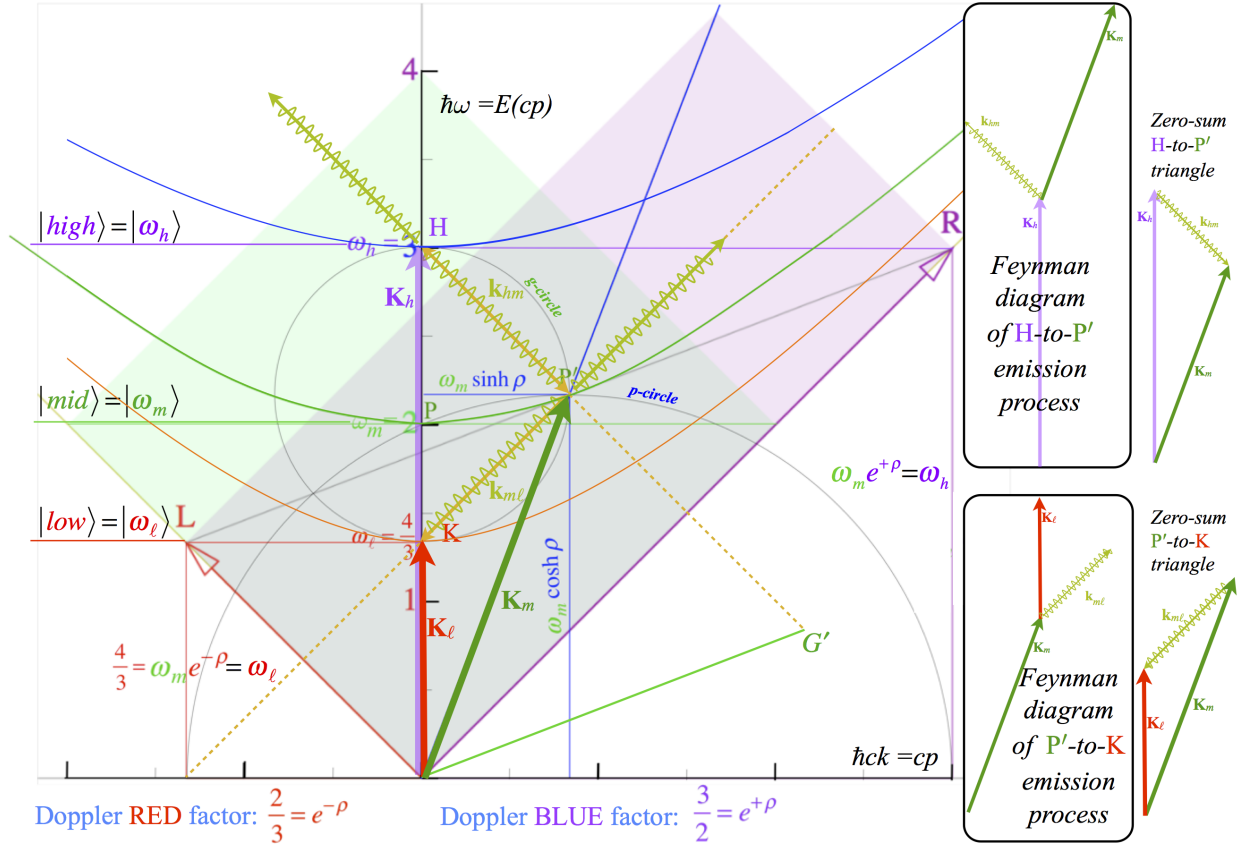


FIG. 29: Feynman diagrams of 1-photon transitions connecting 3-levels ω_l , ω_m , and ω_h .

sequence $\omega_L = \omega_m e^{L\rho}$ ($L = -2, -1, 0, 1, 2, \dots$). (Here base constants $b = e^\rho = \frac{3}{2}$ and $\omega_m = 2$ are fixed.) At the intersections of R and L grid-lines are discrete transition (p, q) -points $P_{p,q}$.

$$P_{p,q} = (ck_{p,q}, \omega_{p,q}) = \omega_m e^{q\rho} (\sinh p\rho, \cosh p\rho) \quad (66)$$

3. Half-sum-and-difference transition web

Each coordinate point is related by half-sum and half-difference coordinate transformations.

$$p = \frac{R-L}{2}, \quad q = \frac{R+L}{2} \quad \Leftrightarrow \quad R = p+q, \quad L = q-p \quad (67)$$

These are integer versions of the phase and group relations 13 and (15) to right and left laser \mathbf{K} -vectors, yet another result of factoring optical wave coordinate functions. The geometric structure represented here might become a useful basis for a kind of lattice-gauge theory to

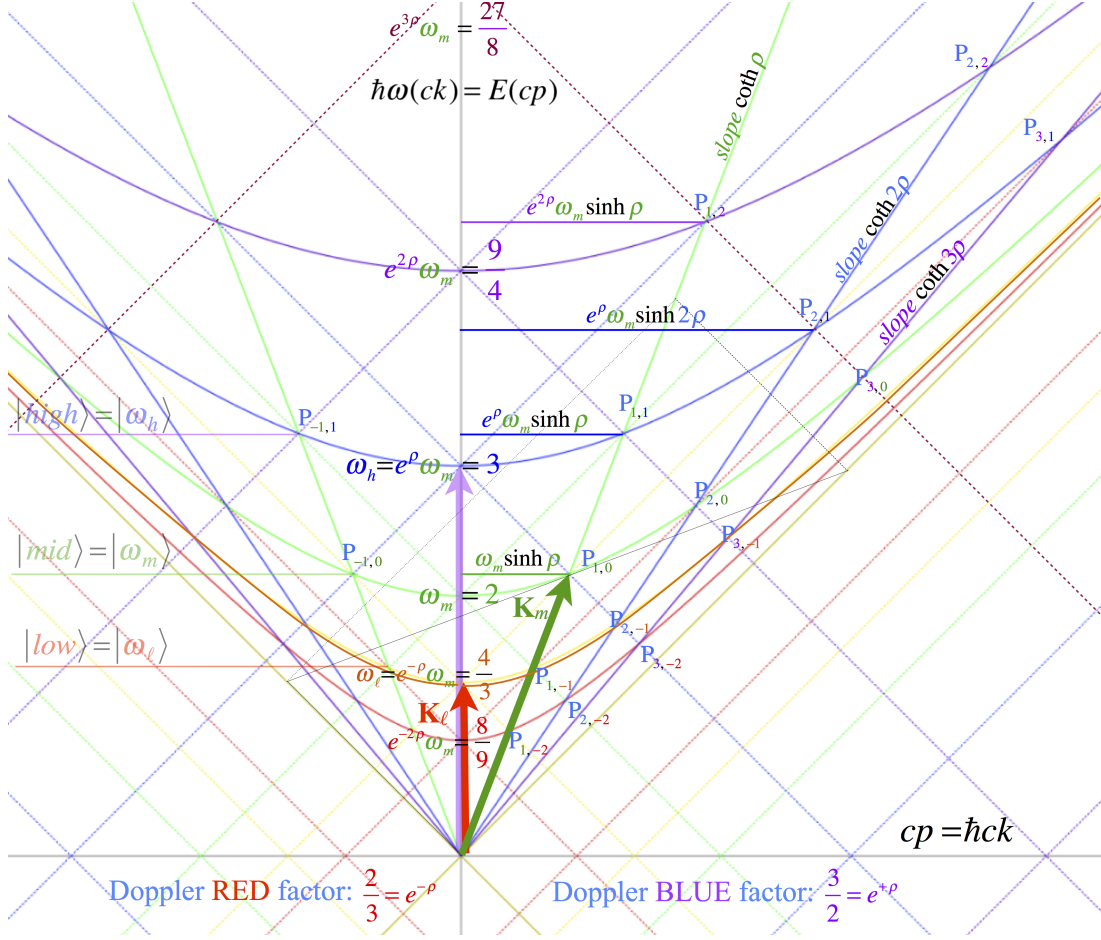


FIG. 30: Rapidity- $\rho_p = p\rho$ and rest-frequency- $\omega_m e^{q\rho}$ and $P_{p,q}$ -lattice based on integer powers of $b = e^\rho = \frac{3}{2}$.

explore cavity quantum electro-dynamics (CQED) or pseudo-relativistic theories of graphene gauge dynamics. Such a structure offers a possible solution to the flaw that made Feynman path integration so difficult due its uncountable universe of possible paths. The structure in Fig. 31 offers a labeling of every discrete path and state by an operation in a discrete subgroup of the continuous Poincare-Lorentz group (PLG) that has a discrete Poincare-Lorentz algebra (PLA). The discrete paths may be made as fine as desired so that each PLA becomes a larger and better approximation to the parent PLG. Each PLA has a discrete spectral decomposition that could derive and solve a range of Hamiltonian eigensolutions and transition amplitudes parametrized by discrete paths.

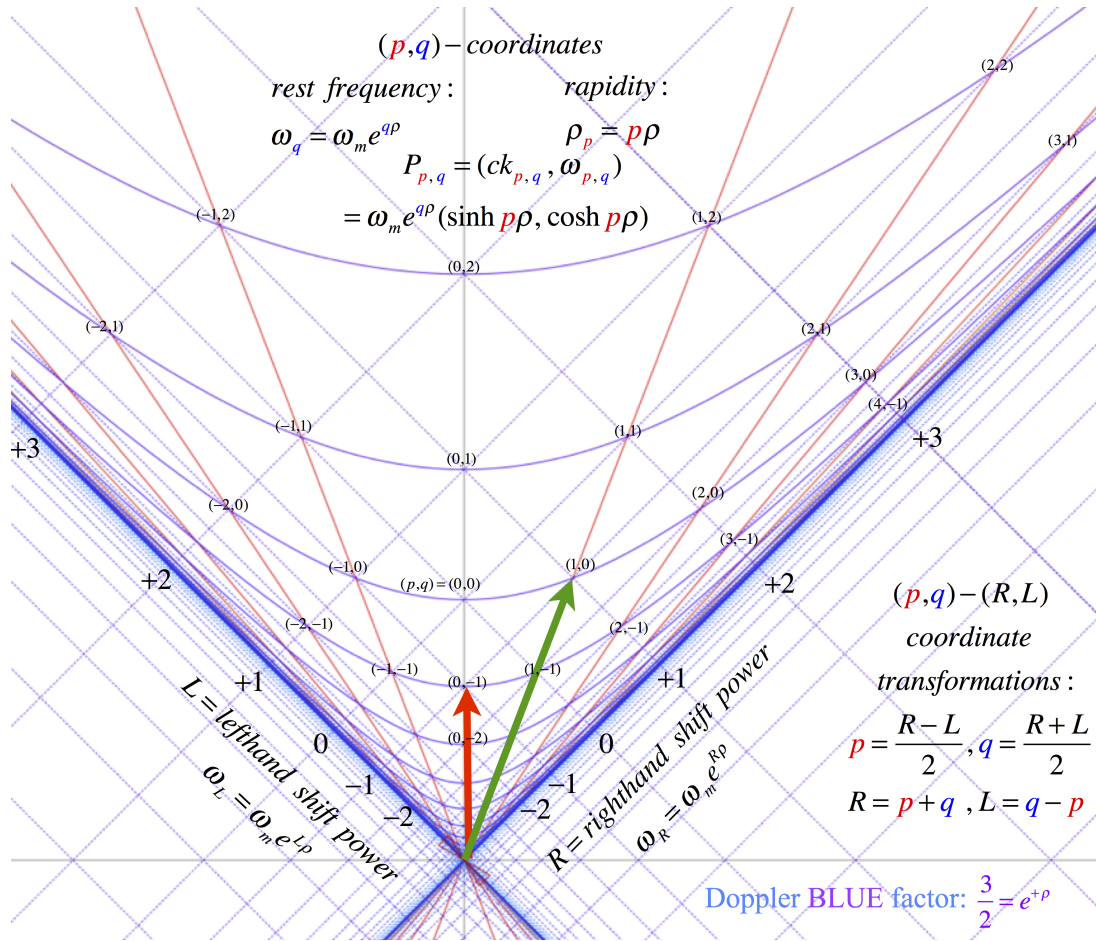


FIG. 31: Hyperbolic lattice of (p,q) -transition points for base $b=e^p=\frac{3}{2}$ and half-sum-difference coordinate relations.

IX. ACCELERATED FRAMES AND OPTICAL EINSTEIN-ELEVATOR

Fig. 9b and Fig. 10b show Lorentz-Minkowski space-time frames made by a 2-CW pair of lasers. Fig. 9b shows a Cartesian (x, ct) -grid made as Alice's and Carla's lasers collide 600THz beams. Fig. 10b shows Bob's view of Alice closing at $u/c=3/5$ with her laser beam Doppler blue-shifted by an octave factor $(B|A)=2=e^{+\rho}$ to 00THz and Carla going away at $u/c=-3/5$ with her beam Doppler red-shifted by $(B|C)=1/2=e^{-\rho}$ to 300THz. If Bob attenuates Alice's beam **E**-field amplitude by 1/2 so its amplitude matches Carla's then he may see the Alice-Carla (x, ct) -grid in Fig. 9b form the Minkowski $(\acute{x}, \acute{c}t')$ -grid shown in Fig. 10b.

Alice and Carla can provide Bob with the same $\rho=\ln 2=0.69$ grid without expending the energy needed to move their lasers to enormous speeds of $u/c=3/5$ relative to him. Instead they may be at rest in his frame and gradually tune up or up-chirp Alice's laser from $\nu_A=600\text{THz}$ to $e^{+\rho}\nu_A=00\text{THz}$ while Carla is down-chirping from ν_A to $\nu_A e^{-\rho}=300\text{THz}$.

This opens the possibility of projecting accelerating frames for optical "Einstein elevators" with curving space-time coordinates that span a finite region between the lasers for a finite time interval. One may imagine Bob has a space ship that accelerates to a velocity $u=c\tanh\rho$ that Doppler shifts the Alice and Carla beams back to their initial green frequency $\nu_A=600\text{THz}$. (Or else, an excited atom b could be imagined to be trapped in a single group-wave anti-node space-time cell so b accelerates with that cell while staying in resonance with the cell's constant phase frequency ν_A .)

The instantaneous velocity u of Bob (or the atom b) relative to Alice and Carla depends on their chirp factors $e^{\pm\rho}$ that vary with rapidity ρ . Bob can find his ρ relative to Alice if she broadcasts a fixed frequency ν_A that he sees at $\nu_B=\nu_A e^{-\rho}$. Rapidity is a function $\rho=\rho(\tau)$ of proper time τ for Bob (or atom b) and τ is related by (42) to time t for Alice or Carla.

$$u = \frac{dx}{dt} = c \tanh \rho \quad \text{where : } \frac{dt}{d\tau} = \cosh \rho \quad \text{and : } \frac{dx}{d\tau} = \frac{dx}{dt} \frac{dt}{d\tau} = \tanh \rho \cosh \rho = c \sinh \rho \quad (68a)$$

Integrating the relations (66a) gives Bob's time-space path (ct, x) as seen by Alice or Carla.

$$ct = c \int \cosh \rho(\tau) d\tau \quad \text{and : } x = c \int \sinh \rho(\tau) d\tau \quad (68b)$$

Constant rapidity $\rho = \text{const.}$ gives a Minkowski τ -axis of slope $x/ct = \sinh\rho/\cosh\rho$.

$$ct = c\tau(\cosh \rho) \quad \text{and : } x = c\tau(\sinh \rho) \quad (68c)$$

This case is sketched in Fig. 32a as a tiny CW Minkowski frame at the intersection of paths of PW light waves from Alice and Carla and repeats the situation in Fig.10. Fig.32b path

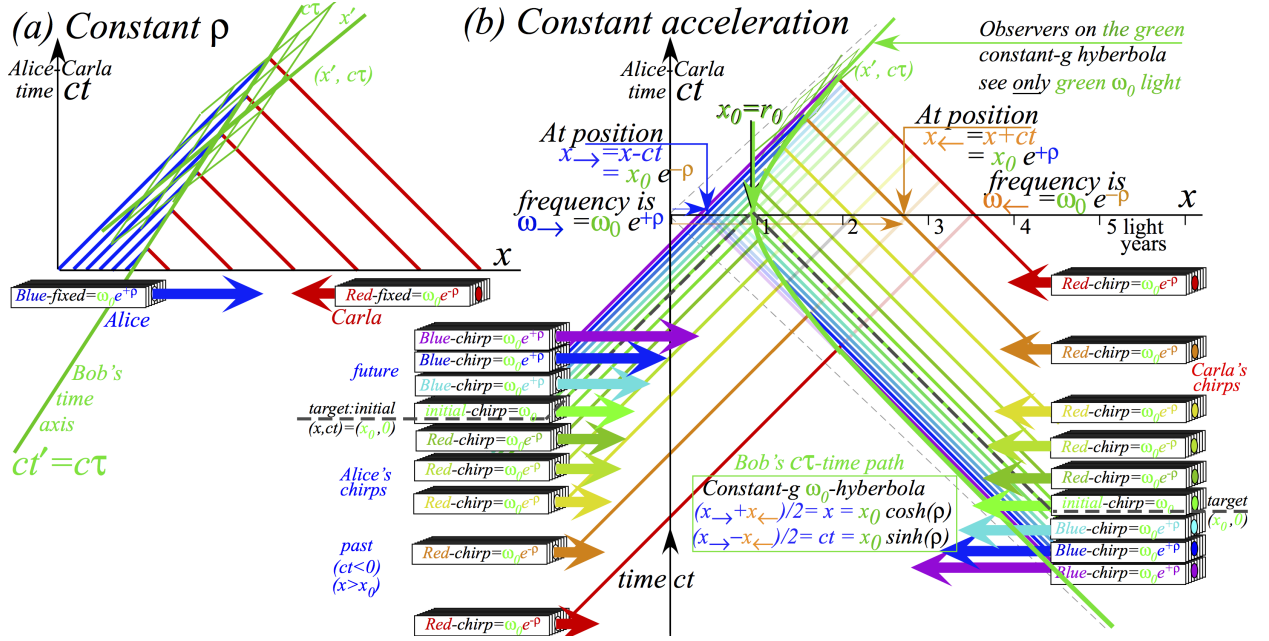


FIG. 32: Space-time laser-formed paths of constant g -acceleration (a) $g=0$, (b) $g=9.8m/s^2$

has constant acceleration $g=9.8m/s^2$ with rapidity linear in Bob's proper time $c\rho = g\tau$.

$$ct = \int \cosh \rho d\tau = \frac{c^2}{g} \sinh \left(\frac{g\tau}{c} \right) \quad (\text{for } u \simeq \rho c = g\tau), \quad x = c \int \sinh \rho d\tau = \frac{c^2}{g} \cosh \left(\frac{g\tau}{c} \right) \quad (69)$$

Recall that low rapidity ($\rho \ll 1$) is approximated by u/c , and so setting $c\rho$ equal to $g\tau$ gives the classical uniform acceleration equation $u=g\tau$. The resulting space-time path shown in Fig.32b is a hyperbola of radius $a=c^2/g$. That radius is enormous unless "gravity" g is also enormous. For terrestrial $g=9.8m/s^2=9.8$ the radius is $a=0.97\text{LightYr}$. However, a traveler with even this small $1g$ acceleration can, over several years, rack up considerable light-year mileage. One should recall both $\cosh\rho$ and $\sinh\rho$ contain e^ρ .

After the first year of $\tau_1=3.15 \cdot 10^7 \text{sec}$. the rapidity is $\rho_1=g\tau_1/c=1.03$ giving an x -coordinate of $x=a \cosh(g\tau_1/c)=1.53 \text{ LightYr}$ with a total mileage of $x-a=0.56 \text{ LightYr}$. But, after 21years (the age of legality) x balloons to $x=a \cosh(21g\tau_1/c) = 1.22 \cdot 10^9 \text{ LightYr}$! Now hyperbolic radius a is an insignificant part of a billion light-year journey. After 25 years (about the age of Einstein as he developed relativity theory) the mileage is 76 billion

light-years, well beyond age-of-universe estimates in the frame of Alice. (Who, by then has long since passed away in the lab frame. Why *did* she have to stay at home?).

The geometric and exponential behavior of relativistic Doppler components dominates this example of space-time inflation and takes Alice-Bob sagas beyond any realm of possibility. Still it is instructive to explore such surprising thought experiments as far as possible and note the asymptotic extremes of scaling and curvature. Recall that rapidity ρ is defined in Fig. 2b as twice the area subtended by a unit hyperbola, its radius vector, and the horizontal axis. Half that is the area shaded in Fig 33a.

$$\alpha(\rho_1) = \frac{x \cdot ct}{2} - \int_0^{x_1} ct dx = \frac{x \cdot ct}{2} - \int_0^{\rho_1} ct \cdot \frac{dx}{d\rho} d\rho = a^2 \frac{\cosh \rho_1 \sinh \rho_1}{2} - \int_0^{\rho_1} a \sinh^2 \rho d\rho = a^2 \rho_1 / 2 \quad (70)$$

Coordinates $x = a \cosh \rho$ and $ct = a \sinh \rho$ from (68) are used. (Circle area is $\alpha = r^2 \sigma / 2$.) Hyperbolic radius $r_0 = a = c^2 / g$ gives c -scaled proper time $c\tau_1$ as a radius-rapidity product $a\rho_1$.

$$a\rho_1 = c\tau_1 \quad (71)$$

Colliding Alice-versus-Carla laser beams in Fig. 32b are detailed in Fig. 33b, a plot of an inertial space-time (x, ct) -frame with Alice and Carla sitting on left or right sides, respectively. Alice gradually up-tunes from infrared while Carla just as gradually down-tunes from ultra-violet. They start their beams over a year before and time their tuning so the central GREEN (lab frequency $\nu_0 = 600 \text{ THz}$) beam-pair meets at $t_0 = 0$ on the x -axis at $x_0 = a_0$ where Bob is briefly stationary but accelerating right at his constant $g_0 = c^2 / a_0$. (See Fig. 33b. Tuning is gradual but only two other tuning paths are plotted and labeled.)

The right-hand RED (lab frequency $\nu_1 = \nu_0 e^{-\rho_1}$) beam-pair meet at $t_0 = 0$ on the x -axis at the point $x_1 = a_1 = a_0 e^{+\rho_1}$ where Bob's companion Carl is also briefly stationary but accelerating right at $g_1 = c^2 / a_1$. The left-hand BLUE (lab frequency $\nu_{-1} = \nu_0 e^{+\rho_1}$) beam-pair meet at $t_0 = 0$ on the x -axis at the point $x_1 = a_1 = a_0 e^{-\rho_1}$ where Bob's companion Al is also briefly stationary but accelerating right at $g_1 = c^2 / a_1$.

Bob and his companions share a line of rising slope $x/ct = \coth \rho$ as they travel up their respective hyperbolic paths in Fig. 33b according to (68). All points on such a line share the same rapidity ρ and the same tangent slope $dx/dct = \tanh \rho$ or lab velocity u/c , and so Al, Bob, and Carl on the ρ_1 -line in Fig. 33b apply the same Doppler blue-shift factor $b_1 = e^{+\rho_1}$ to light they meet head-on and the same red-shift factor $r_1 = e^{-\rho_1}$ to light that catches them from behind. Thus Bob down-shifts Carla's blue beam from its lab BLUE frequency

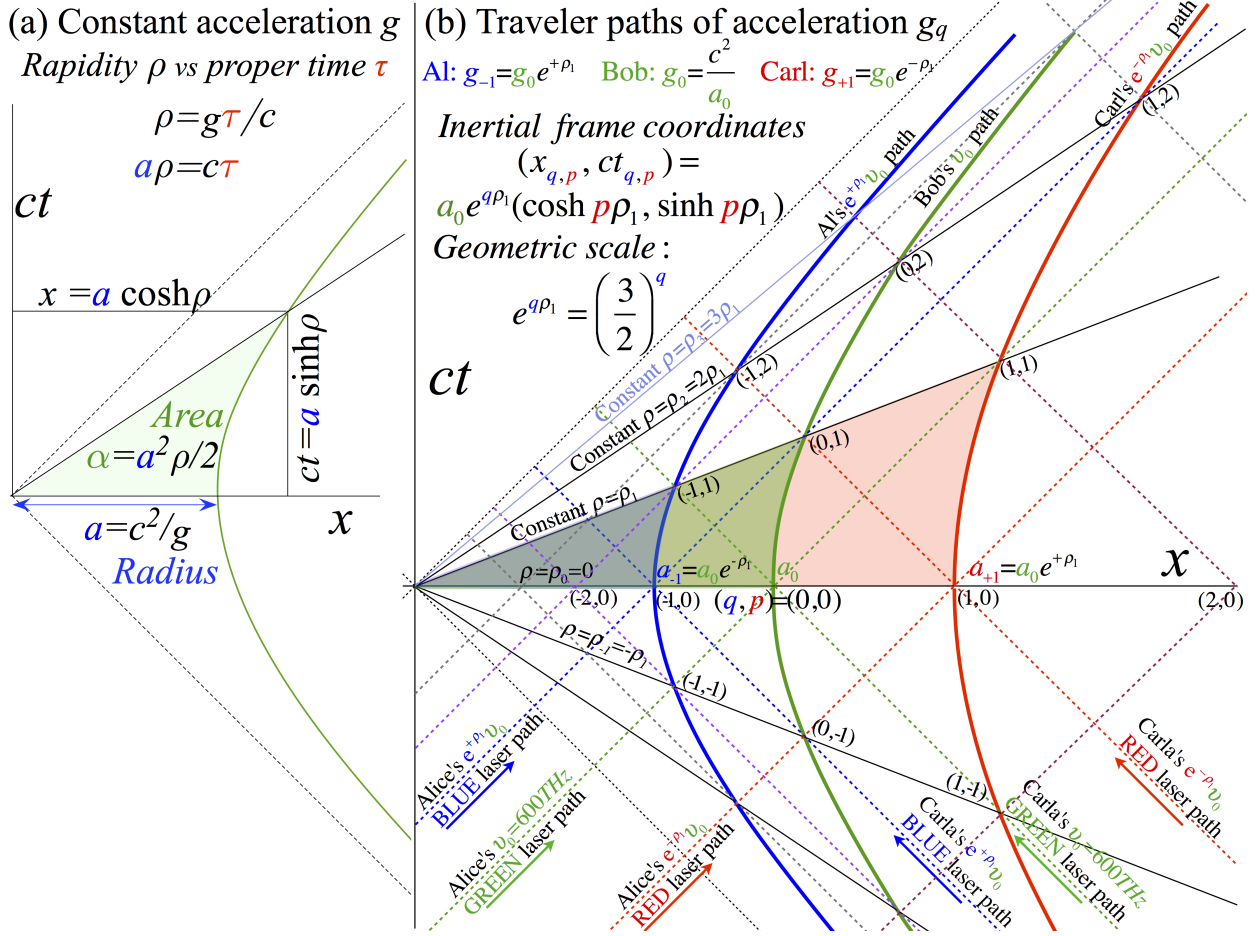


FIG. 33: (a) Constant- $g_q = c^2/a_q$ paths proper time *vs* area
(b) $q_{Al} = -1, q_{Bob} = 0, q_{Carl} = 1$ $\rho_p = p\rho_1 = p \cdot \ln(3/2)$ from $p = -1$ to 3 .

$v_{BLUE} = e^{+\rho_1}$ to his observed GREEN $v_0 = 600\text{THz}$ and up-shifts Carla's red beam from its lab RED frequency $v_{BLUE} = v_0 e^{-\rho_1}$ to the same base frequency $v_0 = 600\text{THz}$.

This is consistent with Alice and Carla's original plan for Bob on an optically accelerated "Einstein elevator" but now it includes two companions Al and Carl that travel in spatial lock-step beside Bob in Fig. 33b with Al maintaining a fixed distance $\Delta a_0 = a_0 - a_1$ below Bob as Carl maintains a larger fixed distance $\Delta a_1 = a_1 - a_0 = e^{+\rho_1} \Delta a_0$ above Bob (As plotted in their frames of equal rapidity ρ_1 .)

Meanwhile, the lab x -view in Fig. 33b clearly shows their relative spatial separations suffering Lorentz contraction. Each hyperbolic path is invariant so a boost in rapidity by $\Delta\rho$ moves any of its points of rapidity ρ_p to $\rho_p + \Delta\rho$ on the same hyperbola.

While Al, Bob, and Carl maintain initial spatial separations tallied by Alice and Carla

at zero rapidity or velocity $\rho_0 = 0 = u_0/c$, they do not maintain equal proper time- τ readings. According to (70) proper time $c\tau_{p,q}$ on hyperbola- q is a product of its radius $a_q = e^{q\rho_1} a_0$ with rapidity $\rho_p = p\rho_1$ for any given p -line shared by travelers $q = -1$, 0 , and $+1$, namely, Al, Bob, and Carl.

$$c\tau_{q,p} = a_q \rho_p = a_0 e^{q\rho_1} p \rho_1 \quad \text{where : } q = -1(\text{Al}), 0(\text{Bob}), \text{ and } +1(\text{Carl}). \quad (72)$$

Hyperbolas of smaller radius a_q have proportionally slower local or proper time evolution and proportionally greater acceleration $g_q = c^2/a_q$ hence more curvature of hyperbolas closer to origin in Fig. 33. Indeed, each (q,p) -cell has the same number of wavelengths and wave-periods packed into a tighter space-time as the radius a_q is reduced.

The hyperbolic acceleration geometry of space-time in Fig. 33b has similar geometry (rotated by 90°) to that of Compton scattering in per-space-time of Fig. 31, but the physics is inverted. A boost of Bob ($q=0$) from ρ_0 to ρ_1 ($p=0 \rightarrow 1$) in Fig. 33b corresponds to a Compton transition of a rest-mass $q=0$ from ρ_0 to ρ_1 in Fig. 31. Increased energy $E = h\nu$ and momentum $p = h\kappa$ on reciprocal (E, cp) lattice Fig. 31 is decreased wave length $\lambda = 1/\kappa$ and wave period $\tau = 1/\nu$ for space-time (x, ct) in Fig. 33. And vice-versa, a low-hyper-radius $a_q = c^2/g_q$ or high acceleration $g_q = c^2/a_q$ in Fig. 33 has high energy E (or frequency ν) and momentum p (or wavenumber κ) in Fig. 31.

This mythical odyssey of intrepid accelerating voyagers (Al, Bob, and Carl) depends on optical metrology provided by a pair of laser-chirping Sirens (Alice and Carla) stationed for years at the left and right edges of Fig. 32b and Fig. 33b. While Carla leisurely de-tunes her right-to-left beam, Alice tries to meet an impossible up-tuning schedule of her left-to-right beam, planned to end with an exponential chirp and explosion of infinite frequency at $ct=0$. Her $ct_0 = -a_0$ emission of frequency $\nu_0 = 600\text{THz}$ hits Bob at $x = a_0$, one of a geometric sequence of frequencies $\nu_q/\nu_0 = e^{\rho_1}, e^{2\rho_1}, e^{3\rho_1}, \dots, e^{q\rho_1}$ emitted at times $ct_q = -e^{-\rho_1}, -e^{-2\rho_1}, -e^{-3\rho_1}, \dots, -e^{-q\rho_1} \rightarrow 0$ to hit a point $x_q = a_0 e^{-q\rho_1}$ at $ct=0$. (The geometric ratio in Fig. 33b is $e^{\rho_1} = 3/2$ and arbitrarily chosen to provide a lattice in the (x, ct) -continuum.)

No light emitted by Alice after $t=0$ can reach Al, Bob, Carl or any fellow traveler- q maintaining enough acceleration to stay under hyperbolic asymptote or “event-horizon” $x=ct$ in Fig. 33b. Carla, the right-to-left half of this 2-CW metrology, hits the same q -points $x_q = a_0 e^{-q\rho_1}$ on the $ct=0$ -line (x -axis) with the same frequencies $\nu_q = \nu_0 e^{q\rho_1}$ that Alice sent

to each traveler- (q) . She can continue hitting Carl(traveler $q=1$) at (q,p) -points $(1,1)$ and $(1,2)$ with beams that later hit Bob (traveler $q=0$) at (q,p) -points $(0,1)$, $(0,2)$ and $(0,3)$ and Al (traveler $q=-1$) at (q,p) -points $(-1,2)$, $(-1,3)$ and $(-1,4)$. However, Carl passes Carla soon thereafter (upper right hand corner of Fig. 33b) and so also will Bob followed by Al. Thus laser coordination by either Siren, Alice or Carla, is quite restricted in its coverage.

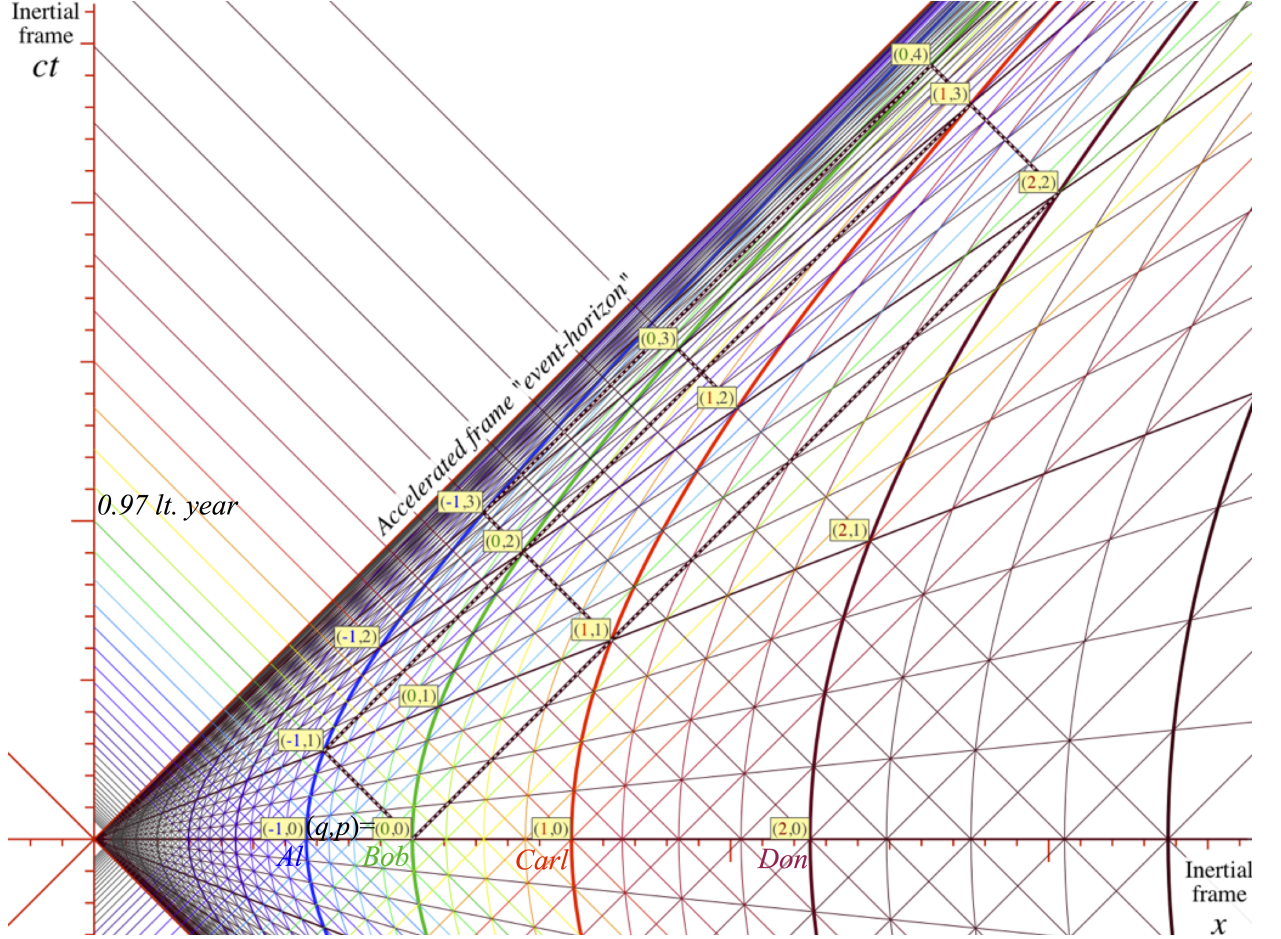


FIG. 34: CW Doppler and PW radar metrology for frame of constant acceleration
 $g = 9.8m \cdot s^2$.

A. Metrology in accelerated frames

Accelerated frame metrology of space, time, and relative velocity is quite counter-intuitive and easily misinterpreted. The space-time grid of CW and PW paths provided by Alice and Carla in Fig. 32b (and with greater detail in Fig. 33b) help to analyze what Al, Bob, and

Carl might be able to observe at each (q,p) -intersection of light beams sent by Alice and Carla.

Let us assume each intersection marks colliding pulse waves (PW) that are separated by the same number N of CW wavelengths in space and N wave periods in time. In Fig. 34 the CW paths for $N=4$ are drawn as the finer CW grid for the sake of clarity, but it should be evident that increasing integer scale N sharpens the space-time fine-grid precision.

The course-grid defined by integer coordinates (q,p) mark equally spaced proper time p -instants $c\tau_{q,p} = a_q\rho_p$ along the q -path hyperbola of traveler q according to (71). Bob ($q=0$), starting from his origin ($p=0$) at rest in Fig. 34, accelerates past his proper time points $c\tau_{0,p}=a_1\rho_1(0,1,2,3,4)$ before exiting at the very top of the plot. Bob sees the same proper time interval $c\tau_{0,1}=a_0\rho_1$ between each of his p -instants wherein he gains the same unit $\rho_1=\ln(3/2)=0.405$ of rapidity per interval or velocity $u/c=\tanh\rho_1=0.385$.

The distance x traveled in inertial frame (x,ct) of Fig. 34 grows only quadratically at first but soon explodes exponentially due to hyperbolic cosine $x=a_0\cosh\rho$ in (68).

Meanwhile, Bob's companions, Al ($q=-1$) and Carl ($q=+1$), also see equal proper time intervals between p -points, but each $c\tau_{q,p}$ is proportional to q_{th} hyperbolic radial constant $a_q = a_0e^{q\rho_1}$. So Al's proper time interval $c\tau_{-1,1} = a_0e^{-\rho_1} = (2/3)a_0$ is $(2/3)$ of Bob's interval while Carl's interval $c\tau_{1,1} = a_0e^{\rho_1} = (3/2)a_0$ is $(3/2)$ -times greater. But, each traveler gains the same rapidity $\rho_1=\ln(3/2)=0.405$ in each interval.

Having uniform proper $\Delta\tau_q$ -intervals allows spatial intervals between each pair of accelerating neighbors to be easily measured by radar echo ranging. A dash-line rectangle connecting $[q,p]$ -points $[0,0]$, $[1,1]$, $[0,2]$, and $[-1,1]$ outlines paths of Bob's radar pulses he might send rightward (That is "up" in his perceived "gravity" field.) from $[0,0]$ to reflect from Carl at $[1,1]$ and leftward (that is down-field) to reflect from Al at $[-1,1]$. Both pulses return to Bob simultaneously at $[2,2]$ at precisely $c\tau_{0,2} = 2a_0\rho_1$ or two "ticks" of his proper time given in distance units. ($a_0=0.97lt-yr$ derived by (69) for $g=9.8m\cdot s^{-2}$.)

Thus Bob finds a radar-range distance $x_{[-1,1]} = -a_0\rho_1 = -0.39lt - yr$ for Al below him and a distance $x_{[1,1]} = a_0\rho_1 = 0.39lt - yr$ of equal distance for Carl above him. Bob gets the same $\pm a_0\rho_1$ distances if he sends out radar pulses one "tick" earlier from the $[0,-1]$ point (below $[0,0]$ and not visible in Fig. 34) that return to him simultaneously two "ticks" later at point $[0,1]$.

If Bob's radar pulses could echo off next-nearest neighbor's paths having radius $a_{\pm 2} =$

$a_0 e^{\pm 2\rho_1}$ or $a_{\pm 3} = a_0 e^{\pm 3\rho_1}$ then they would return four “ticks” later at $[0,4]$ (as shown in Fig. 34) or six “ticks” later at $[0,6]$ (not shown in Fig. 34). Such echo range values would indicate uniformly spaced neighbors at constant positions $\pm a_0 \rho_1$, $\pm 2a_0 \rho_1$, and $\pm 3a_0 \rho_1$, above and below Bob. Such uniformity of spacing seems paradoxical in light of a decidedly non-uniform spacing of neighbor- q positions $x_q(0) = a_q = a_0 e^{q\rho_1}$ on the x -axis of Alice and Carla’s inertial frame at time $ct = 0$ (and rapidity $\rho = 0$). They see a geometric series $a_q = a_0 \{ \dots, e^{-2\rho_1}, e^{-\rho_1}, 1, e^{+\rho_1}, e^{+2\rho_1}, \dots \}$ of hyperbolic radii that includes Bob’s radius a_0 at origin $[0,0]$.

However, the initial ($ct=0$)-spacing of travelers, that is $\Delta a_q = a_0(e^{q\rho_1} - e^{(q-1)\rho_1})$ in Alice’s inertial frame, is to 1st-order in ρ_1 , a uniform $\Delta a_q = a_0 \rho_1$ that agrees with Bob’s radar-range values. Later, as traveler- q gains speed according to its respective acceleration $g_q = c^2/a_q$, Alice will see neighbor intervals Lorentz contract non-uniformly by $\Delta a_q \text{sech} \rho_p$ factors.

When a neighbor- q of Bob sends his own inquiring radar-echo ranging pulses he will get results that differ by the same exponential factor $e^{q\rho_1}$ relating his proper time value $\tau_{q,p}$ to the corresponding value $\tau_{0,p}$ for Bob intercepting echo-return- p . Bob’s radar-range intervals are all seen by up-stairs neighbor- $(+|q|)$, to be uniformly expanded by $e^{+q\rho_1}$, while down-stairs neighbor- $(-|q|)$, sees them uniformly contracted by $e^{-q\rho_1}$.

Consider Doppler blue-shifts $e^{+q\rho_1}$ seen by Bob for CW light sent by up-stairs neighbor- $(+|q|)$ or a red-shift $e^{-q\rho_1}$ for a down-stairs neighbor- $(-|q|)$ source. Each light beam on $\pm 45^\circ$ -paths in Fig. 33b is a copy of laser light sent much earlier by Alice ($+45^\circ$) or Carla (-45°) and Doppler-shifted due to Bob’s velocity so that he always sees a fixed green from either direction. Al and Carl are similarly seeing fixed colors as long as they can maintain their respective accelerations $g_q = g_{-1}$ and $g_q = g_{+1}$ through a field of up-chirped frequency sent by Alice and down-chirped frequency sent by Carla.

Thus each traveler only sends or receives its unique frequency: blue for Al, green for Bob, and red for Carl. So Bob always receives a green from Al down-stairs that is Doppler red-shifted by $e^{-q\rho_1}$ from Al’s blue or else a green from Carl up-stairs that is blue-shifted by $e^{+q\rho_1}$ from Carl’s red. It might seem travelers sharing a line of equal rapidity ρ and fixed radar-range separation should see no Doppler shift between them, that is $(R|S)=1$.

However, each $\pm 45^\circ$ -path connects a $[q,p]$ -point to the nearest up-stairs $[q+1, p\pm 1]$ -points of traveler $q+1$ who deals in reduced frequency and to the nearest down-stairs $[q-1, p\pm 1]$ -points of traveler $q-1$ who deals in higher frequency. In each case rapidity differs by one

ρ_1 -unit implying a Doppler blue-shift factor $e^{+q\rho_1}$ for light is falling down-stairs or a Doppler red-shift factor $e^{-q\rho_1}$ for light having to rise up-stairs. Travelers must have identical and *constant* rapidity for their shifts to go away.

B. Mechanics in accelerated frames

The curved space-time in Fig. 34 and Fig. 35 facilitate tracking light waves going back-and-forth between the co-accelerating travelers Al($q=-1$), Bob($q=0$), Carl($q=1$) and Don($q=2$) and reconciling them to Alice and Carla with their inertial frame laser sources. The same may be done for freely flying massive objects that travelers might drop or throw at each other. A simple example involves travelers dropping objects on downstairs companions at just the moment they all have zero velocity in the inertial (x, ct) frame. Alice and Carla would see such objects to be stationary and represented by vertical lines parallel to their inertial ct -axis as shown in Fig. 35.

Each object dropped by traveler-($q=Q$) will hit (or pass closely by) traveler-($q=Q-1$) then traveler-($q=Q-2$) and so forth as seen by examples in Fig. 35. The first example has Don($q=2$) drop something onto Carl($q=1$), Bob($q=0$), and Al($q=-1$) as is indicated at the top of the figure. Don's object hits Carl (or as witnessed by Alice and Carla: Carl hits Don's stationary object.) when Carl's x -coordinate equals a_2 of Don's object.

$$x_{2\text{HIT}1} = a_2 = a_0 e^{2\rho_1} = x_{\text{Carl}} = a_1 \cosh \rho_{2\text{HIT}1} = a_0 e^{\rho_1} \cosh \rho_{2\text{HIT}1} \quad (73a)$$

This is solved for the relative rapidity $\rho_{2\text{HIT}1}$ between Carl and Don's "falling" object.

$$\rho_{2\text{HIT}1} = \cosh^{-1} e^{\rho_1} = \cosh^{-1} \frac{3}{2} = 0.962 \Rightarrow u_{2\text{HIT}1} = 0.745c \quad (73b)$$

Course-grid scale factor $e^{\rho_1} = 3/2$ yields high relative velocity. So, one hopes Don's object misses Carl. But, then it falls toward Bob ($q=0$) and Al ($q=-1$) with an ever increasing relative velocities.

$$\rho_{2\text{HIT}0} = \cosh^{-1} e^{2\rho_1} = 1.451 \Rightarrow u_{2\text{HIT}0} = 0.896c \quad (73c)$$

$$\rho_{2\text{HIT}-1} = \cosh^{-1} e^{3\rho_1} = 1.887 \Rightarrow u_{2\text{HIT}-1} = 0.955c \quad (73d)$$

From Fig. 35 it is seen that Don's object hits (or passes) Carl with the same relative speed that Carl's object hits Bob or that Bob's object hits Al. These hits (or passings) lie on a

single line of rapidity $\rho_{Q\text{HIT}_q}$ as seen by generalizing (73a).

$$x_{Q\text{HIT}_q} = a_Q = a_0 e^{Q\rho_1} = a_q \cosh \rho_{Q\text{HIT}_q} = a_0 e^{q\rho_1} \cosh \rho_{Q\text{HIT}_q} \quad (74a)$$

Thus rapidity $\rho_{Q\text{HIT}_q}$ and its hyper-cosine vary with the q -index difference (Q-q).

$$e^{(Q-q)\rho_1} = \cosh \rho_{Q\text{HIT}_q} \quad (74b)$$

The $[p, q]$ points or dots in Fig. 35 mark intersections of light rays or massive objects with

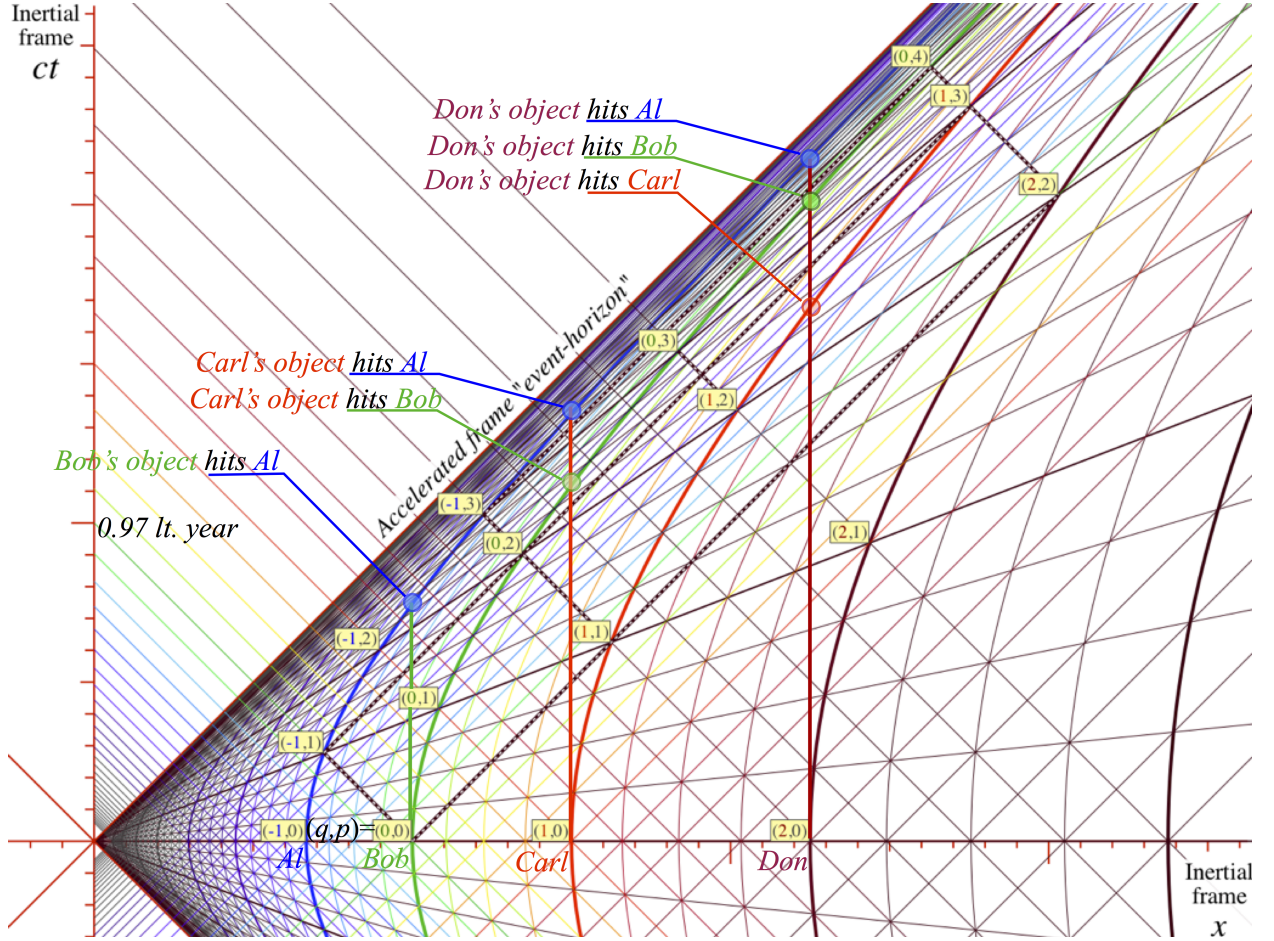


FIG. 35: Space-time paths of dropped objects hitting accelerating travelers.

members of a fleet of co-accelerating ships ($q = \dots -2, -1, 0, 1, 2, \dots$) located at each moment ($p = \dots -2, -1, 0, 1, 2, \dots$) on a line of equal rapidity $\rho_p = p\rho_1$ or velocity $u_p = c \tanh \rho_p$ with low- q ships accelerating more in the (x, ct) frame to have the same velocity u_p as their neighbors by gaining it sooner in local time τ or inertial time t than their high- q “upstairs” neighbors. Light acquires Doppler shift $e^{\rho_1} = 3/2$ in “falling” from a traveler to one below. A mass

shifts its phase frequency ν_{phase} and Hamiltonian $H = Mc^2 \cosh \rho = h\nu_{phase}$ in the Planck-law equation (34) by e^{ρ_1} according to (74b).

X. VARIATION AND QUANTIZATION OF OPTICAL AMPLITUDES

What has been deduced so far has ignored classical and quantum dynamics of *amplitude* or *quantity* of light waves and concentrated mostly on their *quality* as described by *phase* parameters such as angular frequency ω and wave vector k . The Evenson 1-CW phase axiom (*All colors go c.*) leads to Lorentz-Doppler transformation (15a) and (15b) and Planck-DeBroglie dispersion relations (34) while 2-CW amplitudes in (12) and (13) are not defined beyond assuming that head-on 1-CW component amplitudes match. White-line standing wave grid reference frames in Fig.9b and Fig.10b are just points where amplitudes are zero, that is, loci of real wave function *roots*.

Discussion of non-zero amplitude variation begins with counter-propagating 2-CW dynamics of two 1-CW amplitudes A_{\rightarrow} and A_{\leftarrow} that may be *unmatched*. ($A_{\rightarrow} \neq A_{\leftarrow}$)

$$A_{\rightarrow}e^{i(k_{\rightarrow}x-\omega_{\rightarrow}t)} + A_{\leftarrow}e^{i(k_{\leftarrow}x-\omega_{\leftarrow}t)} = e^{i(k_{\Sigma}x-\omega_{\Sigma}t)}[A_{\rightarrow}e^{i(k_{\Delta}x-\omega_{\Delta}t)} + A_{\leftarrow}e^{-i(k_{\Delta}x-\omega_{\Delta}t)}] \quad (75)$$

This uses half-sum(or half-difference) k -vector k_{Σ} (or k_{Δ}) and frequency ω_{Σ} (or ω_{Δ}).

$$k_{\Sigma} = (k_{\rightarrow} + k_{\leftarrow})/2, \quad k_{\Delta} = (k_{\rightarrow} - k_{\leftarrow})/2, \quad \omega_{\Sigma} = (\omega_{\rightarrow} + \omega_{\leftarrow})/2, \quad \omega_{\Delta} = (\omega_{\rightarrow} - \omega_{\leftarrow})/2.$$

Amplitude mean $A_{\Sigma} = (A_{\rightarrow} + A_{\leftarrow})/2$ and half-difference $A_{\Delta} = (A_{\rightarrow} - A_{\leftarrow})/2$ make standing-wave-ratio SWR or inverse standing-wave-quotient SWQ that measure wave dynamics.

$$\text{SWR} = \frac{A_{\rightarrow} - A_{\leftarrow}}{A_{\rightarrow} + A_{\leftarrow}}, \quad \text{SWQ} = \frac{A_{\rightarrow} + A_{\leftarrow}}{A_{\rightarrow} - A_{\leftarrow}}. \quad (76)$$

These are analogous to frequency ratios for group velocity (2.3b) or phase velocity (2.3a).

$$V_{group} = c \frac{\omega_{\Delta}}{k_{\Delta}} = c \frac{\omega_{\rightarrow} - \omega_{\leftarrow}}{\omega_{\rightarrow} + \omega_{\leftarrow}}, \quad V_{phase} = c \frac{\omega_{\Sigma}}{k_{\Sigma}} = c \frac{\omega_{\rightarrow} + \omega_{\leftarrow}}{\omega_{\rightarrow} - \omega_{\leftarrow}}. \quad (77)$$

A 2-state amplitude continuum is bounded by a pure right-moving 1-CW ($A_{\rightarrow}=1, A_{\leftarrow}=0$) of SWR=1 and a left-moving 1-CW ($A_{\rightarrow}=0, A_{\leftarrow}=1$) of SWR=-1. Midway between these limits is a normalized 2-CW standing-wave having SWR=0. ($A_{\rightarrow} = \frac{1}{\sqrt{2}} = A_{\leftarrow}$)

Wave paths for other SWR values are drawn in Fig.36.1a-e for 600THz 2-CW pairs and in Fig.36.2a-e for Doppler shifted 300THz and 1200THz 2-CW pairs at the same SWR values. The SWQ is the ratio of the envelope peak (interference maximum) to the envelope valley (interference minimum), and vice versa for SWR=1/SWQ. Single frequency 2-CW paths of nonzero-SWR in Fig.36.1 do a galloping motion described below while dichromatic 2-CW in Fig.36.2d-e have zero paths that follow a time switchback or staircase.

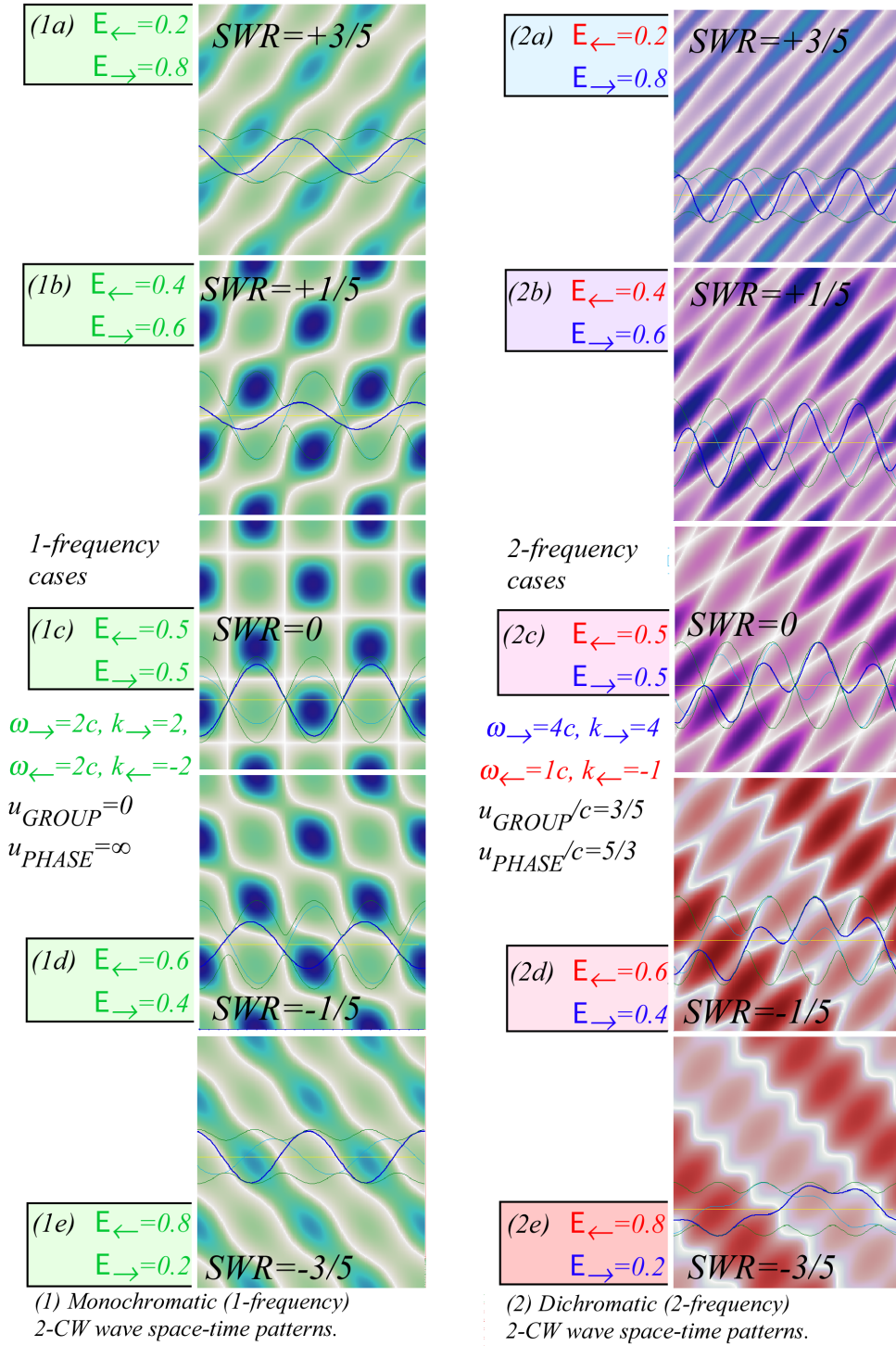


FIG. 36: 2-CW (x, ct) -paths for $\frac{3}{5} \leq SWR \leq \frac{3}{5}$ (1a-e) Single-frequency (2a-e) 2-frequency.

Waves in Fig.36.1b speed up to a peak speed of $c/SWR=5c$ as it shrinks to squeeze

through its envelope minima and then slows to resting speed $c\text{SWR}=c/5$ as it expands to its maximum amplitude. Only at zero-SWR do 2-CW zero-paths appear to travel at a constant group speed (77a) and phase speed (77b) as in Fig.36.1c and in Fig.36.2c. For $\text{SWR}=1$ or $\text{SWR}=-1$ there is just a single wave and one speed $\pm c$ following Evenson's axiom.

The real and imaginary parts take turns with one galloping while the other rests and vice versa and this occurs twice each optical period. Galloping is a fundamental interference property that may be clarified by analogy with elliptic orbits of isotropic 2D-harmonic oscillators and in particular with elliptic polarization of optical wave amplitudes. Fig.37 relates polarization states and wave states of Fig.36.1 beginning with left (right)-circular polarization that is analogous to a left (right)-moving wave in Fig.37g (Fig.37a). As sketched in Fig.37(b-e), galloping waves are general cases analogous to general states of elliptic polarization or general 2D-HO orbits obeying a Keplerian geometry shown in Fig.37h. Standing waves correspond to plane-polarization. Polarization in x -plane of Fig.37d corresponds to a standing cosine wave. y -plane polarization (not shown) would correspond to a standing sine wave.

Isotropic oscillator orbits obey Kepler's law of constant orbital momentum. Orbit angular velocity slows down by a factor b/a at the aphelion a and then speeds up by a factor a/b at the perihelion b just as a galloping wave, twice in each period, slows down to $\text{SWR}c$ and speeds up to $\text{SWQ}c$. The galloping or eccentric motion of the eccentric anomaly angle $\phi(t)$ in Fig.37h is a projection of a uniformly rotating mean anomaly (phase angle ωt) of the isotropic oscillator, and this gives a Keplerian relation of the two angles seen in the figure.

$$\tan \phi(t) = \frac{b}{a} \tan(\omega t) \quad (78)$$

Eccentric anomaly t -derivative gallops between $\omega \frac{b}{a}$ and $\omega \frac{a}{b}$.

$$\dot{\phi} = \frac{d\phi}{dt} = \omega \frac{b \sec^2 \omega t}{a \sec^2 \phi} = \frac{\omega b/a}{\cos^2 \omega t + (b/a)^2 \cdot \sin^2 \omega t} = \begin{cases} \omega b/a \text{ for: } \omega t = 0, \pi, 2\pi \dots \\ \omega a/b \text{ for: } \omega t = \pi/2, 3\pi/2, \dots \end{cases} \quad (79)$$

Angular moment r^2 times $\dot{\phi}$ is proportional to orbital momentum and orbit ellipse area πab .

$$r^2 \frac{d\phi}{dt} = \text{constant} = (a^2 \cos^2 \omega t + b^2 \cdot \sin^2 \omega t) \frac{d\phi}{dt} = \omega \cdot ab \quad (80)$$

(79) galloping also occurs in monochromatic ($\omega_{\rightarrow} = \omega_0 = \omega_{\leftarrow}$) wave (75) having SWQ (76).

$$0 = \text{Re}\Psi(x, t) = \text{Re}A_{\rightarrow} e^{i(k_0 x - \omega_0 t)} + \text{Re}A_{\leftarrow} e^{i(-k_0 x - \omega_0 t)} \quad \text{where: } \omega_{\rightarrow} = \omega_0 = \omega_{\leftarrow} = ck_0 = -ck_{\leftarrow}$$

This real-zero relation factors: $(A_{\rightarrow} + A_{\leftarrow})[\cos k_0 x \cos \omega_0 t] = -(A_{\rightarrow} - A_{\leftarrow})[\sin k_0 x \sin \omega_0 t]$. So space $k_0 x$ varies with time $\omega_0 t$ quite like eccentric anomaly $\phi(t)$ varies in (78) or (79).

$$\tan k_0 x = -SWQ \cdot \cot \omega_0 t = SWQ \cdot \tan \omega_0 \bar{t} \quad \text{where : } \omega_0 \bar{t} = \omega_0 t - \pi/2$$

$$\frac{dx}{dt} = c \cdot SWQ \frac{\sec^2 \omega_0 \bar{t}}{\sec^2 k_0 x} = \frac{c \cdot SWQ}{\cos^2 \omega_0 \bar{t} + SWQ^2 \cdot \sin^2 \omega_0 \bar{t}} = \begin{cases} c \cdot SWQ & \text{for: } \bar{t} = 0, \pi, 2\pi \dots \\ c \cdot SWR & \text{for: } \bar{t} = \frac{\pi}{2}, \frac{3\pi}{2}, \dots \end{cases} \quad (81)$$

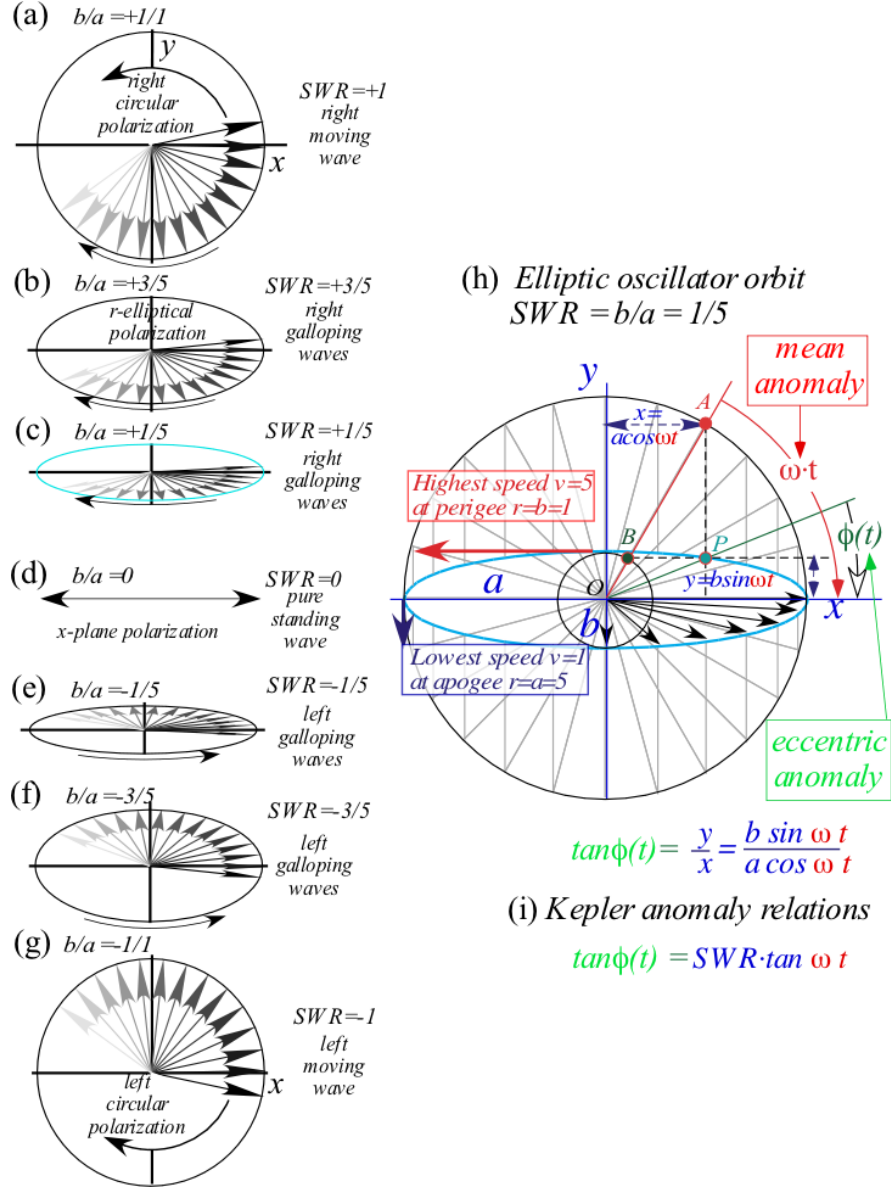


FIG. 37: (a-g) Elliptic polarization ellipses are analogous to galloping waves in Fig. 36.1. (h-i) Elliptical oscillator conserves orbit momentum while obeying Kepler relation (i).

Single frequency 2-CW paths in Fig. 6.1 have a constant product of instantaneous wave velocity and wave amplitude analogous to the constant product of orbital velocity and radius. So vacuum optical amplitude and phase motion obey a strange version of Keplerian rules. The extent to which 14th century geometric relations underlie basic wave physics may be surprising to some. Quantum aspects of wave amplitudes described next are surprising, too.

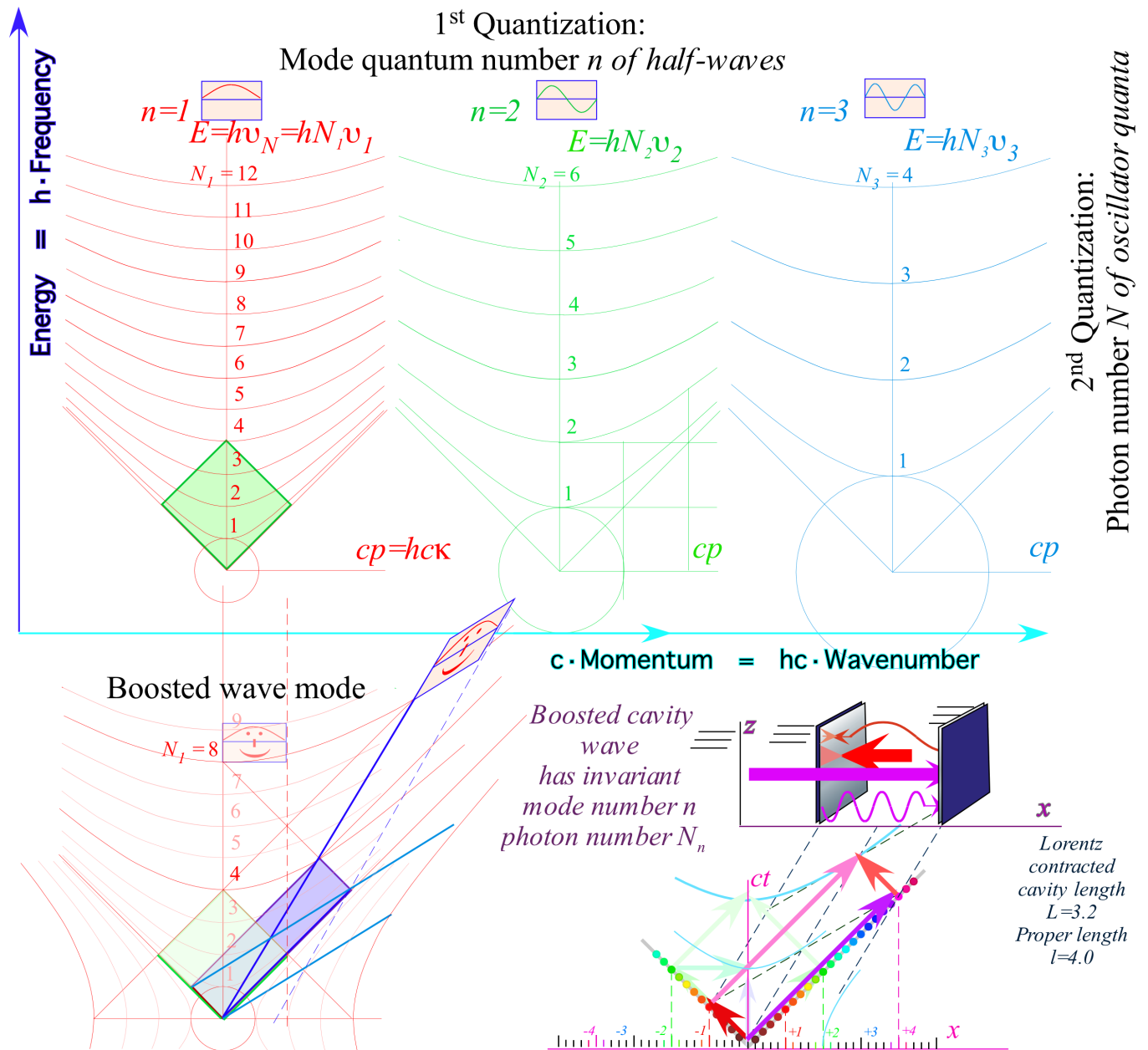


FIG. 38: 1st quantized mode stacks $n=1,2,3$ of 2nd quantized photon levels $N_n=1,2,3..\infty$

A. Quantizing Maxwell waves

Since the beginning of the 20th-century, the *classical* mechanical world has revealed an underlying ethereal wave-like *quantum* mechanical world. There classical quantities such as energy and momentum become “quantized” or restricted to discrete values like notes of a musical instrument in analogy to frequency spectra of molecules, atoms, nuclei and subatomic particles. Quantization occurs when waves bounce around in a trap or some kind of cavity where they self-interfere. There results a natural selection of survival-by-the-fittest wave best able to fit discrete quantum wave-numbers n of undulations in a cavity.

For light (electromagnetic wave mode sums $\sum A_{\mathbf{k},\omega} e^{i(\mathbf{k}\cdot\mathbf{r}-\omega t)}$) there are two kinds of quantization. 1st-quantization is of phase- $(\mathbf{k}\cdot\mathbf{r}-\omega t)$ variables \mathbf{k} and ω . 2nd-quantization is of field amplitudes $A_{\mathbf{k},\omega}$. Modes for 1st-quantum numbers $n=1,2,3,..$ of half-waves must fit in a model cavity of length- ℓ and satisfy 1st quantization conditions for $\omega_n=ck_n$ in that cavity.

$$\text{wave vector : } k_n = \frac{\pi}{\lambda_n} = n\frac{\pi}{\ell} \quad \text{---frequency : } \omega_n = ck_n = cn\frac{\pi}{\ell} \quad (82)$$

A wave-in-cavity for mode $n=1, 2,$ and 3 is sketched above stack- n of photon energy levels for 2nd-quantum numbers $N_n=1,2,..$ of photons in Fig.38. Each photon level- N_n is drawn as a relativistic hyperbola in a stack labeled by mode- n and its photon number. Each hyperbola and its quanta n and N are invariant to Lorentz transformation of space-time and (ω_n, ck_n) .

2nd-quantization of cavity mode k_n (or \mathbf{k} in 3D cavity) uses normal coordinates $A_{k_n}=A_{\mathbf{k}}$ satisfying Maxwell equations that behave as harmonic oscillators. A 2-CW-standing-wave vector potential amplitude $A_{\mathbf{k}} \equiv \mathbf{A} = \mathbf{e}_1 |A| \sin(\mathbf{k}\cdot\mathbf{r}-\omega t+\phi)$ has Maxwell \mathbf{E} -and- \mathbf{B} -fields.

$$\mathbf{E} = -\frac{\partial \mathbf{A}}{\partial t} \quad \mathbf{B} = \nabla \times \mathbf{A} \quad (83)$$

$$\mathbf{E} = \mathbf{e}_1 E_0 \cos(\mathbf{k}\cdot\mathbf{r}-\omega t+\phi) \quad \mathbf{B} = (\mathbf{k} \times \mathbf{e}_1) B_0 \cos(\mathbf{k}\cdot\mathbf{r}-\omega t+\phi)$$

Two unit polarization directions \mathbf{e}_1 of \mathbf{E} and $\mathbf{e}_2=\mathbf{k}\times\mathbf{e}_1 \frac{1}{k}$ of \mathbf{B} share equal energy.(Let: $k=\frac{\omega}{c}$)

$$(a) E_0 \mathbf{e}_1 = |A| \omega \mathbf{e}_1 \quad (b) B_0 (\mathbf{k} \times \mathbf{e}_1) = |A| k \mathbf{e}_2 \quad (84)$$

Maxwell equations gives orthonormal unit vectors $\{\mathbf{e}_1,\mathbf{e}_2,\mathbf{e}_k\}$ and average field energy $\langle U \rangle V$ in a volume V containing the 2-CW vector potential amplitude: $\mathbf{A}=\mathbf{e}_1 |A| \sin(\mathbf{k}\cdot\mathbf{r}-\omega t+\phi)$.

$$\begin{aligned} \langle U \rangle V &= \left\langle \frac{\varepsilon_0}{2} \mathbf{E} \cdot \mathbf{E} + \frac{1}{2\mu_0} \mathbf{B} \cdot \mathbf{B} \right\rangle V = V \left(\frac{\varepsilon_0}{2} |A|^2 \omega^2 + \frac{|A|^2}{2\mu_0} k^2 \right) \langle \cos^2(\mathbf{k} \cdot \mathbf{r} - \omega t + \phi) \rangle \\ &= \frac{\varepsilon_0}{2} \omega^2 |A|^2 V = \frac{1}{2\mu_0} k^2 |A|^2 V \text{ given average: } \langle \cos^2(\mathbf{k} \cdot \mathbf{r} - \omega t + \phi) \rangle = \frac{1}{2} \end{aligned} \quad (85)$$

Constants $\epsilon_0=8.854 \cdot 10^{-7} \frac{Nm^2}{C^2}$ and $\mu_0=4\pi 10^{-7} \frac{N}{A^2}$ have geometric mean $c^{-1}=\sqrt{\epsilon_0\mu_0}$, a still awe inspiring expression for the speed of light. Feynman's approach to field quantization favors Fourier combinations of complex moving waves $e^{i(kr-\omega t)}$ rather the real forms in (83).

$$\mathbf{A} = \sum_{\mathbf{k}} [(a_{\mathbf{k}1}\mathbf{e}_1 + a_{\mathbf{k}2}\mathbf{e}_2) e^{i(\mathbf{k}\cdot\mathbf{r}-\omega t)} + \text{c.c.}] = \sum_{\mathbf{k}} \sum_{\alpha=1}^2 [a_{\mathbf{k}\alpha}\mathbf{e}_\alpha e^{i(\mathbf{k}\cdot\mathbf{r}-\omega t)} + a_{\mathbf{k}\alpha}^*\mathbf{e}_\alpha e^{-i(\mathbf{k}\cdot\mathbf{r}-\omega t)}] \quad (86)$$

The \mathbf{k} -sum $k_\alpha = N_\alpha \frac{2\pi}{\ell}$ ($N_\alpha=1, 2, \dots \infty$; $\alpha=x, y, z$) separates the the 2D polarization base vectors of (84) belonging to its \mathbf{E} and \mathbf{B} oscillator dimensions. Fourier amplitudes $a_{\mathbf{k}\alpha}$ of 1-CW modes in (86) are complex and half the magnitude of the 2-CW amplitude $A_{\mathbf{k}\alpha}$ in (85) since $A \cos \phi = \frac{A}{2} e^{i\phi} + \frac{A}{2} e^{-i\phi}$. Setting $\langle U \rangle V$ in (85) to Planck's $\epsilon_N = \hbar N \omega$ relates A to N .

$$\langle U \rangle V = \hbar N \omega = \frac{\epsilon_0}{2} \omega^2 |A|^2 V \quad \Rightarrow \quad |A| = \sqrt{\frac{2\hbar N}{\epsilon_0 \omega V}} \quad \Rightarrow \quad |\mathbf{E}| = \omega |A| = \sqrt{\frac{2\hbar N \omega}{\epsilon_0 V}} \quad (87)$$

This assumes energy is confined to one quantum level $N_{\mathbf{k}\alpha}$ of one cavity mode \mathbf{k} of one polarization- α . Laser coordinate grids in Fig.9 and Fig.10 require coherent 2-CW Poisson N -distributions seen later where pure photon number N -states wash out grids in Fig.41d.

Planck knew that classical oscillator energy is proportional to the square of the product $|A|\omega$ of amplitude and frequency and worried that his hypothetical $\hbar N \omega$ had to be wrong.

1. Quantum numbering of photons and modes

Building 1-CW Fourier expansions of fields \mathbf{E} and \mathbf{B} to construct their energies $U_E V$ and $U_B V$ from vector potential \mathbf{A} in (86).

$$\begin{aligned} U_E V &= \sum_{\mathbf{k}\alpha} \frac{\epsilon_0 V}{2} [2|a_{\mathbf{k}\alpha}|^2 \omega^2 - a_{-\mathbf{k}\alpha}^* a_{\mathbf{k}\alpha}^* \omega^2 e^{-2i\omega t} - a_{-\mathbf{k}\alpha} a_{\mathbf{k}\alpha} \omega^2 e^{-2i\omega t}] \\ U_B V &= \sum_{\mathbf{k}\alpha} \frac{\epsilon_0 V}{2} [2|a_{\mathbf{k}\alpha}|^2 \omega^2 + a_{-\mathbf{k}\alpha}^* a_{\mathbf{k}\alpha}^* \omega^2 e^{-2i\omega t} + a_{-\mathbf{k}\alpha} a_{\mathbf{k}\alpha} \omega^2 e^{-2i\omega t}] \quad (88) \end{aligned}$$

Cancellation of cross-terms simplifies total energy sum.

$$UV = (U_E + U_B) V = \sum_{\mathbf{k}\alpha} 2\epsilon_0 \omega^2 |a_{\mathbf{k}\alpha}|^2 V = \sum_{\mathbf{k}\alpha} 2\epsilon_0 V \omega^2 a_{\mathbf{k}\alpha}^* a_{\mathbf{k}\alpha} \quad (89)$$

This may be factored and relabeled into a harmonic oscillator Hamiltonian.

$$\begin{aligned}
UV &= \sum_{\mathbf{k}\alpha} \frac{1}{2} \left[2\omega\sqrt{\varepsilon_0 V} (a_{\mathbf{k}\alpha}^{\text{Re}} - ia_{\mathbf{k}\alpha}^{\text{Im}}) \right] \left[2\omega\sqrt{\varepsilon_0 V} (a_{\mathbf{k}\alpha}^{\text{Re}} - ia_{\mathbf{k}\alpha}^{\text{Im}}) \right] \\
&= \sum_{\mathbf{k}\alpha} \frac{1}{2} [\omega Q_{\mathbf{k}\alpha} + iP_{\mathbf{k}\alpha}] [\omega Q_{\mathbf{k}\alpha} + iP_{\mathbf{k}\alpha}] \\
&= \sum_{\mathbf{k}\alpha} \frac{1}{2} (P_{\mathbf{k}\alpha}^2 + \omega^2 Q_{\mathbf{k}\alpha}^2)
\end{aligned} \tag{90}$$

Real and imaginary parts of phasor amplitudes $a_{\mathbf{k}\alpha}$ are coordinates $Q_{\mathbf{k}\alpha}$ and momenta $P_{\mathbf{k}\alpha}$.

$$\begin{aligned}
Q_{\mathbf{k}\alpha} &= 2\sqrt{\varepsilon_0 V} a_{\mathbf{k}\alpha}^{\text{Re}} = \sqrt{\varepsilon_0 V} (a_{\mathbf{k}\alpha} + a_{\mathbf{k}\alpha}^*) \quad \text{where: } a_{\mathbf{k}\alpha} = a_{\mathbf{k}\alpha}^{\text{Re}} + ia_{\mathbf{k}\alpha}^{\text{Im}} = \frac{1}{2\sqrt{\varepsilon_0 V}} \left(Q_{\mathbf{k}\alpha} + \frac{iP_{\mathbf{k}\alpha}}{\omega} \right) \\
P_{\mathbf{k}\alpha} &= 2\omega\sqrt{\varepsilon_0 V} a_{\mathbf{k}\alpha}^{\text{Im}} = \omega\sqrt{\varepsilon_0 V} (a_{\mathbf{k}\alpha} - a_{\mathbf{k}\alpha}^*)/i \quad \text{and: } a_{\mathbf{k}\alpha}^* = a_{\mathbf{k}\alpha}^{\text{Re}} - ia_{\mathbf{k}\alpha}^{\text{Im}} = \frac{1}{2\sqrt{\varepsilon_0 V}} \left(Q_{\mathbf{k}\alpha} - \frac{iP_{\mathbf{k}\alpha}}{\omega} \right)
\end{aligned} \tag{91}$$

Amplitudes $a_{\mathbf{k}\alpha}$ and $a_{\mathbf{k}\alpha}^*$ become operators of photon destruction $\mathbf{a}_{\mathbf{k}\alpha}$ and creation $\mathbf{a}_{\mathbf{k}\alpha}^\dagger$ that find 2D oscillator waves and energy spectrum for each \mathbf{k} -mode and each polarization $\alpha=x, y$.

$$E_{\mathbf{k}} = \hbar\Omega_{\mathbf{k}} = \hbar(N_{\mathbf{k}} + 1)\omega_{\mathbf{k}} = \hbar(N_{x,\mathbf{k}} + N_{y,\mathbf{k}} + 1)\omega_{\mathbf{k}} \tag{92}$$

The ground quantum state has zero ($N_{\mathbf{k}}=0$) photons with zero-point energy $\hbar\omega_{\mathbf{k}}$. (Zero point energy is $\frac{1}{2}\hbar\omega_{\mathbf{k}}$ for each polarization dimension.) There are two energy-degenerate states having one photon ($N_{\mathbf{k}}=1$) each with energy $E_{\mathbf{k}}=\hbar 2\omega_{\mathbf{k}}$, that is, one photon with x -polarization or else one photon with y -polarization. Similarly, there are three states of two photons ($N_{\mathbf{k}}=2$) with energy $E_{\mathbf{k}}=\hbar 3\omega_{\mathbf{k}}$, that is, $(N_{x,\mathbf{k}}, N_{y,\mathbf{k}})=(2,0)$, $(1,1)$, or $(0,2)$. A general $N_{\mathbf{k}}$ -photon energy level $E_{\mathbf{k}}=\hbar(N_{\mathbf{k}}+1)\omega_{\mathbf{k}}$ has polarization degeneracy of $N_{\mathbf{k}}+1$.

A sketch of the first few quantum cavity wave states is given in Fig.39. It is companion to Fig.38 showing a stack of $N_{\mathbf{k}}$ -labeled energy-level hyperbolas for each cavity mode $k_n=\mathbf{k}$. The quantum numbers N (Number of photons) and n (number of “kinks” or anti-nodes per cavity dimension ℓ) are invariant to observer rapidity ρ while wave energy (frequency) and momentum (wave number) vary with observer rapidity as $\cosh\rho$ and $\sinh\rho$, respectively.

Newton might be consoled that number N of photons in a box is invariant to speed $\rho \simeq \frac{u}{c}$ so they act like self-respecting corpuscles without “fits” that he saw waves suffer. However, photon number N is a wave-based property, a wave kink-count in amplitude (A_x, A_y) space, just as mode number n of wavenumber k_n counts wave kinks in real (x, y, z) space.

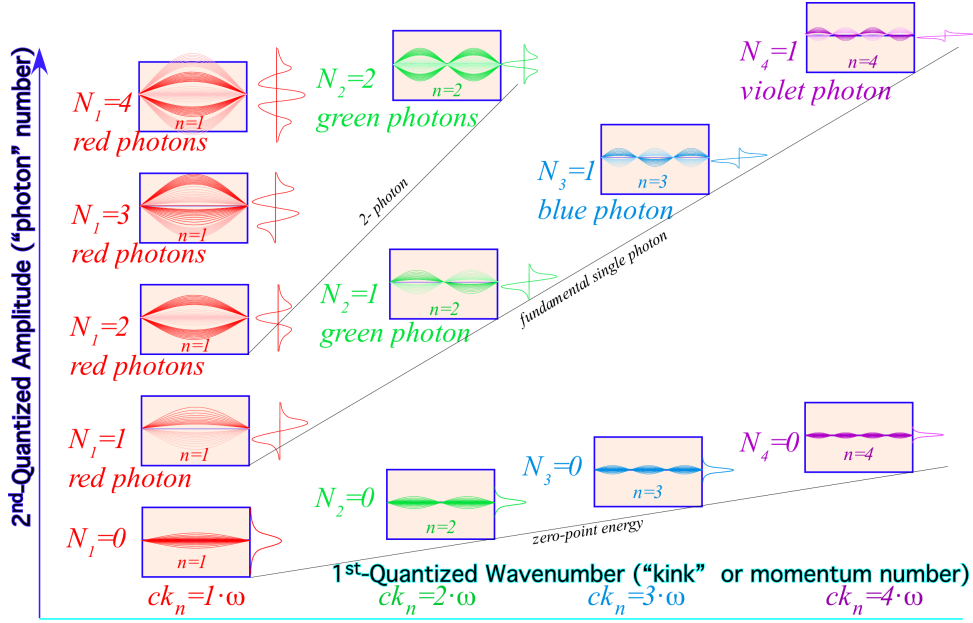


FIG. 39: 1st and 2nd quantized harmonic-oscillator cavity waves

2. Quantum wave normalization

Classical variables such as momentum, energy, or fields become operators whose eigenvalues are observed. This is discussed in a following section devoted to Hamiltonian and Lagrangian mechanics. Here the focus is upon field oscillators whose classical energy (89) has a form of 2nd-power amplitude-frequency product $E=kA^2\omega^2$, while quantum eigenvalues have the Planck form (92) that is only 1st-power in a frequency-quantum-number product $E_N=\hbar N\omega$. Planck may have had some anxious doubts about this.

This and other issues are resolved by re-examining quantum $|\mathbf{E}|$ -amplitude in (87). It shows that product $N\omega$ is proportional to $\omega^2|\mathbf{A}|^2$ in the expression for energy density U .

$$\langle U \rangle = \frac{\hbar N\omega}{V} = \frac{\varepsilon_0}{2}|\mathbf{E}|^2 = \frac{\varepsilon_0}{2}\omega^2|\mathbf{A}|^2 \quad \Rightarrow \quad |\mathbf{E}| = \omega|\mathbf{A}| = \sqrt{\frac{2\hbar N\omega}{\varepsilon_0 V}} \quad (93)$$

Scaling \mathbf{E} by $s = \sqrt{\frac{V\varepsilon_0}{2\hbar\omega}}$ gives an N -photon wave Ψ amplitude whose norm is N .

$$\vec{\Psi} = \begin{pmatrix} \Psi_x \\ \Psi_y \end{pmatrix} = s\mathbf{E} = \sqrt{\frac{\varepsilon_0 V}{2\hbar\omega}}\mathbf{E} \quad \Rightarrow \quad \vec{\Psi}^*\vec{\Psi} = |\Psi_x|^2 + |\Psi_y|^2 = N \quad (94)$$

Having the absolute-square $\Psi^*\Psi = |\Psi|^2$ or norm of a Ψ -wave function equal to the number N of quanta is a familiar axiom of modern quantum theory. If the wave is a variable

wave-function $\Psi(x, y, z)$ then a volume integral is required to sum up energy density U .

Elementary quantum theory of a single particle requires unit normalization $\int d(xyz)\Psi^*\Psi=1$.

$$\iiint \Psi(\mathbf{r})^*\Psi(\mathbf{r})d^{(3)}\mathbf{r} \quad (95)$$

Elementary quantum theory of a single particle requires unit normalization $\int d(xyz)\Psi^*\Psi=1$.

Poynting flux $\mathbf{S}=\mathbf{E}\times\mathbf{B}$ or “photon current” of a plane moving wave (1-CW ψ) also has a classical 2^{nd} -power expression that reduces to a Planck 1^{st} -power form. Flux \mathbf{S} has direction along \mathbf{k} and magnitude $S=cU$. The quantum number n for S is flux rate: $n=cN/V(m^{-2}s^{-1})$.

Poynting flux $\mathbf{S}=\mathbf{E}\times\mathbf{B}$ or “photon current” of a plane moving wave (1-CW ψ) also has a classical 2^{nd} -power expression that reduces to a Planck 1^{st} -power form. Flux \mathbf{S} has direction along \mathbf{k} and magnitude $S=cU$. The quantum number n for S is flux rate: $n=cN/V(m^{-2}s^{-1})$.

$$S = cU = c\varepsilon_0|\mathbf{E}|^2 = \hbar n\omega \quad \text{where:} \quad n = cN/V(\text{per } m^2s) \quad (96)$$

The 1-CW flux rate of photons n per square-meter per second is not invariant to observer rapidity ρ as is the cavity count of N/V photons per cubic meter of cavity in (87). Instead n transforms like frequency ω and suffers the same Doppler factor e^ρ for an observer approaching the source or else $e^{-\rho}$ when fleeing the source.

This amounts to a double-whammy for an approaching observer experiencing a Doppler increase in both *quality* (color or frequency $\omega=2\pi\nu$) and *quantity* (N of photon hits) and raises flux impact to 2^{nd} -power (e^ρ)². This matches the 2^{nd} -power $|\mathbf{E}|^2$ of the \mathbf{E} -field and implies that the \mathbf{E} -field *amplitude* shifts by e^ρ just like 1-CW wave vector \mathbf{k} and frequency $\omega=c|\mathbf{k}|$. Perhaps, this is a lesson from Planck quantum axiom reminding us that the relativistic wave amplitude is a (per-space-time) *frequency*, too, just like energy and momentum.

3. Relativistic 1-CW covariance of Poynting flux

Maxwell-Planck energy density $U[\text{Joule}/m^3]$ (85) times c is Poynting flux $S[\text{Joule}/m^2s]$.

$$\mathbf{S} = \mathbf{E}\times\mathbf{B} = \langle U_k \rangle c\hat{\mathbf{k}} = 2\varepsilon_0c \langle \mathbf{E}_k \bullet \mathbf{E}_k \rangle \hat{\mathbf{k}} = \hbar\omega_k \bar{n}_k \hat{\mathbf{k}} \quad \text{where:} \quad n_k = cN_k/V [m^{-2}s^{-1}] \quad (97)$$

Flux \mathbf{S} contains two frequency factors, the fundamental laser frequency ω_k and the photon count rate n_k per $[m^2s]$. Frequency ω_k is quantum *quality* of a laser beam and rate n_k is its quantum *quantity*.The product $\hbar\omega_k n_k$ is Poynting *flux*. Rate n_k and frequency ω_k both

Doppler shift by an exponential $e^{\pm\rho}$ of rapidity ρ in (2.16). So do 1-CW fields \mathbf{E}_k as may be shown by Lorentz transforming a laser beam transverse electric field directly.

$$E'_{+k'} = e^{+\rho} E_{+k} \quad E'_{-k'} = e^{-\rho} E_{-k} \quad (98)$$

Thus both electric field polarization \mathbf{E} -amplitudes E_x and E_y of a 1-CW field undergo the same $e^{\pm\rho}$ Doppler shift that the frequency ω_k or wavevector \mathbf{k} experience. If \mathbf{E} in (97) is scaled by single-photon factor $s = \sqrt{\frac{V\epsilon_0}{2\hbar\omega}}$ (after (93)) a probability wave Ψ follows whose square $\Psi^*\Psi$ is a per-volume photon density N/m^3 .

$$\Psi_k = \sqrt{\frac{2\epsilon_0 V}{\hbar\omega_k}} E_k \Rightarrow \langle \Psi_k^* \Psi_k \rangle = \langle N_k \rangle = \bar{N}_k = \bar{n}_k \frac{V}{c} \quad (99)$$

Flux probability wave ψ is defined so its square $\psi^*\psi$ is an expected photon flux count n/m^2s .

$$\psi_k = \sqrt{\frac{2\epsilon_0 c}{\hbar\omega_k}} E_k \Rightarrow \langle \psi_k^* \psi_k \rangle = \langle n_k \rangle = \bar{n}_k = \frac{c}{V} \bar{N}_k \quad (100)$$

Scaling $1/\sqrt{\omega_k}$ of E_k adds a factor $e^{\pm\rho/2}$ to Doppler factor for $E_{\mp k}$ in (98).

$$L_z(\rho) |\psi\rangle = \begin{pmatrix} \psi'_{+k} \\ \psi'_{-k} \end{pmatrix} = \begin{pmatrix} e^{+\rho/2} & 0 \\ 0 & e^{-\rho/2} \end{pmatrix} \begin{pmatrix} \psi_{+k} \\ \psi_{-k} \end{pmatrix} = e^{\sigma_z \rho/2} |\psi\rangle \quad (101)$$

This is a starting point for the spinor form of Lorentz transformation for Dirac amplitudes.

4. Relativistic 2-CW invariance of cavity quanta

Mean photon number \bar{N}_k of a 2-CW cavity mode is invariant to cavity rapidity ρ , quite unlike the 1-CW wave in (101) or flux n_k . Also, the 2-CW mode has ρ -invariant geometric mean wave velocity $c = \sqrt{V_{group} \cdot V_{phase}}$ and mean frequency $\bar{\omega} = \sqrt{\omega_{+k}\omega_{-k}} = \sqrt{\omega^2 - c^2k^2}$. Transformation of the phase and group velocity (24) and of 2-CW fields is not so simple.

$$\frac{V_{phase}}{c} = \frac{\omega_{+k} + \omega_{-k}}{\omega_{+k} - \omega_{-k}}, \quad \frac{V_{group}}{c} = \frac{\omega_{+k} - \omega_{-k}}{\omega_{+k} + \omega_{-k}}. \quad (102)$$

Linear dispersion $\omega_{\pm k} = \pm ck$ of component 1-CW apply. *SWR* relations (76) are used.

$$SWR = \frac{E_{+k} - E_{-k}}{E_{+k} + E_{-k}}, \quad SWQ = \frac{E_{+k} + E_{-k}}{E_{+k} - E_{-k}}. \quad (103)$$

The *SWR* is a wave velocity and Doppler-transforms like relativistic velocity u/c .

$$SWR' = \frac{SWR + u/c}{1 + SWR \cdot u/c}, \quad \frac{V'_m}{c} = \frac{V_m/c + u/c}{1 + (V_m/c) \cdot (u/c)}. \quad (104)$$

Velocity $\frac{u_{AB}}{c} = \tanh \rho_{AB}$ is a hyper-tan sum. Rapidity is sum $\rho_{AB} = \rho_A + \rho_B$ by Fig.8.

$$\frac{u_{AB}}{c} = \tanh \rho_{AB} = \tanh(\rho_A + \rho_B) = \frac{\tanh \rho_A + \tanh \rho_B}{1 + \tanh \rho_A \tanh \rho_B} = \frac{u_A/c + u_B/c}{1 + u_A u_B / c^2} \quad (105)$$

B. E-Field 2-CW flux relations

Total flux energy E and momentum p are found for counter- k 2-CW beam wave Ψ .

$$\Psi_{k\rightleftharpoons} = \psi_{\rightarrow} e^{i(k_{\rightarrow}x - \omega_{\rightarrow}t)} + \psi_{\leftarrow} e^{i(k_{\leftarrow}x - \omega_{\leftarrow}t)} \quad (106)$$

Lab 1-CW flux number values $|\psi_k|^2 = \langle n_k \rangle$ give 2-CW flux expectations in lab.

$$\begin{aligned} \langle E \rangle &= \langle \hbar\omega \rangle = \hbar\omega_{\rightarrow} \langle n_{\rightarrow} \rangle + \hbar\omega_{\leftarrow} \langle n_{\leftarrow} \rangle = \hbar\omega_{\rightarrow} |\psi_{\rightarrow}|^2 + \hbar\omega_{\leftarrow} |\psi_{\leftarrow}|^2 \\ \langle cp \rangle &= \langle \hbar ck \rangle = \hbar ck_{\rightarrow} \langle n_{\rightarrow} \rangle + \hbar ck_{\leftarrow} \langle n_{\leftarrow} \rangle = \hbar\omega_{\rightarrow} |\psi_{\rightarrow}|^2 - \hbar\omega_{\leftarrow} |\psi_{\leftarrow}|^2 \end{aligned}$$

The relation (100) of quantum field ψ_k and classical E_k -field expectation is used.

$$\begin{aligned} \langle E \rangle &= \hbar\omega_{\rightarrow} |\psi_{\rightarrow}|^2 + \hbar\omega_{\leftarrow} |\psi_{\leftarrow}|^2 = 2\varepsilon_0 c (|E_{\rightarrow}|^2 + |E_{\leftarrow}|^2) \\ \langle cp \rangle &= \hbar\omega_{\rightarrow} |\psi_{\rightarrow}|^2 - \hbar\omega_{\leftarrow} |\psi_{\leftarrow}|^2 = 2\varepsilon_0 c (|E_{\rightarrow}|^2 - |E_{\leftarrow}|^2) \end{aligned} \quad (107)$$

Values $\langle cp \rangle$ and $\langle E \rangle$ lie on invariant hyperbola of constant geometric means $\varpi \bar{N}$ or $|\bar{\mathbf{E}}|^2$.

$$\begin{aligned} \langle E \rangle^2 - \langle cp \rangle^2 &= (2c\varepsilon_0)^2 \left[(|E_{\rightarrow}|^2 + |E_{\leftarrow}|^2)^2 - (|E_{\rightarrow}|^2 - |E_{\leftarrow}|^2)^2 \right] = (2c\varepsilon_0)^2 [4|E_{\rightarrow}|^2 |E_{\leftarrow}|^2] \\ \langle E \rangle^2 - \langle cp \rangle^2 &= 4 (2c\varepsilon_0 |E_{\rightarrow}|^2) (2c\varepsilon_0 |E_{\leftarrow}|^2) = 4 (\hbar\omega_{\rightarrow} \langle n_{\rightarrow} \rangle) (\hbar\omega_{\leftarrow} \langle n_{\leftarrow} \rangle) \end{aligned} \quad (108)$$

The $E(cp)$ hyperbolic dispersion equation reduces to simple expressions.

$$\sqrt{\langle E \rangle^2 - \langle cp \rangle^2} = 2c\varepsilon_0 |2\bar{\mathbf{E}}|^2 = (\hbar\bar{\omega}) (2\bar{n}) \quad (109)$$

These involve geometric mean frequency $\bar{\omega}$, mean quantum number \bar{n} , and mean field $|\bar{\mathbf{E}}|$.

$$\bar{\omega} = \sqrt{\omega_{\rightarrow}\omega_{\leftarrow}}, \quad \bar{n} = \sqrt{n_{\rightarrow}n_{\leftarrow}}, \quad |\bar{\mathbf{E}}| = \sqrt{E_{\rightarrow}E_{\leftarrow}}. \quad (110)$$

Doppler relations imply Lorentz invariance for the mean number \bar{n} and for the mean frequency $\bar{\omega}$. Also invariant is their geometric mean that is $2c\varepsilon_0$ times the mean field $|\bar{\mathbf{E}}|$ as it applies to a general 2-CW beam wave function ψ . The factors of 2 in (109) are consistent with 1-photon 2-CW states having $n_{\rightarrow} = \bar{n} = n_{\leftarrow} = \frac{1}{2}$ and total 1-photon Planck energy expectation $E = \hbar\omega$. Ideal cavities balance field ($E_{\rightarrow} = \bar{E} = E_{\leftarrow}$), frequency ($\omega_{\rightarrow} = \bar{\omega} = \omega_{\leftarrow}$), and number ($n_{\rightarrow} = \bar{n} = n_{\leftarrow}$). However, a general beam has unbalanced frequency $\omega_{\rightarrow} \neq \omega_{\leftarrow}$, number $n_{\rightarrow} \neq n_{\leftarrow}$, or field $E_{\rightarrow} \neq E_{\leftarrow}$. According to (107) a 2-CW field with unbalanced E field-amplitudes, that is unbalanced $\hbar n\omega$, has non-zero momentum cp . A center-of-momentum COM-frame of zero momentum cp has a group velocity determined by (102). Consider

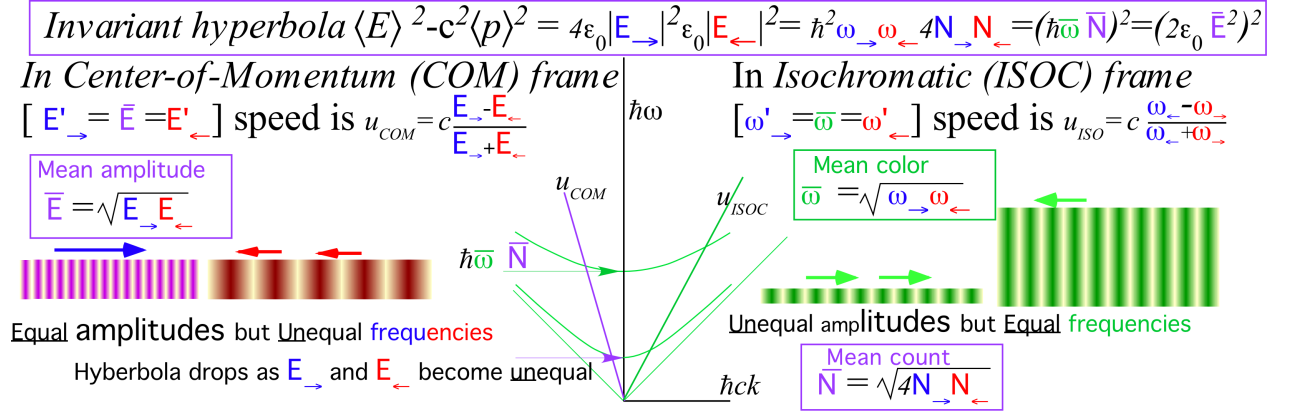


FIG. 40: Cavity 2-CW modes and invariant hyperbolas. (a) COM frame. (b) ISOC frame.

speeds for frames balancing field $E_{\rightarrow}^{com} = E_{\leftarrow}^{com}$, frequency $\omega_{\rightarrow}^{isoc} = \omega_{\leftarrow}^{isoc}$, or number $n_{\rightarrow}^{ison} = n_{\leftarrow}^{ison}$. The first two cases are sketched in Fig. 40.

$$\frac{u^{COM}}{c} = \frac{E_{\rightarrow} - E_{\leftarrow}}{E_{\rightarrow} + E_{\leftarrow}}, \quad \frac{u^{ISOC}}{c} = \frac{\omega_{\rightarrow} - \omega_{\leftarrow}}{\omega_{\rightarrow} + \omega_{\leftarrow}} = \frac{V^{Group}}{c}, \quad \frac{u^{ISON}}{c} = \frac{n_{\rightarrow} - n_{\leftarrow}}{n_{\rightarrow} + n_{\leftarrow}}. \quad (111)$$

C. Photon-number vs. Coherent-alpha waves

Optical fields $\mathbf{A}(x, t)$ or $\mathbf{E}(x, t)$ have quantum eigenvalues (92) of field operators based on mode amplitudes a_k or a_k^* in classical energy expressions (89) thru (91). Each a_k or a_k^* is replaced by oscillator boson operator \mathbf{a}_k or \mathbf{a}_k^\dagger in a quantum field Hamiltonian

$$\mathbf{H} = \sum \hbar \omega_k (\mathbf{a}_k^\dagger \mathbf{a}_k + \bar{\alpha}) \quad (112)$$

whose eigenstates $|N_1 N_2 \cdots N_k\rangle$ have exact quantized photon numbers for each mode- k_m .

Each mode phase 1st-quanta m and amplitude 2nd-quanta N_m define invariant constants for another hyperbola with Einstein-Planck proper frequency $\Omega_{N,m} = \hbar N_m \omega_m$ as sketched in Fig.38 and Fig.39. The problem is that absolute certainty of photon number N_m implies totally uncertain field phase just as absolutely certain (ck, ω) for 1-CW symmetry implies totally uncertain position in space and time. Space-time position coordinates were defined by taking 1-CW combinations to make 2-CW coordinates of Fig.9 or Fig.10. Ultimately an n-CW pulse-wave (PW) of Fig.15 or Fig.16 was localized with a low space-time uncertainty $\Delta\tau$, but then it acquires per-space uncertainty or bandwidth $\Delta\nu$ according to Fourier-Heisenberg relation $\Delta\tau \cdot \Delta\nu \geq 1$ discussed around Fig.14.

So also must photon-number states be combined if amplitude and phase uncertainty are to be reduced to the point where wave space-time coordinates can emerge. Such combinations are known as coherent states or α -states of harmonic oscillation. Sharper wave zeros require fuzzier hyperbolas *vice-versa*.

1. Fuzzy hyperbolas vs. fuzzy coordinates

Model micro-laser states $|\alpha\rangle = \sum_N \psi_N |N\rangle$ are coherent states made of single-mode eigenstates $|N\rangle = (\mathbf{a}_1^\dagger)^N |0\rangle$ with amplitudes $\psi_N = \alpha^N e^{-\alpha^2/2} / \sqrt{N!}$ parametrized by the variable $\alpha = x + ip = |\alpha| e^{i\Phi}$. That is, average mode phase components ($x = \text{Re } \alpha, p = \text{Im } \alpha$), rescaled by a quantum field factor f , are field averages $(\langle A \rangle, \langle \dot{A} \rangle = -\langle E \rangle)$.

$$\langle \alpha | A | \alpha \rangle = \langle A \rangle = (\alpha + \alpha^*) f = (\alpha + \alpha^*) \sqrt{\frac{\hbar}{2\varepsilon_0 \omega V}} \quad (113)$$

Amplitude factor f turns Planck relation $\bar{E} = \hbar\omega\bar{N}$ into Maxwell field energy $\bar{E} = \bar{U} \cdot V$.

$$\langle U \rangle V = 2\varepsilon_0 \omega^2 V \langle A^2 \rangle = \hbar\omega |\alpha|^2 = \hbar\omega\bar{N} \quad (114)$$

A fundamental laser mode in a $0.25\mu\text{m}$ cubic cavity (See **E**-wave in a strip of Fig. 9.) contains green laser light with $\hbar\bar{\omega} = 4 \cdot 10^{-19} \text{Joule}$ or about 2.5eV per photon. Average photon number $\bar{N} = |\alpha|^2 = 10^{10}$ models a laser with energy $\bar{E} = \bar{U} \cdot V = \hbar\bar{\omega}\bar{N} = 4.0 \text{ nanoJ}$ in a volume $V = (\frac{1}{4}\mu\text{m})^3$. Photon number uncertainty varies inversely to phase uncertainty.

$$\Delta\Phi \cdot \Delta N = \pi \quad \text{or:} \quad \Delta\Phi = \pi/\alpha \sim 3 \cdot 10^{-5} \quad \text{where: } \Delta N = |\alpha| = 10^5 \quad (115)$$

Amplitude expectation value $\langle N | A | N \rangle$ is zero for $|N\rangle$ states due to *incoherence* of phase, but number value $\langle N | \mathbf{a}_k^\dagger \mathbf{a}_k | N \rangle = N$ is exact as is proper frequency $\bar{\omega}N$ due to the phase factor $(e^{-i\bar{\omega}t})^N$ of $(\mathbf{a}_k^\dagger)^N$. Approximate N -quantum number uncertainty is $\Delta N = \sqrt{\bar{N}}$.

A volume V with ($N=10^{10}$)-photons has energy $E = \hbar\bar{\omega}N$. That is a mass-equivalent of $M = E/c^2 = 10^{-25} \text{kg}$ on a hyperbola 10^{10} quanta above the $N=1$ hyperbola. A coherent-state $|\alpha = 10^5\rangle$ has a mass $M = 10^{-25} \text{kg}$ with uncertainty $\Delta M = 10^{-30} \text{kg}$ so its phase uncertainty $3 \cdot 10^{-5}$ is low enough to make an (x, ct) -grid (Fig.41b) but a low- α state (Fig.41a) has too few photon counts-per-grid to plot sharply. Photon-number eigenstate $|N\rangle$ in Fig.41d is a total wash even for high- N since $\Delta N = 0$ implies maximal phase uncertainty ($\Delta\Phi = \infty \gg 2\pi$). The coherent wave amplitude dynamics of the (x, ct) gridlines in Fig.41b is revealed more clearly in Fig.42 that shows real amplitudes plotted over (x, ct) .

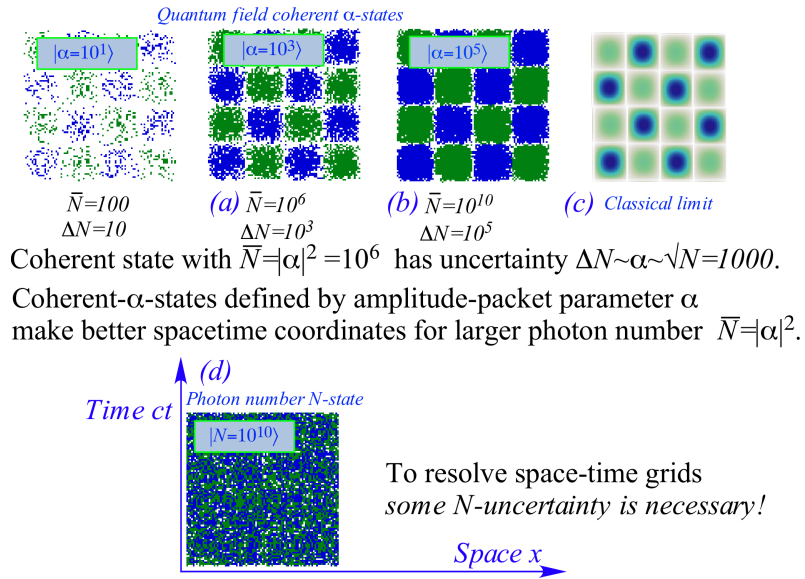


FIG. 41: Coherent α -wave grids $\alpha \sim \Delta N$ (a) 10^3 , (b) 10^5 , (c) ∞ , (d)0.

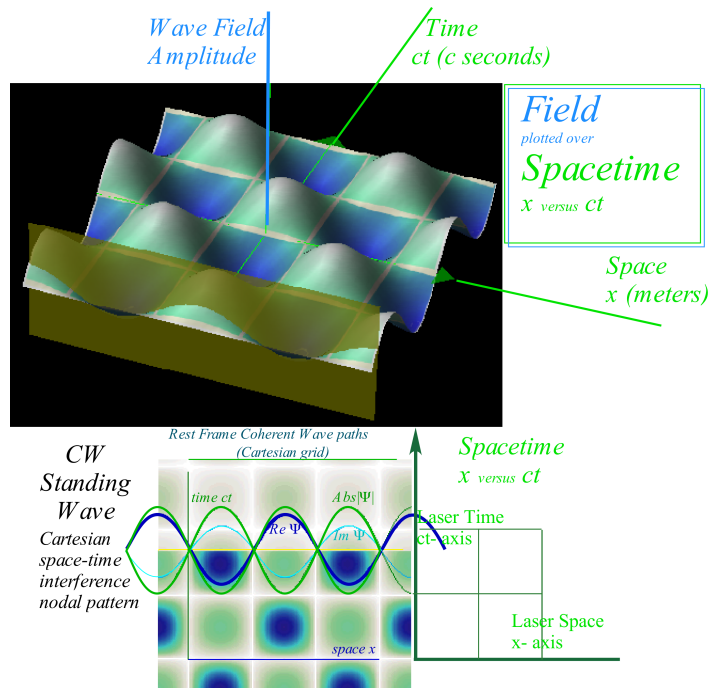
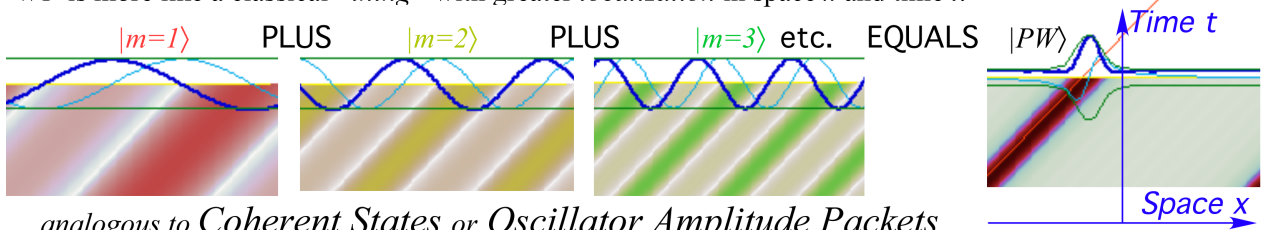


FIG. 42: Coherent real α -wave plotted over space-time.

Cosine waves in Fig.42 are coherent α -waves shown in Fig.43 as weighted sums of oscillator N -eigenstates analogous to wave packets that are weighted sums of plane wave k -eigenstates. Coherent amplitude $\psi_N = \alpha^N e^{-\alpha^2/2} / \sqrt{N!}$ has a built-in tapering of each N -state as can be seen in the tapered phasor sizes in the lower right-hand corner of Fig.43.

Wave Packets...

Adding CW's (Continuous Waves $m=1,2,3\dots$) makes PW (Pulse Wave) or WP (Wave Packet)
 WP is more like a classical "thing" with greater localization in space x and time t .



...analogous to Coherent States or Oscillator Amplitude Packets

Adding photons (Quantized amplitude $N=0,1,2\dots$) can make a CS (Coherent State) or OAP (Oscillator Amplitude Packet) that is more like a classical wave oscillation with more localization in field amplitude.

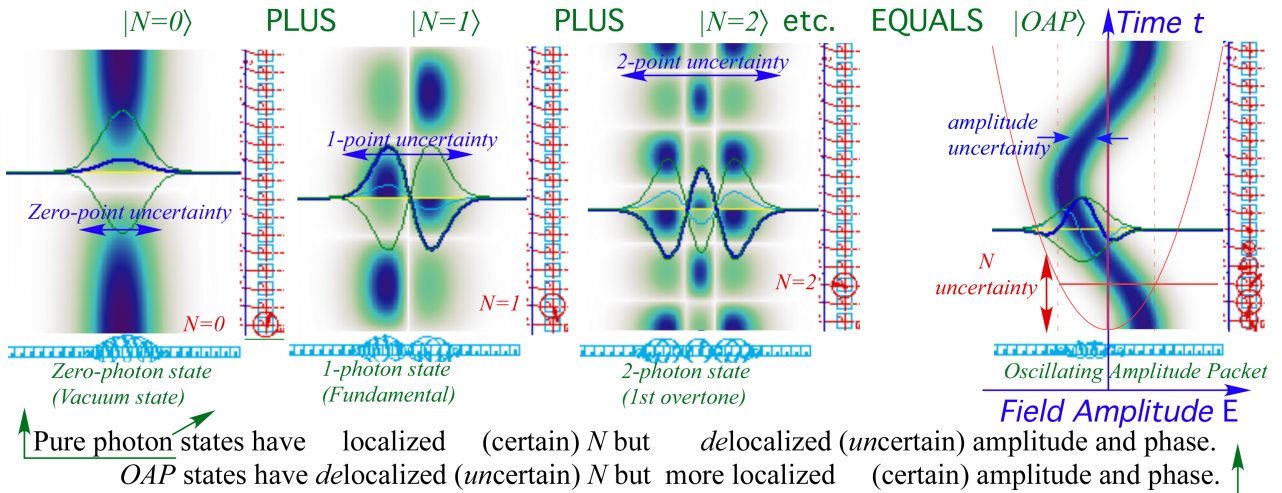


FIG. 43: Analogy: $e^{i(kx-\omega t)}$ -wave packet and Coherent α -wave oscillator amplitude packet.

It helps to recall the tapered wave-sum amplitudes in eq(26) that suppress the ringing along wave pulses in Fig.14 and make smoothly formed PW peaks in Fig.15 or the pulse wave packet in the top portion of Fig.43. This example and the coherent oscillator wave in the lower portion are as close as we get to having quantum wave dynamics that mimics the corresponding classical mechanics.

It remains to be seen whether this coherent classical correspondence can also be seen in transition mechanics described by Feynman diagrams in Fig.29 or Fig. 31. In particular the dynamics of pair-creation and pair-annihilation diagrammed on all four energy hyperbolas in Fig.44 deserves to have some coherent light shed upon its seminal process.

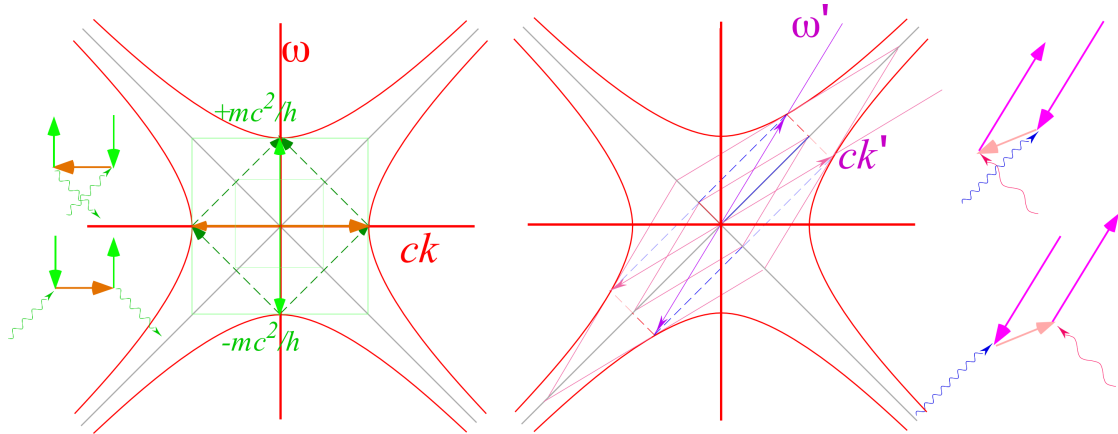


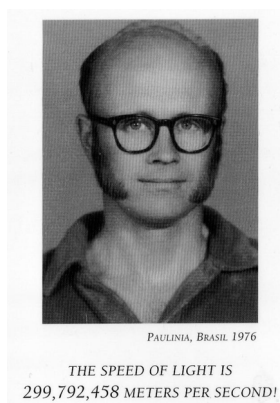
FIG. 44: Pair production or annihilation diagrammed in different reference frames.

XI. APPENDIX

A. The Purest Light and a Wave-Resonance Hero —Ken Evenson (1932-2002)

The Purest Light and a Wave-Resonance Hero —Ken Evenson (1932-2002) – When travelers punch up their GPS coordinates they owe a debt of gratitude to an under sung hero who, alongside his colleagues and students, often toiled 18 hour days deep inside a laser laboratory lit only by the purest light in the universe. Ken was an "Indiana Jones" of modern physics. While he may never have been called "Montana Ken" such a name would describe a real life hero from Bozeman, Montana, whose extraordinary accomplishments in many ways surpass the fictional characters in cinematic thrillers like *Raiders of the Lost Arc*. Indeed, there were some exciting real life moments shared by his wife Vera, one together with Ken in a canoe literally inches from the hundred-foot drop-off of Brazil's largest waterfall. But, such outdoor exploits, of which Ken had many, pale in the light of an in-the-lab brilliance and courage that profoundly enriched the world. Ken is one of few researchers and perhaps the only physicist to be twice listed in the Guinness Book of Records. The listings are not for jungle exploits but for his lab's highest frequency measurement and for a speed of light determination that made c many times more precise due to his lab's pioneering work with John Hall in laser resonance and metrology³³. The meter-kilogram-second (mks) system of units underwent a redefinition largely because of these efforts. Thereafter, the speed of light c was set to $299,792,458\text{ms}^{-1}$. The meter was defined in terms of c , instead of the

other way around since his time precision had so far trumped that for distance. Without such resonance precision, the Global Positioning System (GPS), the first large-scale wave space-time coordinate system, would have been much less practical. Ken's courage and persistence at the Time and Frequency Division of the Boulder Laboratories in the National Bureau of Standards (now the National Institute of Standards and Technology or NIST) are legendary as are his railings against boneheaded administrators who seemed bent on thwarting his best efforts. Undaunted, Ken's lab painstakingly exploited the resonance properties of metal-insulator diodes, and succeeded in literally counting the waves of near-infrared radiation and eventually visible light itself. Those who knew Ken miss him terribly. But, his indelible legacy resonates today as ultra-precise atomic and molecular wave and pulse quantum optics continue to advance and provide heretofore unimaginable capability. Our quality of life depends on their metrology through the Quality and Finesse of the resonant oscillators that are the heartbeats of our technology. Before being taken by Lou Gehrig's disease, Ken began ultra-precise laser spectroscopy of unusual molecules such as HO₂, the radical cousin of the more common H₂O. Like Ken, such radical molecules affect us as much or more than better known ones. But also like Ken, they toil in obscurity, illuminated only by the purest light in the universe.[?] In 2005 the Nobel Prize in physics was awarded to Glauber, Hall, and Hensch³⁴ for laser optics and metrology.



LIST OF FIGURES

1 Circular TRM's (a) Primary circular function triplet. (b) Full TRM sextet of circular functions. 8

2 TRM Hyperbolic labeling of Fig. 1b. 9

3 More detailed TRM expanding hyperbolic labeling of Fig. 2. 10

4 (a) Single-phasor plot of wave-function at (x,ct) . (b) 1-CW Array of phasors at many (x,ct) -points. 12

5 Comparing a wave point in Kaiser-Hertz per-space-time to its Minkowski space-time view of resulting wave. 19

6 600THz plots c-scaled in per-space-time $(c\kappa, v)$ and space-time (x,ct) 20

7 Alice's 300THz laser approaches Bob. (a) Bob sees $v=600$ THz. (b) What $\lambda=1/\kappa$ does Bob measure? 21

8 Doppler $\langle R|S \rangle$ and Rapidity ρ_{RS} (a) Alice's source and basic definitions. (b-c) Example of rapidity addition 23

9 (x,ct) wave plots (a) Alice's **R**-CW (b) Bob's Group **G** over Phase **P** (c) Carla's **L**-CW (d) $(c\kappa, v)$ plots of **P** over **G**
BohrIt Web Simulation: *Unshifted MultiPanel* ? 26

10 (x,ct) wave plots (a) Alice's **R'**-CW (b) Bob's Group **G'** over Phase **P'** (c) Carla's **L'**-CW (d) $(c\kappa, v)$ plots of **P'** over **G'**
BohrIt Web Simulation: *Doppler Shifted MultiPanel* ? 27

11 Relativity parameters given as ρ -functions as they appear in (a) Per-space-time and (b) Space-time 30

12 (a) Thales-Euclid geometric and arithmetic means (b) Hyperbola construction step by circle radius **CP'**. 36

13 (a) Sum $\Psi_{AB} = \Psi_A + \Psi_B$. (b) Sum of individual phasors. (c) Phasor A moves relative to B and vice-versa. 37

14 Sums of $n=(1,2,5,10$ and $50)$ CW with "boxcar" harmonic spectrum 38

15 (x, ct) -plots:(a-c)R&L moving PW $k=2,4,6\dots$,(b)Sum:(a)+(c) 39

16 Colliding PW of Fig. 15 as viewed in frame moving at $u=3c/5$ 40

17 Stellar aberration angle σ of light beam normal to direction of velocity **u**. ... 42

18 Epstein space-proper- $c\tau$ geometry of relativistic effects in terms of ρ or σ 42

19	Bob- $(v', c\kappa')$ -view of Alice- $(v_A, c\kappa_A)$ tangent geometry and (inset) Occam-Sword pattern relates σ , ρ , and v angles.	43
20	TE-Waveguide and Occam sword geometry for stellar angle (a-b) $\sigma = 60^\circ$ and (c-d) $\sigma = 30^\circ$	45
21	Plot of Table II values versus group velocity u/c . (List is labeled for $u/c =$ $3/5$.)	47
22	(a) Einstein-Planck energy-momentum dispersion (b) Bohr-Schrodinger ap- proximation.	54
23	(a) Slope,intercept $(u/c,-L)$ of $H(p)$ -tangent LP' give (u,L) point \mathbf{S} on $L(u)$ - circle. (b) Slope,intercept (cp,H) of $L(u)$ -tangent $C'\mathbf{S}$ give (p,H) point \mathbf{P}' on $H(p)$ -hyperbola.	59
24	Relativistic Legendre contact transformation between (a) Hamiltonian $H(p)$ (b) Lagrangian $L(u)$	61
25	Geometric elements of positive-energy relativistic quantum mechanics.	62
26	Feynman's flying clock contest winner has the greatest advance of time.	64
27	Quantum waves interfere constructively on "True" path but mostly cancel elsewhere.	65
28	Energy-momentum diagram for 1-photon transition \mathbf{H} -to- \mathbf{P}' having recoil $u/c=5/13$	69
29	Feynman diagrams of 1-photon transitions connecting 3-levels ω_l , ω_m , and ω_h	71
30	Rapidity- $\rho_p=p\rho$ and rest-frequency- $\omega_m e^{q\rho}$ and $P_{p,q}$ -lattice based on integer powers of $b=e^\rho=\frac{3}{2}$	72
31	Hyperbolic lattice of (p,q) -transition points for base $b=e^\rho=\frac{3}{2}$ and half-sum- difference coordinate relations.	73
32	Space-time laser-formed paths of constant g -acceleration (a) $g=0$, (b) $g=9.8m/s^2$	75
33	(a) Constant- $g_q = c^2/a_q$ paths proper time vs area (b) $q_{Al} = -1$, $q_{Bob} = 0$, $q_{Carl} = 1$ $\rho_p = p\rho_1 = p \cdot \ln(3/2)$ from $p = -1$ to 3	77
34	CW Doppler and PW radar metrology for frame of constant acceleration $g = 9.8m \cdot s^2$	79
35	Space-time paths of dropped objects hitting accelerating travelers.	83
36	2-CW (x,ct) -paths for $\frac{-3}{5} \leq \text{SWR} \leq \frac{3}{5}$ (1a-e) Single-frequency (2a-e) 2-frequency.	86

37	(a-g) Elliptic polarization ellipses are analogous to galloping waves in Fig. 36.1. (h-i) Elliptical oscillator conserves orbit momentum while obeying Kepler relation (i).	88
38	1 st quantized mode stacks $n=1,2,3$ of 2 nd quantized photon levels $N_n=1,2,3..\infty$	89
39	1 st and 2 nd quantized harmonic-oscillator cavity waves	93
40	Cavity 2-CW modes and invariant hyperbolas.(a) COM frame. (b) ISOC frame.	97
41	Coherent α -wave grids $\alpha \sim \Delta N$ (a)10 ³ , (b)10 ⁵ , (c) ∞ , (d)0.	99
42	Coherent real α -wave plotted over space-time.	99
43	Analogy: $e^{i(kx-\omega t)}$ -wave packet and Coherent α -wave oscillator amplitude packet.	100
44	Pair production or annihilation diagrammed in different reference frames. . . .	101

LIST OF TABLES

I	Relativity parameter formulae. Last row gives numeric values for blue-shift $b_{BLUE}^{Doppler}=2$ or $\beta = \frac{u}{c} = \frac{3}{5}$	31
II	Includes rapidity- ρ and Stellar angle- σ parameters	48

-
- ¹ Note1. Max Planck, "Zur Theorie des Gesetzes der Energieverteilung im Normal-spectrum". Deutsche Physikalische Gesellschaft. Verhandlungen 2: 237-245 (1900). [Cited on page 4.]
- ² Note2. A. Einstein, Annalen der Physik 17,891(1905). (Translation by W. Perrett and G.B. Jeffery, *The Principle of Relativity*(with notes by A. Sommerfield) (Methuen, London 1923), (republished by Dover, London 1952). [Cited on page 4.]
- ³ Note3. Albert Einstein "Zur Elektrodynamik bewegter Korper." Annalen der Physik 18,639 (1905); Annalen der Physik 17,891(1905). (Translation: Perrett and Jeffery, *The Principle of Relativity*, (Methuen, London 1923), (Dover, 1952). [Cited on page 4.]
- ⁴ Note4. Albert Einstein "Uber einen die Erzeugung und Verwandlung des Lichtes betreffenden heuristischen Gesichtspunkt." Annalen der Physik 17: 132-148 (1905). (Translation by A.B. Aarons and M.B. Peppard, Am. J. Phys. 33, 367(1965).). [Cited on page 4.]
- ⁵ Note5. Louis de Broglie, Nature 112, 540 (1923); Annalen der Physik (10) 2 (1923). [Cited on page 4.]
- ⁶ Note6. W.G. Harter and T. C. Reimer, 2005; http://www.uark.edu/ua/pirelli/html/poincare_inv_2.html. [Cited on page 4.]
- ⁷ Note7. R. P. Feynman, R. Leighton, and M. Sands, *The Feynman Lectures* (Addison Wesley 1964) Our development owes a lot to Feynman's treatment cavity wave dispersion in Vol. II Ch. 24 and Vol. III Ch. 7. [Cited on page 4.]
- ⁸ Note8. R. P. Feynman, F. B. Morinigo, and Wm. G. Wagner, *Feynman Lectures on Gravitation*, Perseus Books, Reading MA(1995). [Cited on page 4.]
- ⁹ Note9. W. G. Harter, J. Evans, R. Vega, and S. Wilson, Am. J. Phys. 53, 671(1985). [Cited on page 4.]
- ¹⁰ Note10. W. G. Harter, J. Mol. Spectrosc. 210, 166(2001). [Cited on page 5.]
- ¹¹ Note11. L. C. Epstein, *Relativity Visualized*. (Insight Press 1981) Transverse rotation provides an alternative view of SR that is described later. [Cited on page 5.]
- ¹² Note12. E.F.Taylor and J.A. Wheeler, *Spacetime Physics* (W. H. Freeman San Francisco 1966) p. XX. [Cited on page 5.]
- ¹³ Note13. D. F. Steyer, M. S. Balkin, K. M. Becker, M. R. Bums, C. E. Dudley, S. T. Forth, J. S. Gaumer, M. A. Kramer, D. C. Oertel, L. H Park, M. T. Rinkoski, C. T. Smith, and T.

- D. Wotherspoon, “Nine Formulations of Quantum Mechanics” *A. J. Phys.* 70. 288 (2002). The need for a more efficient logic is shown quite well. [Cited on page 5.]
- ¹⁴ Note14. K. M. Evenson, J.S. Wells, F.R. Peterson, B.L. Danielson, G.W. Day, R.L. Barger and J.L. Hall, *Phys. Rev. Letters* 29, 1346(1972). [Cited on page 5.]
- ¹⁵ Note15. Michelson, Albert A.; Morley, Edward W. (1887). “*On the Relative Motion of the Earth and the Luminiferous Ether*”. *American Journal of Science*. **34**: 333–345. [Cited on page 6.]
- ¹⁶ Note16. H. Minkowski, *Mathematisch-Physikalische Klasse*, vol. 1, 53 (1908). [Cited on page 12.]
- ¹⁷ Note17. Einstein never used Minkowski’s graphical view of SR (or even answer his teacher’s letter). Minkowski died in 1909. [Cited on page 17.]
- ¹⁸ Note18. At this point a Faustian pact with the devil is made. For waves to make a Cartesian (x, ct) rest frame there must be a phase wave-zero traveling at infinite speed drawing a space-x grid-lines each with time ct constant. Here waves get weird! [Cited on page 25.]
- ¹⁹ Note19. H. A. Lorentz Koninklijke Akademie van Wetenschappen te Amsterdam. Section of Science. Proc. 6: 809-831 (1904). Albert Einstein “Zur Elektrodynamik bewegter Körper.” *Annalen der Physik* 18,639 (1905); *Annalen der Physik* 17,891(1905). (Translation: Perrett and Jeffery, *The Principle of Relativity*, (Methuen, London 1923), (Dover, 1952). [Cited on page 32.]
- ²⁰ Note20. L. C. Epstein, *Relativity Visualized*. (Insight Press 1981). [Cited on page 41.]
- ²¹ Note21. L. C. Epstein, *Relativity Visualized*. (Insight Press 1981) This novel approach to SR theory did not catch on likely due to not being connected to the conventional approaches. Perhaps this can be remedied as shown here. [Cited on page 41.]
- ²² Note22. Albert Einstein “*Über einen die Erzeugung und Verwandlung des Lichtes betreffenden heuristischen Gesichtspunkt.*” *Annalen der Physik* 17: 132-148 (1905). (Translation by A.B. Aarons and M.B. Peppard, *Am. J. Phys.* 33, 367(1965).). [Cited on page 50.]
- ²³ Note23. Louis de Broglie, *Nature* 1, 540 (1923); *Annalen der Physik* (10) 2 (1923). [Cited on page 50.]
- ²⁴ Note24. Max Planck “*Zur Theorie des Gesetzes der Energieverteilung im Normal-spectrum.*” *Deutsche Physikalische Gesellschaft. Verhandlungen* 2: 237-245 (1900). [Cited on page 50.]
- ²⁵ Note25. N. Bohr, *Zeitschrift für Physik*, 9, 1-2, (1922). [Cited on page 52.]
- ²⁶ Note26. E. Schrodinger, *Annalen der Physik* (4) 79 361 and 489 (1923). Schrodinger’s protests about prevailing quantum mechanical interpretations are well circulated. So far we have not located more solid references. [Cited on page 52.]

- ²⁷ Note27. Ken Ford, *Building the H Bomb: A personal history*, World Scientific (2015) p. 70. [Cited on page 56.]
- ²⁸ Note28. . [Cited on page 56.]
- ²⁹ Note29. C. Sykes, *No Ordinary Genius: The Illustrated Richard Feynman* , W. Norton (1994) p. 84 (Meets Dirac in July 1964). [Cited on page 57.]
- ³⁰ Note30. P. A. M. Dirac, *of Relativistic Dynamics*” Rev. Mod. Physics, 21: 392 (1949). [Cited on page 57.]
- ³¹ Note31. Feynman’s Thesis: A New approach to Quantum Theory, Edited by Laurie M. Brown, World Scientific (2005) has edited copy of 1941 thesis and discussion of RPF Space-time approach to non-relativistic quantum mechanics, Rev. Mod. Phys. 20 (1948) pp. 367-387; and R. P. Feynman and A. R. Hibbs, *Quantum Mechanics and Path Integrals* (McGraw-Hill 1965). [Cited on page 57.]
- ³² Note32. A. Einstein, *”I shall never believe that god plays dice with the universe”* Albert Einstein Archives, The Jewish National and University Library, The Hebrew University of Jerusalem (<http://www.albert-einstein.org>), Einstein Archives Online, Volume 15, 294, Letter to Cornelius Lanczos, March 21, 1942; <http://www.alberteinstein.info/db/ViewDetails.do?DocumentID=30893>. [Cited on page 64.]
- ³³ Note33. K. M. Evenson, J.S. Wells, F.R. Peterson, B.L. Danielson, G.W. Day, R.L. Barger and J.L. Hall, Phys. Rev. Letters 29, 1346(1972). [Cited on page 101.]
- ³⁴ Note34. The Nobel Prize in Physics, 2005. https://www.nobelprize.org/nobel_prizes/physics/laureates/2005